Effects of magmatic intrusions on temperature history and diagenesis in sedimentary basins - and the impact on petroleum systems

Magnhild Sydnes

Thesis for the degree of Philosophiae Doctor (PhD)
University of Bergen, Norway
2020

UNIVERSITY OF BERGEN

Effects of magmatic intrusions on temperature history and diagenesis in sedimentary basins - and the impact on petroleum systems

Magnhild Sydnes

Thesis for the degree of Philosophiae Doctor (PhD)
at the University of Bergen

Date of defense: 23.04.2020

Year: 2020

Title: Effects of magmatic intrusions on temperature history and diagenesis in sedimentary basins - and the impact on petroleum systems

Name: Magnhild Sydnes

Print: Skipnes Kommunikasjon / Universitetet i Bergen

Nothing would be done at all

if one waited until one could do it so well

that no one could find fault with it.

-*Cardinal John Henry Newman*

I can accept failure,

everyone fails at something.

But I can't accept not trying.

-*Michael Jordan*

Preface

This dissertation is submitted as a partial fulfillment of the requirements for the degree Philosophiae Doctor at the Department of Earth Science, University of Bergen. The project was jointly funded by the Research Council of Norway (RCN) and Tectonor AS through RCN's Industrial Ph.D. program. Professor Nestor Cardozo was the supervisor at the beginning of the project from January 2016 to December 2017 at the University of Stavanger. From December 2017 to January 2020 the project was continued and finalized at the University of Bergen with Professor Rolf Mjelde as the supervisor. Throughout the whole project period colleagues from Tectonor have been involved, Dr. Willy Fjeldskaar as the main industrial supervisor and Drs. Ingrid Fjeldskaar Løtveit and Ivar Grunnaleite as co-supervisors.

The motivation to carry out the present investigation is essentially due to my employment in Tectonor, an enterprise "providing specialized geological expertise to the petroleum exploration industry" (www.tectonor.com). Through the work for the company I was exposed to a number of geological problems, and it was interesting and educational to experience how challenges, faced by the oil and gas industry, raised questions where no clear answer could be found in the research literature. Among the questions surfacing in this way was if it was possible to predict fairly accurately how magmatic intrusions influences the petroleum potential in a sedimentary basin due to acceleration of the maturation of organic material in areas that otherwise would remain immature.

References cited in the papers in Part II are found at the end of each paper, whereas references in Part I of the thesis follow at the very end of the dissertation.

Acknowledgements

First of all, sincere thanks to Tectonor, which had faith in me and presented me with a number of questions that could form the basis for a Ph.D. thesis of relevance to the petroleum industry. Financial support from the company and the Research Council of Norway is highly appreciated.

My Tectonor colleagues and supervisors, mainly Dr. Willy Fjeldskaar, but also Dr. Ingrid Fjeldskaar Løtveit and Dr. Ivar Grunnaleite, are thanked for guidance and inspiring discussions throughout the project. My university supervisors, Professor Nestor Cardozo at the University of Stavanger and Professor Rolf Mjelde at the University of Bergen are thanked with gratitude for the input and advice they furnished. Thanks are also due to Professor Emeritus Olav Eldholm for encouragement and interesting discussions, a result of which was valuable contact with Professor Emeritus Elen Roaldset, who shared with me interesting information about her studies on diagenesis. Communications with Associate Professor Christian Haug Eide is highly appreciated and I am grateful for his permission to use photographic material. Fellow Ph.D. students are thanked for uplifting conversations.

My family is thanked for tremendous patience and understanding for years. I want to thank my dad for patiently discussing issues related to chemistry and furnishing literature to study to improve my understanding; my mom for taking care of the kids when time was scarce; and my siblings, in-laws, nieces, and nephews for cheering me up when they sensed that the spirit needed a boost.

Lastly, but not least: Sincere thanks and gratitude to my husband Anders for believing in me, supporting me, and keeping order when I was unable to do so, and our three boys, Martin, Olav and Magnus, for reminding me what is really important in life. I love you guys!

Magnhild Sydnes
Bergen, January 13th, 2020

Abstract

For many volcanic basins, the thermal effect of igneous intrusions is decisive for their petroleum potential because such thermal impact may lead to maturation of organic material in areas that otherwise would remain immature. Many factors contribute to the outcome of such intrusions, and in this thesis the influence of a number of parameters, including sill thickness, timing of emplacement, structural changes of sedimentary basins, lithologies and diagenesis, have been modeled to improve the ability to predict the development of the whole petroleum system as a function of its thermal history. By quantifying the effect of several of these factors, the aim of this project has been to estimate the thermal impact of magmatic intrusions on maturation and diagenesis, from the very first temperature increase in the host rock to the long term influence, in terms of permeability and migration.

Sill thickness and timing of emplacement is central in the first Paper where the thermal effect of 0 m, 50 m and 100 m thick sills are compared. The results show large differences on the thermal effect of the tested thicknesses, particularly for 0 m versus 100 m, but also 50 m versus 100 m thick sills. Whereas immature areas in the vicinity of sills that are 50 m thick will remain immature, they become fully matured when the sills are twice as thick. Timing of sill emplacement can be essential, particularly if the source rocks are between two or more sills intruded with a time lapse.

Transient thermal effects of normal faulting in basins with magmatic intrusions are in focus in the second Paper. As fault movements occur, the basin momentarily experiences thermal instability in the proximity of the fault zone. How long this thermal instability lasts, depends on several factors, such as the physical properties of the rocks and the time lapse of fault movement. The results show that the largest differences between steady state and transient thermal calculations are found in the hanging wall. If sills intrude shortly after fault movement, the rocks in the hanging wall are colder than the rocks at the same depth in the foot wall. As the thermal effect of magmatic intrusions is dependent on the pre-intrusion host-rock temperatures, the

thermal effect of the sills is smaller in the hanging wall than the foot wall due to the lower host rock temperatures. However, if the sills intrude with a time lapse in relation to the fault slip, the sedimentary rocks have become warmer and the effect of the intruding sills is larger. Other factors that influence the thermal effects of sill intrusions in sedimentary basins are fault displacement, time span of faulting and deposition, fault angle, the thermal conductivity of the rocks, specific heat capacity and basal heat flow. How the faults are restored in the modeling process also influences the thermal development in the basin after fault slip.

Diagenesis/chemical compaction is the focus of the third Paper. The study quantifies the thermal effect of magmatic intrusions on three different diagenetic processes: the transition of opal A to opal CT to quartz; the smectite to illite transition; and the dissolution and re-precipitation of quartz. All these processes are temperature dependent and may induce deterioration of the reservoir quality by reducing the porosity. Diagenetic alterations can contribute to changes in the physical properties of the rocks. These changes can cause rocks to respond differently to stress conditions in the subsurface. Emplacement of magmatic intrusions influences all the studied diagenetic processes and result in porosity loss of rocks in their proximity. Results show that stresses build up in the stiffer rocks, like the sills and diagenetic altered areas. Such stress accumulations may potentially lead to fault slip or opening of fractures and thus increase the permeability and the potential of fluid migration.

Overall, this study shows the need for good representation of the subsurface sill thicknesses and structural development, particularly prior to emplacement of magmatic intrusions. Through magmatic intrusion and their impact on the maturation of organic material, diagenetic processes, location of stress concentrations, and the potential effect on permeability and migration pathways, this study highlights how these factors may have long-term effect on the petroleum system. Other crucial variables are sill thickness and clustering of the sills at multiple levels. The thermal conductivity of host rocks is the factor influencing the transient thermal effects the most, after fault slip and the increased temperatures enhance maturation and diagenesis in their vicinity.

List of Publications

Paper 1:

Sydnes, M., Fjeldskaar, W., Løtveit, I.F., Grunnaleite, I., Cardozo, N. (2018): "The importance of sill thickness and timing of sill emplacement on hydrocarbon maturation", Marine and Petroleum Geology, 89, 500-514, doi: 10.1016/j.marpetgeo.2017.10.017

Paper 2:

Sydnes, M., Fjeldskaar, W., Grunnaleite, I, Løtveit, I.F., Mjelde, R. (2019): "Transient Thermal Effects in Sedimentary Basins with Normal Faults and Magmatic Sill Intrusions – A Sensitivity Study", Geosciences, 9, 160; doi:10.3390/geoscineces9040160, Special Issue "Future Advances in Basin Modeling: Suggestions from Current Observations, Analyses and Simulations".

Paper 3:

Sydnes, M., Fjeldskaar, W., Grunnaleite, I., Løtveit, I.F., Mjelde, R. (2019): "The influence of magmatic intrusions on diagenetic processes and stress accumulation", Geosciences, 9, 477, doi:10.3390/geosciences9110477, Special Issue "Future Advances in Basin Modeling: Suggestions from Current Observations, Analyses and Simulations".

Contents

Part I

Introduction and summary

Chapter 1

Introduction

According to the annual report, Energy outlook 2019, by British Petroleum (BP, 2019); "The demand for energy is set to increase significantly driven by increases in prosperity in the developing world". This report intends to predict the future energy needs and challenges towards 2040 and explore the forces that drive the global energy changes by considering several possible future scenarios. In a world demanding transition from fossil fuels to renewable energy supplies, accompanied by global growth in population and wealth makes this is a particularly difficult task.

This report predicts an increase in the need of hydrocarbons to feed the worlds future energy demands. Although renewable energy is expected to play a larger role to meet these needs, fossil fuels will still be the main source of energy in decades to come. This is a challenge for the energy companies, not only in their search for new "green" energy forms, but also in their handling of the actual transition phase, a phase requiring continued petroleum exploration, search for new commercial hydrocarbon reserves, and investigation of new petroleum plays.

This project explores the petroleum potential of volcanic sedimentary basins and the thermal impact of magmatic intrusions on the petroleum system (Fig. 1). Worldwide there are several producing oil and gas fields located in volcanic basins (Zou et al., 2013). However, on the Norwegian Continental Shelf such reservoirs are considered a fairly new, challenging petroleum play. The intensions of the project are to improve the certainty of the assessment of the hydrocarbon potential in volcanic basins and

increase the knowledge related to the thermal impact of magmatic intrusions. It emphasizes how the interpretation and modeling phase ultimately effect the maturation and diagenetic estimates of basins with magmatic intrusions.

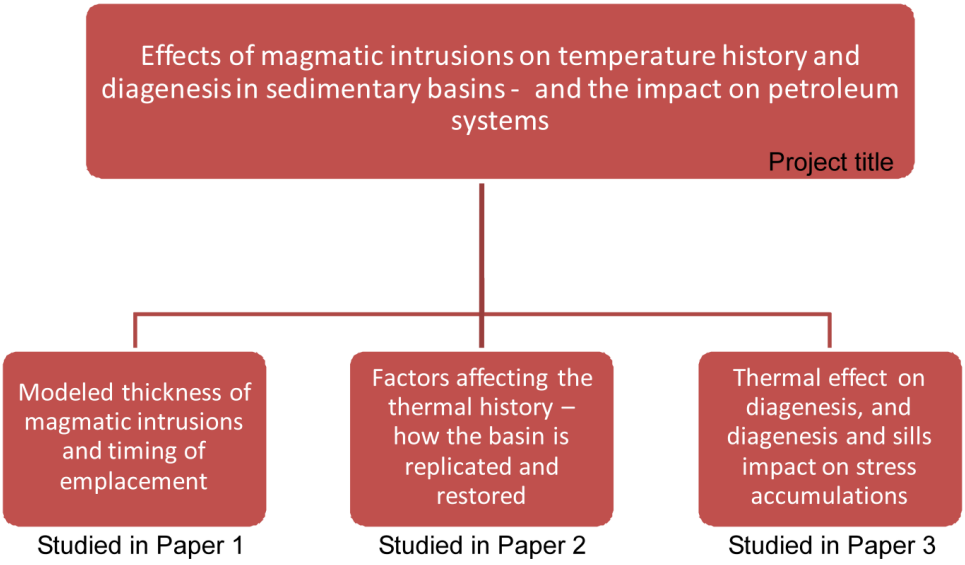

Figure 1: *Simple, schematic presentation of the project. Top: project title. Bottom: the topics of the three Papers. Papers* 1 *and* 2 *explore the consequences of the interpretation and basin modeling process related to volcanic sedimentary basins. Paper 3 explores magmatic intrusions effect on diagenetic processes.*

Below follows a paragraph stating the motivation and objectives of the study followed by a description of different intrusion types in volcanic basins worldwide, as well as factors influencing the petroleum potential of basins with intrusions. Furthermore, the methods used in this study are presented followed by a summary of the results and conclusions of this project. Part II presents the three scientific articles resulting from this work.

1.1 Motivation and objectives of the study

On seismic reflection data magmatic intrusions can be observed and interpreted, however, their effects on temperature, maturation and diagenesis can only be

calculated through basin modeling. Basin modeling commonly operates with time steps representing several millions of years. Such a time-resolution is too coarse when studying the thermal effect of magmatic intrusions, as the main effects are present the first million years. Estimations of the thermal effect of these features demand a high-resolution system in both time and space. Therefore, the motivation for this study is twofold: One relates to how the thermal effect of magmatic intrusions is estimated, the other to the several unanswered questions regarding the impact of magmatic intrusions on the petroleum system.

A large body of knowledge exists on the thermal effect of igneous intrusions in volcanic basins. It is well established that magmatic intrusions influence the thermal development of sedimentary basins (e.g. Galushkin, 1997; Fjeldskaar et al., 2008; Aarnes et al., 2010; Peace et al., 2017; Spacapan et al., 2018). Aarnes et al. (2010) studied the thermal effect of the thickness of sills, vertical spacing between the sills (Aarnes et al., 2011) and timing of emplacement (Aarnes et al., 2015). Neither of the studies model the intrusions emplaced into their natural environment accounting for the effects of the geological, structural and thermal development of the basin prior to emplacement of sills. Fjeldskaar et al (2008) modeled the effect of sill intrusions on the transformation of organic matter emplaced into a structural complex basin. However, the sensitivity of the basin to sill thickness was not pursued.

For a basin without sills, Fjeldskaar et al. (2017) found a large gap in the calculated thermal development when the faults were restored to when they were not restored. This indicates that the estimated thermal development of basins is sensitive to how they are reconstructed and represented. The thermal effect of magmatic intrusions is dependent on the pre-intrusion host rock temperature (e.g. Aarnes et al., 2010; Spacapan et al., 2018). Therefore, it is important to explore the sensitivity of basins to factors influencing the temperature history of structurally complex volcanic basins in order to make good thermal estimates. Very few studies estimate the temperature effect of magmatic intrusions emplaced into structurally complex basins. Such a study requires a modeling system that can restore the geological and structural

history, which forms the foundation for the thermal development and the basis for quantifying the thermal effect of magmatic intrusions in sedimentary basins.

Studies on diagenesis and the effect of igneous intrusions on such processes have resulted in contrasting conclusions. Haile et al. (2018) found that the sill intrusions on Edgeøya (Svalbard) had not affected the diagenesis in their vicinity, while at Wilhelmøya (Svalbard) convection related to igneous intrusions had influenced the diagenetic process (Haile et al. 2019). At Trail Ø (East Greenland), Therkelsen (2016) found that both conductive and convective heat transfer due to magmatic intrusion had contributed to increased diagenetic alterations in their vicinity. However, little has been done to incorporate estimates of diagenesis in basin modeling of volcanic sedimentary basins. Because diagenesis may alter reservoir properties through dissolution and precipitation of minerals, it is of interest to the oil and gas industry to predict reservoir quality.

The overall goal of this project is to contribute to better prediction of thermal development and hydrocarbon potential of basins with magmatic intrusions (Fig. 1), and to attempt answering some of the challenges faced by the petroleum industry. It aims at broadening the perspectives on how magmatic intrusions affect all parts of the petroleum system. From the very first temperature increase in the basin sediments, to the long term influence due to the accelerated maturation and diagenesis and the potential alteration of permeability and porosity in rocks. More specifically the goals of the project can be summarized as follows:

1. Analyze the effect of sill thickness and timing of emplacement on the temperature and hydrocarbon maturation of sedimentary basins.
2. Quantify the thermal effects of the most important factors affecting the thermal history in structurally complex sedimentary basins with magmatic intrusions.
3. Quantify the effect of magmatic intrusions on transitions of opal A to opal CT to quartz, smectite to illite and quartz diagenesis. Assess the influence of diagenetic processes and the sills themselves on the stress field in a sedimentary basin, and the potential impact on fracture and fault permeability.

Chapter 2

Magmatic intrusions in sedimentary basins

Magmatic intrusions, in contrast to magmatic extrusions, represent magma emplaced and solidified beneath the surface of the earth. Intrusions emplaced as hot liquid magma, penetrates upwards due to buoyancy caused by the density difference between the magma and the host rock (Gudmundsson and Løtveit, 2012). There are four main types of intrusions; batholiths, laccoliths, sills and dykes (Fig. 2). Batholiths are the largest types of intrusions and are commonly formed when several smaller intrusions merge into one large unit which is layer discordant. Laccoliths are layer concordant features responsible for substantial doming of the overlying sequences, exerting a high magma pressure on the overlying units. Commonly magma is fed into laccoliths directly from underneath (Fig. 2). Sills are also layer concordant, but are tabular in shape and typically thinner than laccoliths. There are examples of sills forcing overlying sequences to bulge upwards (e.g. Hansen and Cartwright, 2006; Jackson et al., 2013; Eide et al., 2017; Omosanya et al., 2017; Magee et al., 2019), however, not to the same degree as laccoliths. Dykes are considered the smallest of the intrusions and are layer discordant. Although generally smallest, they are vital for the magma plumbing system to function as they feed the system with magma from deeper sources.

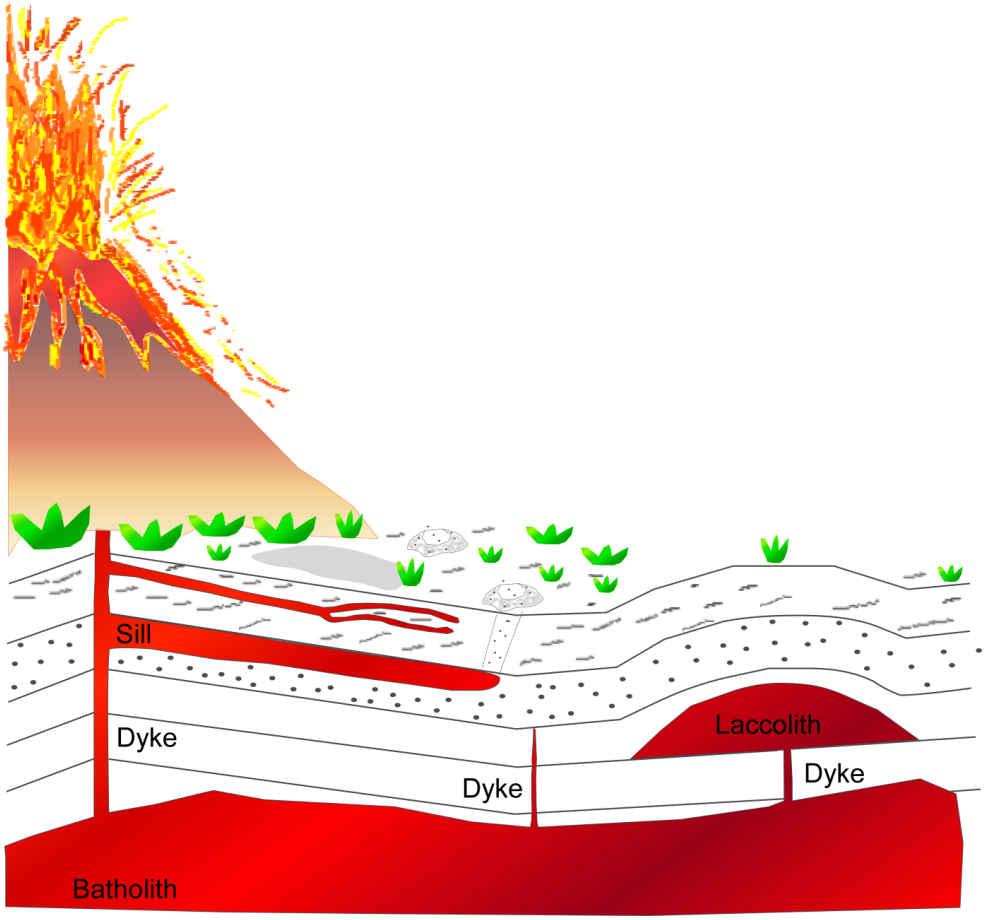

Figure 2: *Simple sketch of a system containing batholiths, laccoliths, sills and dykes*.

The focus of this study is on the sills, as this is the group of intrusions often observed in sedimentary basins having an intense thermal effect on their host rocks. However, the results of this study are applicable for magmatic intrusions of all kinds. Sills may feed other sills with magma (e.g. Eide et al., 2017), however, one or more dykes must be present to supply magma from a source deeper within the crust. Dykes are deflected into sills when local stresses change into favoring sill emplacement, usually at interfaces between two layers (Gudmundsson, 1990, 2011a). Sills are known to act as both low permeable seals and fractured reservoirs (Zou et al., 2013; Gudmundsson and Løtveit, 2012).

2.1 Observations of sills in the field and on seismic data

Sills commonly have large acoustic impedance relative to their host rocks, which often make them easy to locate on seismic images (Fig. 3a) (Smallwood and Maresh, 2002). However, determining the upper and lower boundaries of sills can be difficult. How well a sill can be detected and separated from the host rock depends on its thickness, the acoustic impedance contrast and the frequency bandwidth of the seismic wavelet (Hart, 2000; Osagiede et al., 2014; Magee et al., 2015). Dykes are commonly beyond seismic resolution due to their small size/proportions, and sub vertical dykes are ordinarily impossible to locate on reflection seismic data. However, in some areas dykes are well resolved in high quality 2D and 3D seismic reflection data due to post-emplacement rotation by structural development of the basin (Phillips et al., 2018). If a sufficient number of dykes are present, or if the dykes are thick enough, they will also have a thermal contribution in sedimentary basins. This factor is however, not pursued in this study.

Field observations of sills (Fig. 3b,c) suggest that sill thicknesses commonly are from a few meters to some hundred meters (e.g. Aarnes et al., 2011; Gudmundsson and Løtveit, 2012) and the aspect ratio (lateral dimension versus thickness) normally lies within the 150-500 range (Hansen et al., 2011; Gudmundsson and Løtveit, 2012). A subsurface study by Mjelde et al. (1997a) from the Vøring Basin model sills to be locally more than 500 m thick based on Ocean Bottom Seismograph (OBS) data. Interpretation of multichannel seismic reflection data and amplitude modeling from the same basin suggest that sills are generally around 100 m thick (Berndt et al., 2000).

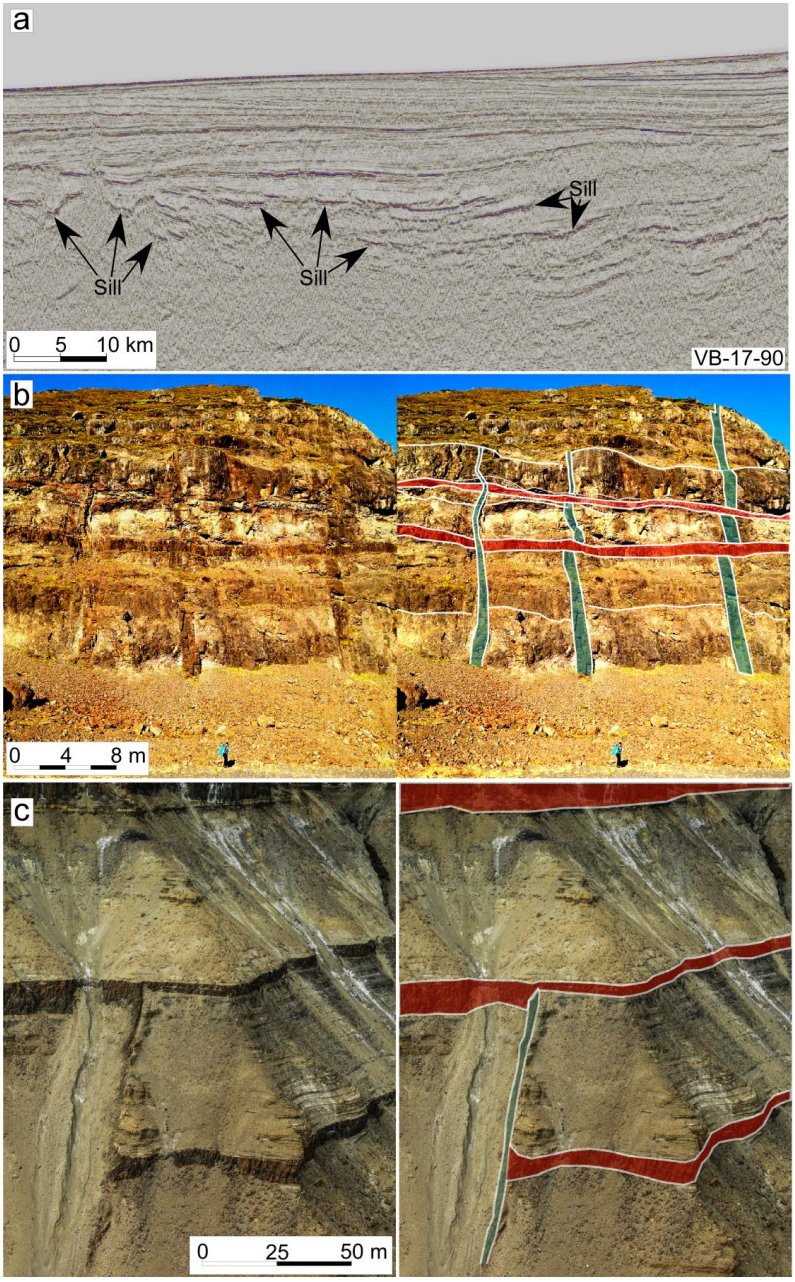

Figure 3: *a) Sills on seismic reflection data. Arrows point at some of the sills. b) Sills intruded into volcanic rocks on Iceland (Photo I. Grunnaleite. Permission granted). c) Magmatic intrusions in a sedimentary basin in East Greenland (Eide et al., 2017. Permission granted).*

2.2 Volcanic basins worldwide and on the Norwegian Continental Shelf

Today, several producing oil and gas fields in Asia, Australia and in North and South America are located within volcanic provinces and many future petroleum exploration activities are expected to be associated with such regions (Zou et al., 2013; Senger et al., 2017). The Neuquen Basin (Argentina), Amazonas Basin (Brazil), North Basin (USA) and Niigata Basin (Japan) (Zou et al., 2013) are some examples of basins with producing volcanic oil and gas fields. Volcanic provinces, also known as large igneous provinces (LIPs) (Fig. 4), are formed under abnormal circumstances, as opposed to conventional continental rifting and oceanic spreading mechanisms (Coffin and Eldholm, 1994). Successful exploration on volcanic margins requires understanding of their tectonic development, heat-flow history, intrusion mechanisms, and the effects of emplacement of magmatic intrusions on the petroleum system.

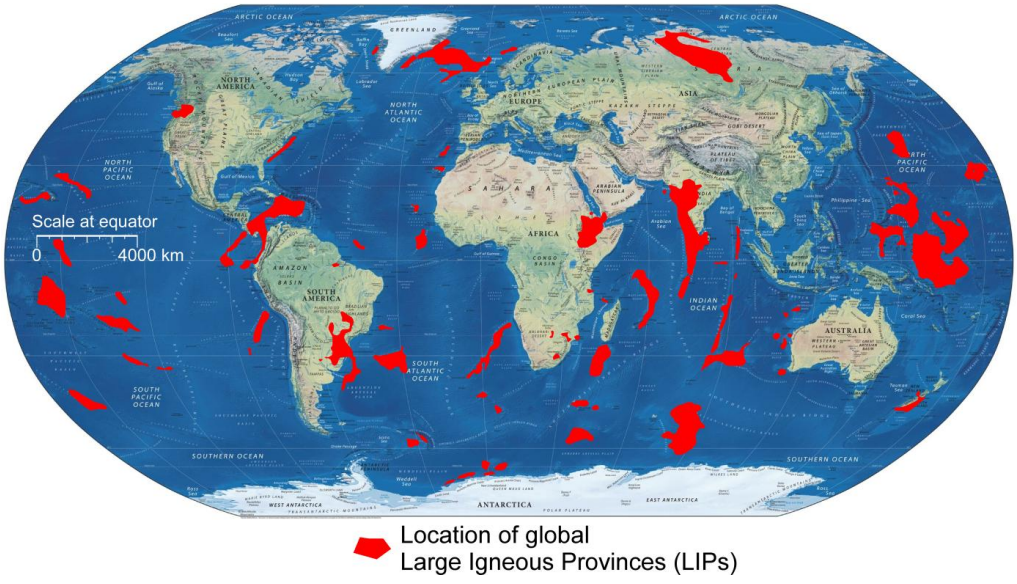

Figure 4: *Map showing approximate location of some of the Large Igneous Provinces (LIPs); modified after Coffin and Eldholm (1994) and Geoffroy (2005). Base map obtained from: https://non-art.info/map-of-thw-world-map/physical-map-of-the-world-land-cover-maps-com/.*

These igneous provinces (Fig. 4) are characterized by their extensive crustal emplacement of iron and magnesium rich (mafic) rocks and include continental flood basalts, volcanic passive margins, oceanic plateaus, submarine ridges, seamount chains, and ocean basin flood basalts (Coffin and Eldholm, 1994).

On the Norwegian Continental Shelf there are a few basins known to accommodate magmatic intrusions. The Vøring and Møre Basins (Fig. 5) (e.g. Planke et al., 2005; Galushkin, 1997; Fjeldskaar et al., 2008) are probably the two basins containing the largest volume of emplaced magmatic material. These basins are located offshore the west coast of Mid-Norway in the Norwegian Sea and are dated to have been intruded by magma simultaneously to the opening of the North Atlantic in Early Eocene (Svensen et al., 2010).

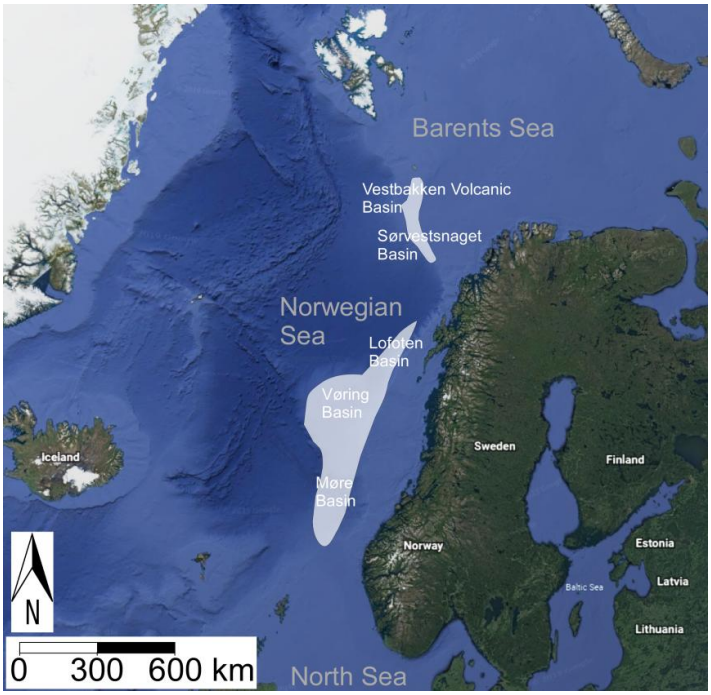

Figure 5: *Approximate location of known basins with magmatic intrusions on the Norwegian Continental Shelf; Vestbakken Volcanic Basin, Sørvestsnaget Basin, Lofoten Basin, Vøring Basin and Møre Basin. Base map obtained from: www.earth.google.com, on December 6th 2019.*

Magmatic intrusions are also known to be present in the Lofoten Basin in the Norwegian Sea (Fig. 5) (Mjelde et al., 2002), and in some locations in the SW Barents Sea, like the Sørvestsnaget Basin (e.g. Mjelde et al., 2002) and in the Vestbakken Volcanic Province (Fig. 5) (e.g. Fjeldskaar et a., 2008; Gac et al., 2018).

Chapter 3

The main effects of magmatic intrusions on sedimentary basins

In a petroleum system, the thermal history is one of the most important factors as it controls the formation and migration of hydrocarbons, the hydrocarbon properties, and the diagenetic processes that are important for the physical properties of the rocks. The emplacement of magmatic intrusions may significantly alter the thermal history of sedimentary basins.

3.1 Effect on temperature

The thermal calculation of any sedimentary basin is founded on its geohistory. Reconstruction of the geohistory, therefore, becomes important, and it is commonly based on a digitized seismic section which can be performed by either forward or backward modeling. All sediments in the digitized section are assigned a lithology with defined porosity/depth trends in order for the system to compact or decompact (depending respectively on forward or backward reconstruction process) the deposits through the geological evolution. Generally, reconstruction methods do not account for the complex structural history of basins. However, some methods restore the structural development, which has been shown by Fjeldskaar et al. (2017) to be crucial, as it can result in underestimation of temperature by ~80 °C (Fig. 6)

The assigned lithologies in a section also contain information about vertical and horizontal thermal conductivity and specific heat capacity which are important parameters for the thermal calculations. For a sedimentary basin following a cycle of depositions and subsidences, the thermal history is a function of the heat flow from the mantle, the surface temperature, sediment deposition and subsidence, uplift and erosion, paleo-water depths, and the ability of sedimentary rocks to transfer heat. Usually, basin thermal calculations are based on heat transfer by conduction, since the main heat flow in the lithosphere occurs through this process (Allen and Allen, 2014). All these factors result in variation of the temperature with depth, often increasing by 30 °C·km^{-1} (Allen and Allen, 2014).

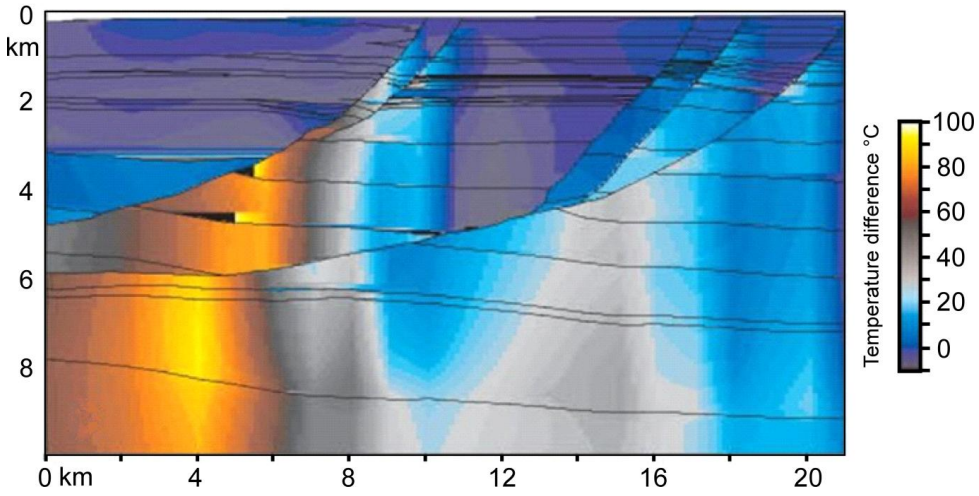

Figure 6*: Thermal differences in a basin when fault movement is accounted for versus when it is not accounted for. The estimated temperatures are higher in the basin when fault movement is restored (modified after Fjeldskaar et al., 2017).*

Thermal calculations can be performed either by the steady-state or the transient models. The steady-state method assumes that the basin maintains thermal equilibrium from one modeled time step to the next. Transient thermal calculations, on the other hand, take into account the time needed for the basin to warm up or cool down, and requires more computer time than the steady-state models. When magmatic intrusions are emplaced, the magma temperature is around 1000 ^{o}C

(Gudmundsson and Løtveit, 2012), which is considerably higher than the surrounding host rock. The resulting thermal effects are short lived in geological terms, and transient thermal modeling with frequent time intervals are required to obtain accurate calculations and study the thermal effect. Calculations of the thermal effects thus require much higher temporal and spatial resolution than is generally the case in basin modeling. Modeling of the temperature and maturity effects of magmatic sills is therefore hardly ever done based on a realistic geohistory of 2D seismic sections.

The ultimate thermal effect of magmatic intrusions is sensitive to the host-rock pre-intrusion temperature (Dow, 1977; Bostick and Pawlewicz, 1984; Raymond and Murchison, 1988; Aarnes et al., 2010; Moorcroft and Tonnlier, 2016; Spacapan et al., 2018) and it has been found to have larger thermal impact than the magma intrusion temperatures and the sill thickness (Aarnes et al., 2010). Unfortunately, this parameter is one of the most difficult to determine as evidence of this temperature is erased with the sill emplacement and further geological development. The host rock pre-intrusion temperature can only be estimated by thorough temperature modeling. Magmatic intrusions are commonly emplaced into structurally complex sedimentary basins where several factors affect the thermal development. It is therefore important to do this modeling as realistic as possible.

3.2 Effect on maturation

Maturation of organic material in source rocks is a function of the temperature (e.g. Gluyas and Swarbrick, 2015). For organic material to transform into oil or gas, the source rock must maintain high temperatures over millions of years; ~80-150 ^{o}C to form oil and ~150-180 ^{o}C to obtain gas (Allen and Allen, 2014; Gluyas and Swarbrick, 2015). The need for good thermal-history calculations to make good maturation predictions is therefore evident.

Kinetics of kerogen degradation is a common approach in maturation modeling (Tissot and Welte, 1984) utilizing the relationship between temperature and chemical-reaction rates given by the Arrhenius equation (1) (Tissot and Welte, 1984; Allen and Allen, 2014).

$$k = A_0 e^{\left(\frac{-E_a}{RT}\right)} \quad (1)$$

where k is the reaction rate, A_0 is the pre-exponential constant/frequency factor (mol/ cm^2s), E_a is the activation energy (J/mol), R is the real gas constant (8.314 J $mol^{-1}K^{-1}$) and T is the temperature. A_0 represents a constant describing how often chemical species collide within a system, whereas E_a represents the energy barrier necessary for a chemical reaction to occur. Both these parameters are unique for any given chemical reaction.

Kerogen type must be defined for the source rocks in the basin. There are three types of kerogen that mainly transform into oil and gas, denoted kerogen type I, II and III. Their unique activation energies and frequency factors result in dissimilar behavior and cracking of oil and gas under different conditions (e.g. Gluyas and Swarbrick, 2015).

The rate of a chemical reaction is doubled when the temperature is increased approximately by 10 °C (Tissot and Welte, 1984; Allen and Allen, 2014). Thus, with emplacement of magmatic intrusions a tremendous increase in the chemical-reaction rates will take place in their proximity. However, the increased temperatures following such emplacement feed the system with a lot of energy, which may lead to a transition from kinetic to thermodynamic control so that more energy-demanding transformations may occur (Atkins et al., 2017). This may in turn result in formation of kerogen less prone to form hydrocarbons (Tissot and Welte, 1984; Michelsen, 2017).

3.3 Effect on diagenesis

Diagenesis is the alteration occurring when chemical compounds dissolve and are either re-deposited or form new components that precipitate (Allen and Allen, 2014). Several diagenetic reactions occur in the subsurface, including quartz diagenesis, transition of opal A to opal CT, dolomitization of carbonate rocks and alterations of clay minerals (e.g. Tissot and Welte, 1984; Allen and Allen, 2014; Dralus et al., 2013; Peltonen et al., 2009). These chemical transformations cause porosity loss and

increase of rock densities, seismic velocities and physical rock strength (e.g. Nobes, et al., 1992; Roalset and Wei, 1997a and b; Peltonen et al., 2009; Neagu et al., 2010). In some cases, potentially good reservoir rocks may be totally destroyed by such chemical transformations leaving little or no porosity for hydrocarbons to accumulate. However, these diagenetic changes are also known to create hydrocarbon traps and fractured reservoirs (Dralus, 2013; Tsuji et al., 2011).

Diagenesis, like maturation, is thermally dependent and is commonly described by kinetics governed by the Arrhenius equation (1) (Dralus, 2013), where k for this reaction is the rate constant of precipitation. As for maturation, increased temperatures due to magmatic intrusions are anticipated to enhance the diagenetic processes, which are determined by the lithology and chemical material in the subsurface. Modeling of these effects caused by sill intrusion had not been performed prior to this work.

3.4 Stress effect of sills

Sedimentary basins commonly consist of multiple heterogeneous layers with rocks of contrasting Young's modulus (stiffness) and contain a network of faults and fractures developed through tectonic events. These faults and fractures are resulting from stresses that have acted on the basin over its lifetime and they constitute weaknesses in the subsurface prone to be reactivated (Gudmundsson, 2011b). The current stress field in a basin determines the faults and fractures that are potentially active and open.

Magmatic intrusions are hydrofractures, primarily extension fractures, usually generated, partly or entirely, by fluid pressure (Gudmundsson and Brenner, 2001). These fractures open up perpendicular to the minimum compressive principal stress, σ_3, and propagate in the direction of the maximum compressive principal stress, σ_1 (Gudmundsson, 2011b). When sills are emplaced, they induce stresses on the host rocks and this may lead to activation/reactivation of faults and open fractures and could possibly cause formation of fractured reservoirs even at distances far away

from the sill itself. In addition, sills can function as hydrocarbon seals and even as fractured reservoirs (Gudmundsson and Løtveit, 2012).

The emplaced sills eventually solidify and become typically stiffer than their sedimentary host rocks (Gudmundsson, 2011b). Areas in close proximity of sills have been identified to have increased diagenetically modified rocks (e.g. Therkelsen, 2016) and constitute together with the sills, the stiffer rocks in the basin, as the diagenesis may have increased the physical strength of the rock by more than 100% (Roaldset and Wei, 1997b). Stiffer rocks tend to accumulate stress as opposed to the softer layers (e.g. Gudmundsson and Brenner, 2001; Gudmundsson et al., 2002; Gudmundsson, 2011b), which make these areas prone to activate/reactivate faults and fractures. The stress effects of sills and the diagenetically modified area have so far received little attention.

Chapter 4

Methods and softwares

The project aims at reaching conclusions applicable to volcanic basins in general. This is accomplished by using the geometry of real basins with magmatic intrusions and applying global instead of site-specific parameters to the sections. The Vøring basin, offshore mid-Norway, is an example of a basin located in a volcanic passive margin that has developed during continental rifting and breakup derived by lithospheric extension due to plate tectonics (Geoffroy, 2005). With extension follows thinning of the lithosphere, subsidence, sedimentation, passive buoyant-driven upwelling of the mantle in the thinned area (McKenzie, 1978; Sengör and Burke, 1978) and possible emplacement of magmatic intrusions (Geoffroy, 2005). Most of the magmatic activity in the Vøring basin is proposed to originate from a LIP related to the Iceland hotspot that has influenced the North Atlantic since Early Cenozoic (Coffin and Eldholm, 1994; Howell et al., 2014; Mjelde et al., 2016). Such an area is ideal for studying the thermal effect of emplaced magmatic intrusions in sedimentary basins, but in some cases it is convenient to use synthetic profiles, which simplifies the modeling, for instance when differentiating the sensitivity of key parameters to the thermal development of sedimentary basins as performed in Paper 2 of this project.

In the mantle, the main heat transfer mechanism is convection, while in the lithosphere it is conduction (Allen and Allen, 2014). The main processes influencing the thermal effect of intrusions have been calculated by conduction modeling.

Convection may locally play a significant role and is a function of lithology, porosity and permeability, but is generally considered a secondary heat transfer mechanism in the lithosphere (Robertson, 1988) and is beyond the scope of this project.

4.1 Basin modeling

The starting point for all geohistory reconstructions in our study is the present basin geometry. All polygons in the digitized section are assigned a lithology with corresponding porosity/depth trend, thermal conductivity and specific heat capacity. An inversed, backstripping process is utilized, where one layer at a time is removed and the underlying sequences are decompacted based on the porosity/depth trend after exponential functions described by Sclater and Christie (1980). Faults are restored by vertical shear, a process that leaves no gaps or overlaps in the geometry and keeps track of rock masses, which is essential for the thermal and maturation modeling (Fjeldskaar et al., 2017). Furthermore, it simplifies and accelerates the compaction calculations (Fjeldskaar et al., 2003). Potential eroded material is added and paleo-water depths may be defined for every timestep but are not accounted for here. For timesteps with presence of sills, the sill polygons are assigned magmatic intrusion lithology with corresponding physical properties. These sill polygons are activated at time of emplacement. Similar procedure repeats itself all the way to the top basement. The result is structural and geological history of the basin, which forms the basis for further thermal and maturation modeling.

The thermal development of the basin is calculated by a conductive finite difference model (cf. Fjeldskaar et al., 2008, 2017) with rectangular finite difference thermal grid (Fig. 7), which is redefined at each timestep. Vertical and horizontal grid lines must be inserted so that the geometries are accurately represented. Particularly fine grid around small features, e.g. sills, must be inserted in order to provide realistic calculations.

In contrast to the modeling of the geological and structural history, the thermal calculation is a forward process, taking the temperatures from the previous timestep into account. The upper boundary condition is the surface temperature, which in this

project is kept constant at 7 °C and the lower boundary condition is the basal heat flow in our calculations kept constant through time (44 $mW \cdot m^{-2}$ for Paper 1 and 47 $mW \cdot m^{-2}$ for Papers 2 and 3). This heat flow value is just above one heat flow unit (Allen and Allen, 2014) and is typical for some continental shelves, e.g. parts of the Norwegian continental shelf and is in agreement with values measured in Europen Archean cratons (Nyblade and Pollack, 1993; Pascal et al., 2010).

Classical first-order kinetics is utilized for the maturation and diagenesis calculations (cf. Fjeldskaar et al., 2008, 2017). For all maturation modeling in this project, kerogen type II is assumed, as it is the most common kerogen type in marine shales (Tissot and Welte, 1984). In order to fully investigate the effect igneous intrusions have on the hydrocarbon maturation, the whole basins are defined as source rocks. However, for a case study of a specific basin, only the actual source rock will be defined as such.

For the modeling of diagenesis, precipitation, which is temperature dependent, is the rate limiting factor for all processes (Walderhaug, 1994, 1996). The precipitation is proportional to the rate constant (k) given by the Arrhenius equation (1).

4.1.1 Basin Modelling Toolbox (BMT)

Basin Modelling Toolbox (BMT^{TM}; a trademark of Tectonor) is a high-resolution, temporal and spatial, 2D basin modeling software that reconstructs the structural and geological development and predicts the thermal and maturation evolution based on digitized seismic sections (Fig. 7). The software enables modeling of complex structural processes, including magmatic intrusions and the heat flow related to these features (Lander et al., 1994; Fjeldskaar et al., 2003, 2017). The thermal finite difference grid consists of minimum 400 x 400 cells, but the grid density and size depends on the complexity of the subsurface geometry. In terms of temporal resolution, the gap between every timestep depends on the digitized horizons. However, after emplacement of igneous intrusions, the timesteps are as small as 100 years.

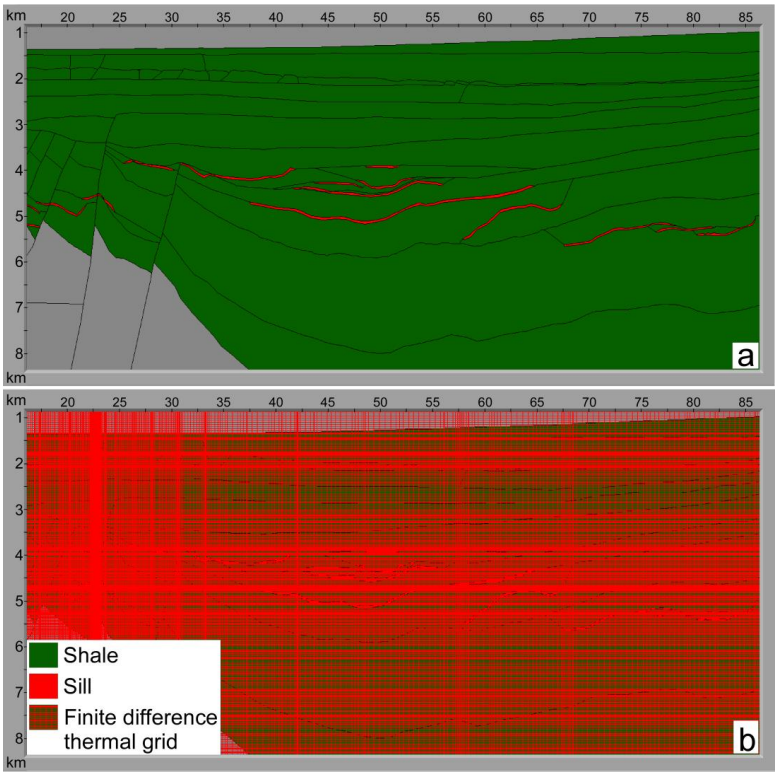

Figure 7: *The appearance of the work suite in BMT. a) Shale basin with magmatic sill intrusions. b) Same shale basin as in a) with the rectangular finite difference thermal gridding included. Please notice the extra fine gridding around smaller features, incorporated to ensure accurate calculations.*

4.1.2 Move

BMT solely restores faults by vertical shear. Fault restoration other than vertical shear, was done by the software Move (Petex Ltd) (www.petex.com/products/move-suite). Move is a structural modeling and analysis software with 2D and 3D kinematic modules that enables e.g. integrating and interpreting data, cross-section construction, kinematic restoration and validation, and geomechanical modeling. For this study, the 2D kinematic reverse modeling was used to perform antithetic and synthetic inclined shear fault restoration on a constructed 2D section in Paper 2 (Fig. 8). The porosity and decompaction calculations are based on exponential functions after Sclater and

Christie (1980) in both Move and BMT, and the same values are used in the two softwares.

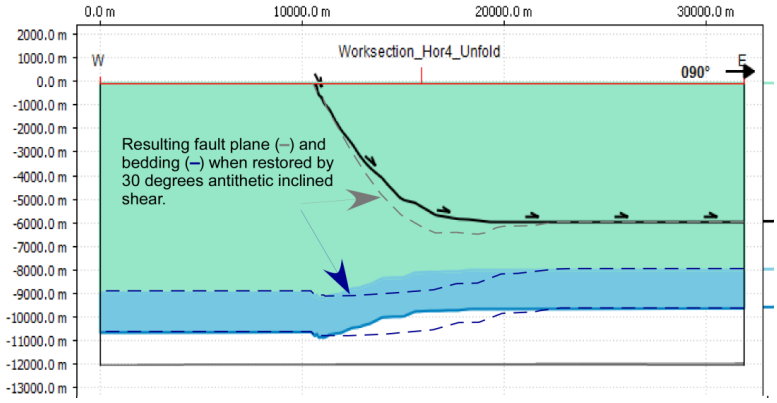

Figure 8: *The appearance of the work suite in Move and the resulting geometries of fault plane and bedding when section is restored by 10 degrees synthetic inclined shear (solid lines) and by 30 degrees anthitetic inclined shear (dashed lines).*

4.2 Stress modeling

Rocks at low temperatures and low pressures commonly behave as a linear elastic material up to 1-3% strain (Farmer, 1983; Paterson and Wong, 2005). Therefore, stress modeling of brittle rocks is commonly based on linear elasticity theory following Hooke's law (2) which states that the strain (ε) in a body is proportional to the applied stress (σ).

$$\sigma = E\varepsilon \qquad (2)$$

where E is Young's modulus. Since the unit for both σ and E is pascals (Pa), ε is unitless. Young's modulus is a measure of the stiffness of a material and its ability to withstand deformation when forces are applied (Gudmundsson, 2011b). Poisson's ratio (ν) is another unitless material constant in linear elasticity theory, and is the ratio of a materials lateral expansion/contraction in relation to the longitudinal contraction/expansion when forces are applied. For rocks, this ratio normally lies within the range 0.15-0.35, but usually it is 0.25 (Bell, 2000; Gudmundsson, 2011b).

Rocks exceeding 1-3% strain will experience irreversible deformation such as fracturing or faulting. Fracturing or faulting occurs when the tensile or shear strength of the rock is exceeded (Gudmundsson, 2011b). For most rocks the shear strength normally is in the range 1-12 MPa and the tensile strength is usually half of the shear strength, 0.5-6 MPa (Haimson and Rummel, 1982; Schultz, 1995; Amadei and Stephansson, 1997).

In this study, 2D modeling was performed for stress calculations in Paper 3. 2D modeling infers the third dimension to be infinite, which is a good approach as sills generally are much larger in the third dimension than the two others (e.g. Gudmundsson and Løtveit, 2012). Setting up the model involves defining the geometry and assigning elastic properties to the polygons. The polygons represent units of material with properties corresponding to the rock types under investigation. Before adding compressional or extensional loading to the model, the lower boundary is fastened to avoid rotation and translation of the rock body.

All polygons in the studied models in this project are given a Poisson's ratio of 0.25, and the assigned Young's modulus values are typical for the rocks they represent (Gudmundsson, 2011b). The models include; host rock (10 GPa), sills and basement (both 50 GPa), area modified by diagenesis (20 GPa), fault core and damage zone (0.1 GPa and 1 GPa respectively) and, fault core and damage zone altered by diagenesis (0.2 GPa and 2 GPa respectively). The densities for all rock units are assumed to be 2700 $kg \cdot m^{-3}$. Before running the models, 5 MPa extensional or compressional loading is applied to the sides of the model to replicate an extensional or compressional stress regime.

4.2.1 Comsol Multiphysics®

In order to investigate stress accumulations related to the sills and areas affected by diagenesis, we used the software Comsol Multiphysics® 5.2.a (www.comsol.com). Comsol Multiphysics® is a numerical simulation software for modeling of key processes within most fields of engineering and scientific research. It is a commercial finite element method (FEM) software that solves 2D and 3D problems based on

partial differential equations. The geometry under investigation is divided into finite, triangular, interacting volume (3D models) or surface (2D models) elements in a process named meshing. The element mesh density increases at boundaries between neighboring domains and particularly where geometries have pointed edges (Fig. 9).

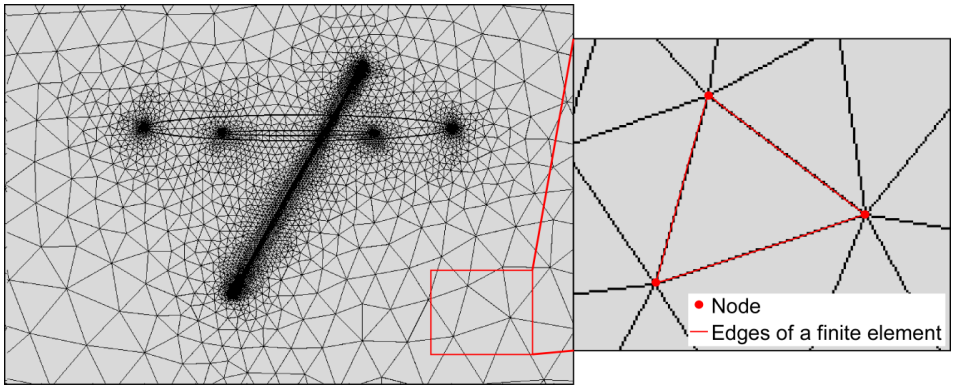

Figure 9: *Illustration of the domain of the model divided into triangular, interacting elements. Areas closest to for instance faults, sills and fractures consist of denser element mesh, and are particularly dense in the proximity of pointed edges/shapes.*

Every triangular element consists of three corners, referenced as nodes, and three edges (Fig. 9). The FEM method is based on the assumption that transfer of forces between element edges can be represented by the interaction of forces at the element nodes. This requires expressions for the forces acting at the nodes that manage to simulate the forces acting along the element boundaries. For assembling a solution for the whole geometry, numerical approximations of the differential equations for each element are then combined (Brady and Brown, 2005).

Chapter 5

Results and future work

5.1 Contribution and conclusions of this study

Schutter (2003) concluded that magmatic intrusions may potentially influence all parts of the petroleum system. The results from this study show that the increased temperatures caused by these features impact the source rocks and the transformation of organic material to hydrocarbons. They also impact the reservoir rocks by enhanced diagenesis and the potential migration by affecting location of stress accumulations.

5.1.1 Sensitivity of sill thickness on basin temperature and maturation

This study has quantified the effect of interpreting and modeling sills that are 0 m, 50 m and 100 m thick. The results document the large difference in the thermal effect and calculated potential of source rocks when sills are accounted for, or not, and also when they are modeled with variable thickness. For source rocks located between clusters of sills, the timing of emplacement can be essential for the hydrocarbon maturation. When the upper sills in a cluster intrude last, it has a positive effect on the area of hydrocarbon maturity.

The main results show that:

- Sill thickness has significant impact on the thermal effect of magmatic intrusions and ultimately the maturation of organic material in sedimentary basins. This is especially true for sills intruding at 3-5 km depth. The main

thermal effect of sills occurs the first 1 million years after emplacement, but thermal differences may last up to ~10 million years after intrusion.

- Modeling sills too thin may lead to underestimation of the petroleum potential of a basin, and overestimation if sills are modeled too thick.
- Considering the timing of emplacement may be necessary in order to estimate the range of possible maturation for source rock between sills. There is a boosted thermal effect of magmatic intrusions when the upper cluster of sills intrudes last.
- The high temperatures of magmatic intrusions impact the source rocks by maturing organic matter at depths that otherwise would be immature.

5.1.2 Effect of faulting on pre-intrusion basin temperature

The transient processes in structurally complex basins with magmatic intrusions have received little attention. This project has highlighted the significance of good representation of the structural development of basins, by quantifying the sensitivity of the most important factors for thermal development in basins with magmatic intrusions. It is particularly important to include transient thermal effects in such cases because the thermal effect of magmatic intrusions are shortlived compared to those caused by other geological processes, and because the pre-intrusion host rock temperature is vital to the ultimate thermal effect (e.g. Aarnes et al., 2010; Spacapan, et al., 2018).

This study shows:

- After fault slip, the sedimentary basin experiences transient thermal effects that may last several million years.
- The amount of fault displacement, time span of faulting and deposition, fault angle, thermal conductivity, specific heat capacity, basal heat flow and restoration method, impact the transient thermal effects of structurally complex basins. The thermal conductivity of the lithology is the most significant parameter that influences the pre-intrusion host rock temperature the most.

- Ignoring the transient thermal effects proceeding normal faulting may lead to under- or overestimation of the pre-intrusion host-rock temperatures and will have implications for the calculated effect of magmatic intrusions on hydrocarbon maturation. This is particularly important when assessing the effect of several sills intruded at multiple levels. The maximum pre-intrusion host-rock temperature sills can intrude into is a basin that has regained steady state after fault slip.

5.1.3 Effect of sills on diagenetic processes

Gudmundsson and Løtveit (2012) showed how sills can act as seals for hydrocarbon accumulations, as well as constitute fractured reservoirs themselves. They also demonstrated how sills may contribute to the formation of fractured reservoirs in stiff rocks at time of emplacement. But sills may also contribute to deterioration of reservoir properties through diagenesis. This study has quantified the porosity loss due to magmatic intrusions for the following diagenetic processes; opal A to opal CT to quartz, smectite to illite and quartz diagenesis. All processes are temperature dependent (e.g. Walderhaug, 1994, 1996; Roaldset and Wei, 1997a, b, 1998) and influenced by the emplacement of magmatic intrusions.

The main conclusions are:

- Conductive thermal effects of magmatic intrusions significantly impact the diagenesis in sedimentary basins. The depth of emplacement determines which diagenetic processes are affected.
- Sill thickness influences the size of the diagenetically altered area and the amount of porosity loss. This is particularly the case when sills are intruded as clusters at multiple levels.
- Diagenetic alterations caused by magmatic intrusions may lead to reduction in the reservoir quality as pores are clogged by precipitation of minerals.

5.1.4 Effect of sills on permeability

The sills and the area modified by diagenesis are commonly stiffer than their host rocks. Stiff rocks tend to concentrate stress in heterogeneous basins (Gudmundsson and Brenner, 2001; Gudmundsson et al., 2002; Gudmundsson, 2011b), possibly leading to opening of fractures and activation of fault slips. As open fractures and active faults increase the permeability (Gudmundsson, 2001), they may act as conduits for fluid flow and therefore influence the migration of hydrocarbons. If the initiated fault or fracture is in the sealing part of the hydrocarbon trap, magmatic intrusions may potentially influence the seal and trap for hydrocarbons and thus lead to leakage.

The main results show that:

- Sills and area altered by diagenesis influence accumulation of stresses in the subsurface. Stresses tend to build up in the sills and in the diagenetically altered area, making the area prone to opening of fractures, activation/reactivation of faults and contribute to increased permeability.
- For the petroleum system this implicates that the effect of magmatic intrusions may influence the permeability and migration pathways not just at time of emplacement, but also long term effects due to their stiffer nature compared to their host rocks.

5.2 Limitations to the modeling

In numerical modeling the quality of the input data defines the quality of the results. This project aims at general conclusions regarding the extended thermal effect of magmatic intrusions in sedimentary basins. The parameters used in this study are thus of typical global average and not site-specific values. This can lead to significant differences between the reported results compared to anticipated results using site-specific input parameters. For the temperature calculations this includes thermal conductivity, specific heat capacity, heat flow from the mantle and surface temperatures.

Thermal convection is not accounted for in this project, but several studies point out that significant convection occurred in Cenozoic time subsurface e.g. the Norwegian Sea (e.g. Svensen et al., 2003, 2004; Planke et al., 2005, Kjoberg et al., 2017). Such a heat transmission would definitely impact the cooling rate around magmatic intrusions (Iyer et al., 2013, 2017) and should be investigated in site-specific studies involving igneous intrusions. Latent heat of crystallization will add heat to the system when magmatic intrusions start to cool and minerals crystallize, as the crystallization process is an exothermic reaction. This additional heat is also not accounted for in the calculations here, and will have impact on the thermal effect, particularly of thick sills (Lander et al., 1994).

Defining the correct kerogen type is crucial for the outcome of the maturation calculations. This is related to the frequency factors and activation energies that are different for the various kerogen types (Tissot and Welte, 1984). The thermal impact of magmatic intrusions will influence all the kerogen types and the resulting maturation, however, the effect may differ. In this study kerogen type II is used, another kerogen type will give different maturation results than those presented in this project.

As maturation, diagenesis is also thermally dependent. The Arrhenius equation (1) gives the reaction rates as a function of the temperature, and the calculations in this study show areas where kinetic requirements are met for different diagenetic processes. However, for diagenesis to occur several other requirements related to lithology, chemical materials and the composition of circulating pore fluids must be fulfilled (e.g. Sachsenhofer et al., 1998; Essene and Peacor, 1995). In the modeling of diagenesis in this project it is assumed that these additional requirements are met. Furthermore, potential reactions in the subsurface, caused by catalysts and/or quenchers (which may retard or accelerate the reactions) (cf. Kastner et al., 1977; Huang et al., 1993; Bjørkum et al., 1998; Roaldset et al., 1998; Ireland et al., 2010) have not been considered. The diagenetic results of this study must therefore be interpreted with care, observing that the diagenesis effect may be overestimated.

In this project the modeling is based on sill intrusions in homogeneous basins. However, typical sedimentary basins are heterogeneous consisting of multiple layers of various stiffnesses. In volcanic sedimentary basins the sills themselves and the rocks modified by diagenesis will likely constitute the stiffest rocks (Gudmundsson, 2011b) and thereby accumulate the most stress when stress is applied (Gudmundsson and Brenner, 2001; Gudmundsson et al., 2002; Gudmundsson, 2011b). For site specific studies it is important to include regional and local stresses acting on the basin. Furthermore, the heterogeneity of the sedimentary basin should be accounted for, as it will influence stress accumulations and thereby areas prone to open fractures or activate/reactivate faults.

5.3 Further implications

The calculations of the thermal effects of magmatic intrusions performed in this study may be of interest beyond the petroleum industry and the geosciences research community. All subsurface kinetic processes may be influenced by the emplacement of magmatic intrusions. Production of coal is a function of pressure and heat (Hatch and Affolter, 2015), and increased temperatures due to magmatic intrusions may therefore possibly lead to coalification and altered coal quality at shallower depths than expected (e.g. Yao et al., 2011). Such intrusions may also accelerate the production of methane gas related from coal deposits (e.g. Jiang et al., 2011; Yao and Liu, 2012; Wang et al., 2014; Shi et al., 2018; Rahman et al., 2018; Chen et al., 2020). Geothermal fields are known to produce energy sourced by intrusions (e.g. Scott et al., 2015, 2018; Montanari et al., 2017). Calculations similar to those performed in this study may therefore be relevant for prediction of heat and possible duration of energy production from such a field.

It is also conceivable that these results may be of interest to the minig industry. Gold, silver and other profitable transition metals are found and produced from ores that are genetically related to intrusions, often hydrothermally deposited (e.g. Moorhouse, 1942; Sillitoe and Thompson, 1998; Parada and Stolyarov, 2012; Fayol et al., 2016; Guice, et al., 2017; Maier and Hanski, 2017; Eldursi et al., 2018). Diamonds and

other gemstones are reported to be present in some magmatic intrusions (e.g. Haggerty, 1999; Dill, 2018). Therefore, to locate magmatic intrusions and study their hydrothermal vents and effect on increased permeability through fracture opening and fault activation/reactivation, similar to what has been performed here, may contribute to exploration of essential metals and gemstones.

5.4 Future work

General conclusions have been the aim of this project. Therefore, a reasonable next step is to use the methodology applied in this thesis in site-specific studies. The magmatic intrusions in the Vøring Basin have been extensively studied from multiple angles (e.g. Mjelde et al, 1997 a, b; Planke et al., 2005; Fjeldskaar et al., 2008; Planke et al., 2017). However, a case study where all available data is combined in order to more specifically determine the thermal effect of the intrusions in a particular area is lacking. A good approach would be to start with the semi-regional ocean bottom seismograph (OBS) data model by Mjelde et al. (1997a) who estimated the sills to be considerably thicker than indicated by the regional procedure and anticipated in this study. These data, combined with conventional seismic reflection data (like those used as basis in this study), vitrinite reflectance and fluid inclusion data, would contribute to estimate the thermal effect of the magmatic intrusions in the Vøring Basin. Furthermore, a detailed interpretation of the structural elements can be implemented, and restoration of the structural development can be executed with several restoration methods, like the ones utilized in Paper 2. Modeling of the diagenetic effect of the igneous intrusions can be added along with a detailed stress modeling based on the regional and local stress fields. Possible permeability changes through time and migration opportunities may be predicted.

In East Greenland, an onshore sedimentary basin with sill intrusions has been studied by Eide et al. (2017a) (Fig. 3c). They have also attacked the “sub-sill imaging problem” (Eide et al., 2017b) by making synthetic seismograms of outcrop lidar data of igneous intrusions in a sedimentary basin. A comparative study of data from this East Greenland basin combined with the seismic reflection and OBS data from the

Vøring basin could be an approach to determine the sill thicknesses and amount of intruded material in this offshore Norwegian Sea basin.

This study has done a first approach in including diagenetic predictions in relation to magmatic intrusions, and the effect such transformations may have on stress accumulations. Magmatic intrusions and the associated increased heat flow will also have implications for other temperature dependent chemical processes occurring in the subsurface than those studied here. Increased porosity is observed in close proximity of magmatic intrusions due to diagenesis of carbonate rocks (Xu et al., 2015), and represents an example of a diagenetic process not studied here, and which can be pursued in the future.

Sills are known to intrude into or in proximity of salt sequences (Schofield et al., 2014). Salts have high thermal conductivity and therefore conduct heat better than other lithologies. This result in higher temperatures above such sequences compared to areas at the same depth without salt (e.g. Grunnaleite and Mosbron, 2019). These increased temperatures above salt structures may lead to more mature organic material at shallower depths than areas at corresponding depth without salt (Grunnaleite and Mosbron, 2019). If magmatic intrusions are emplaced in the vicinity of such structures, these unusual high temperatures may lead to even larger areas with matured organic material overlying these structures than modeled in this study. The extreme heat from magmatic intrusions may possibly also lead to salt movements (Schofield et al., 2014). Salt exerting pressure on the overburden may cause fracturing and potential fault slip, thereby influencing the permeability of the basin. This is an unexplored topic.

Where there are sills, there must be one or more dykes reasonably close by. Some basins are stacked with dykes, like the Farsund Basin located offshore southern Norwegian North Sea (Phillips et al., 2018). Generally, dykes are not visible on seismic data. Minakov et al. (2012) discovered that by combining magnetic and seismic data, dykes could be located. This suggests that by combining these data sets,

the heat contribution of dykes can also be incorporated into the thermal calculations, a topic that has received little attention and is yet to be examined.

Chapter 6

Summary of Papers 1-3

Paper 1: The importance of sill thickness and timing of sill emplacement on hydrocarbon maturation

Magnhild Sydnes, Willy Fjeldskaar, Ingrid Fjeldskaar Løtveit, Ivar Grunnaleite and Nestor Cardozo

From seismic sections it can be difficult to determine the thickness of magmatic intrusions due to insufficient seismic resolution, as well as timing of emplacement. The objective of Paper 1 is to investigate the influence of magmatic sill thickness and timing of emplacement on temperature and maturation of organic matter in sedimentary basins. A 2D seismic section from the Vøring Basin containing some 40 interpreted sills is utilized to study the effect of sill thickness on the thermal and maturation history. Results for sill thicknesses of 0 m, 50 m and 100 m are presented in the study. Furthermore, the sills in the study were divided into an upper and a lower cluster of sills and modeled to intrude with time intervals of 10 000 years and 100 000 years. Additionally, sills beyond seismic resolution and their effect on the surrounding host rocks were studied by performing a 1D modeling of well 7316/5-1 in the Barents Sea, containing 9 sills naturally divided in an upper and a lower cluster. Vitrinite reflectance data from this particular well permit the study of the effect of thin sills on temperature and maturation.

In order to investigate the geological, structural, thermal and maturation development of the studied section, BMT was used. The results show that sill thickness has significant influence on the thermal impact of magmatic intrusions and ultimately the hydrocarbon maturation. The largest thermal differences for scenarios of varying sill thickness are, as expected, closest to the sills, and the thicker the sills, the larger the thermal aureole and area of increased matured organic material. When comparing maturation levels for the tested sill thicknesses, results show up to 100% difference in matured organic matter in close proximity of sills and in particularly in areas between close-lying, neighboring sills. There is a positive thermal effect of sills intruding in one pulse as opposed to two pulses, at least for thinner sills. This is also observed for sills intruding in two pulses when the first pulse intrudes at deeper levels than the second pulse. For sills beyond seismic resolution the results show that thin sills within a cluster consisting of other thicker sills will not influence the maturation significantly. However, thin sills with no thicker sills in their immediate vicinity play an important role in the total maturation of organic material in their surroundings.

Paper 2: Transient thermal effects in sedimentary basins with normal faults and magmatic sill intrusions – A sensitivity study

Magnhild Sydnes, Willy Fjeldskaar, Ivar Grunnaleite, Ingrid Fjeldskaar Løtveit and Rolf Mjelde

The pre-intrusion host-rock temperature has been shown to play a significant role on the thermal effect of magmatic intrusions, and ultimately, their effect on maturation of organic material. This study quantifies the thermal effects of the most important factors affecting the thermal history in structurally complex sedimentary basins with magmatic sill intrusions. These factors are related to faulting, physical properties, and restoration method of the structural evolution of the basin, and are 1) fault displacement, 2) time span of faulting and deposition, 3) fault angle, 4) thermal conductivity, 5) basal heat flow, and 6) restoration method. All modeling examples were executed on the same constructed clastic profile and one parameter at a time

was changed. This method allows for keeping track of the magnitude and impact of the individual factors, while avoiding other factors obscuring the thermal calculations. BMT was utilized to reconstruct the geohistory, as well as the structural development and the thermal and maturation calculations. The software Move was used to restore the structural evolution with 10º, 20º and 30º antithetic inclined shear and 10º synthetic inclined shear. As BMT solely performs fault restoration through vertical shear, and Move does not perform thermal and maturation calculations, the resulting reconstruction from Move was replicated in BMT through a function called "volume editing", enabling thermal calculations of the resulting basin geometries from different restoration methods.

All the tested parameters show, to various degrees, transient thermal effects that will impact the estimation of pre-intrusion host rock temperatures of basins with intruding magmatic sills. Thermal conductivity is the factor that the most influences the basins transient thermal history and steady state is obtained 3-22 million years after fault slip has occurred. The other tested factors obtain steady state within a smaller timespan. Thermal differences up to 40 °C can occur for sills intruding at time of fault slip compared to sills intruding 10 million years later. This 40 °C temperature difference in host rock temperature may have significant impact on the calculated thermal effect of magmatic intrusions and thereby also on the maturation calculations. For sills intruding as clusters and not as individual sills, this pre-intrusion temperature difference will have an even larger impact on the maturation estimations.

Paper 3: The influence of magmatic intrusions on diagenetic processes and stress accumulation

Magnhild Sydnes, Willy Fjeldskaar, Ivar Grunnaleite, Ingrid Fjeldskaar Løtveit and Rolf Mjelde

Chemical compaction, known as diagenesis, is dependent on the temperature in the subsurface. Emplacement of magmatic intrusions provides abrupt thermal changes in

their proximity, which has been clearly presented in Papers 1 and 2. The objective of Paper 3 is to study magmatic intrusions effect on the diagenetic processes in their vicinity and furthermore, the effect they have on stress accumulations in the subsurface.

A section from the Vøring Basin has been utilized in this study to ensure realistic proportions and structures of basins with magmatic intrusions. BMT has been used to perform the geological, structural, thermal, maturation and the diagenetic modeling. The influence of magmatic intrusions on three diagenetic processes has been quantified; opal A to opal CT to quartz, smectite to illite, and quartz diagenesis. The results clearly show enhanced porosity loss due to magmatic intrusions in comparison to areas not intruded. Particularly areas between clusters of sills are prone to intensified diagenesis. However, the effect of sills is dependent on depth of emplacement. This is because maximum diagenetic alterations occur at different temperatures for different processes, making depth of emplacement a crucial factor for sill influence. For diagenetic processes to occur, several other conditions must be met. BMT includes the thermal calculations and the possible porosity loss caused by diagenesis. However, it does not take into account the biogenic and chemical material present, and circulating pore fluids, which ultimately determine the possible diagenetic processes.

During diagenesis, the physical properties of rocks are altered making the diagenetically transformed areas prone to respond differently to stresses. The sills themselves are typically stiffer than their host rocks in sedimentary basins. These features will concentrate stresses, as stiffer rocks tend to concentrate stress in heterogeous basins. The results show that areas altered by diagenesis and the sills themselves, concentrate stresses, which may lead to opening of fractures where tensile stresses concentrate, and initiation or reactivation of fault movement where shear stresses concentrate. This may contribute to increased permeability and influence the hydrocarbon migration, as faults and fractures may act as conduits for fluid flow.

Part II

Papers

1

Paper 1: The importance of sill thickness and timing of sill emplacement on hydrocarbon maturation

Magnhild Sydnes, Willy Fjeldskaar, Ingrid Fjeldskaar Løtveit, Ivar Grunnaleite, Nestor Cardozo

Published in Marine and Petroleum Geology, 89, 500-514

Marine and Petroleum Geology 89 (2018) 500–514

Contents lists available at ScienceDirect

Marine and Petroleum Geology

journal homepage: www.elsevier.com/locate/marpetgeo

Research paper

The importance of sill thickness and timing of sill emplacement on hydrocarbon maturation

Magnhild Sydnes[a,b,*], Willy Fjeldskaar[a], Ingrid Fjeldskaar Løtveit[a], Ivar Grunnaleite[a], Nestor Cardozo[b]

[a] Tectonor AS, P.O. Box 8034, NO-4068, Stavanger, Norway
[b] Department of Petroleum Engineering, University of Stavanger, P.O. Box 8600 Forus, NO-4036, Stavanger, Norway

ARTICLE INFO

Keywords:
Volcanic basins
Sills
Sill thickness
Timing of sill emplacement
Basin modeling
Temperature history
Hydrocarbon maturation

ABSTRACT

Magmatic sills in sedimentary basins can be relatively easy to interpret on seismic data because they stand out due to their high acoustic impedance in relation to the sediments. However, determining sill thickness is challenging unless the sills are drilled. This study explores the influence of magmatic sill thickness and timing of emplacement on temperature and hydrocarbon maturation in sedimentary basins. A 230 km long 2D transect through the Vøring Basin in the Norwegian Sea is modeled and sill thickness and timing of emplacement are the only parameters varied. The transect holds ~40 sills that intruded at ~55 Ma with a temperature of 1000 °C in a shale-dominated sequence. Several sill thickness scenarios were tested, but results for 0 m (no sills), 50 m and 100 m are presented here. Furthermore, the 50 m and 100 m thick sills were tested to intrude as upper and lower clusters separated by time intervals of 10 and 100 kyr. To study the effect of sills below seismic resolution, 1D modeling of well 7316/5-1 in the Barents Sea was performed. This well contains 9 sills distributed in an upper and a lower group. Vitrinite reflectance data from the well allow studying the effect of thin sills on temperature and maturation. The results show a clear connection between sill thickness and the temperature and maturation history of the basin. The largest impact of sill intrusions is at 3–5 km depth. For sills intruding as clusters, there are regionally marginal differences related to timing of emplacement but local differences especially in the close vicinity of the sills occur. This work indicates that the interpretation of sill thickness has a substantial influence on the prediction of the maturation and petroleum potential of sedimentary basins holding magmatic intrusions. Sills below seismic resolution contribute to increased maturation in its surroundings. Differences in the timing of sill emplacement within 10–100 kyr show local effects that may influence the petroleum potential of source rocks between two sill complexes.

1. Introduction

Oil and gas reserves in volcanic provinces are found on all continents and many future petroleum exploration areas will be located in volcanic margins (Caineng et al., 2012; Senger et al., 2017). Magmatic sills in sedimentary basins commonly stand out on seismic images due to their high acoustic impedance (AI) resulting in high amplitude reflections compared to the surrounding sediments (Smallwood and Maresh, 2002). However, determining the boundaries, top and base, of magmatic sills from seismic is not straightforward, unless the intrusions are drilled. How well a layer is detected and separated on seismic depends on its thickness, AI contrast (Hart, 2000), and the seismic wavelet frequency (Osagiede et al., 2014; Magee et al., 2015). The higher the wave frequency the thinner the sills that can be detected and resolved (Brown, 2004; Osagiede et al., 2014; Magee et al., 2015; Schofield et al., 2015). For a typical wave frequency of 30 Hz at 2–3 km depth, the minimum sill thickness that can be clearly interpreted is ~50 m. Heterogeneous host rocks may modify the seismic expression of the sill and create seismic artifacts (Magee et al., 2015).

In outcrops, magmatic sills show thicknesses ranging from a few meters (Burchardt, 2008; Polteau et al., 2008; Galerne et al., 2011; Senger et al., 2014; Button and Cawthorn, 2015; Schofield et al., 2015) to several hundred meters (Chevallier and Woodford, 1999; Polyansky and Reverdatto, 2006; Galerne et al., 2010, 2011; Aarnes et al., 2011; Hansen et al., 2011). Seismically interpreted sill thicknesses are normally within a few tens of meters to a few hundred meters (Hansen and Cartwright, 2006; Cukur et al., 2010; Gudmundsson and Løtveit, 2012; Wang et al., 2012; Inam et al., 2014).

Seismic provides little or no information on the timing of sill emplacement. Dating of magmatic intrusions exists in some areas, and the

* Corresponding author. Tectonor AS, P.O. Box 8034, NO-4068, Stavanger, Norway.
E-mail address: magnhild.sydnes@tectonor.com (M. Sydnes).

http://dx.doi.org/10.1016/j.marpetgeo.2017.10.017
Received 20 March 2017; Received in revised form 10 October 2017; Accepted 18 October 2017
Available online 21 October 2017
0264-8172/

tectonic evolution of the basin may also indicate possible ages of emplacement, but these approaches have high uncertainty. Gleadow and Brooks (1979) estimated an average uncertainty of 1–3 Myr in sill emplacement ages based on fission track dating of sphenes, zircons and apatites. Other studies report similar uncertainties for the dating of magmatic intrusions (Trude et al., 2003; Quinn et al., 2005; Svensen et al., 2010, 2012; Zhong et al., 2011). Outcrop studies of volcanic basins such as central East-Greenland and the Karoo Basin, South Africa, indicate that clusters of sills consisting of many levels of intrusions possibly were emplaced simultaneously (Planke et al., 2005; Svensen et al., 2012). A study of intrusions in the Guaymas Basin, Gulf of California (Einsele, 1982), suggests that sill clusters were emplaced in pulses separated by 10–100 kyr, which fits well with the 10–20 kyr interval for basalt interruptions in the Mid-Atlantic Ridge (Moore et al., 1974). Works by Svensen et al. (2010, 2012) in the Vøring and Karoo basins suggest even longer time intervals.

Several studies have shown and acknowledged that magmatic intrusions affect the temperature history and hydrocarbon maturation of sedimentary basins (Galushkin, 1997; Othman et al., 2001; Aarnes et al., 2010, 2011; Wang, 2012; Wang et al., 2013; Peace et al., 2017; Schofield et al., 2017). Fjeldskaar et al. (2008) studied the impact of sills on temperature, vitrinite reflectance, and transformation ratio in the Vøring Basin and Gjallar Ridge area, Norwegian Sea. Their results show that the temperature in the vicinity of the sills increases drastically just after the emplacement and diminishes with time, increasing the transformation ratio in the sediments. In the same region, Aarnes et al. (2015) found that gas generation in the host rock due to sill intrusions can be significant, despite relatively poor total organic content (TOC) in the source rocks.

These examples show that magmatic intrusions influence the basin temperature and maturation, but how sensitive the petroleum potential of basins is to sill thickness and timing of emplacement has received little attention. The aim of the present study is to analyze the impact of these factors on the temperature and hydrocarbon maturation of sedimentary basins. This is done by modeling of a 2D geological section across the Vøring Basin in the Norwegian Sea and 1D modeling of well 7316/5-1 in the Barents Sea. Different modeling scenarios reflecting uncertainties in sill thickness and timing of emplacement have been tested. The modeled well and geological section represent specific locations, but the paper aims at conclusions applicable to volcanic basins in general. The results show that uncertainties in sill thickness and timing of sill emplacement influence the prediction of temperature and maturation history, i.e. the evaluation of petroleum potential of the basin.

2. Geological setting

The Vøring Basin lies offshore mid-Norway (Fig. 1), and is known for its numerous magmatic intrusions. This region is bounded by the Bivrost Lineament to the NE and the Vøring Transform Margin to the SW (Fig. 1). During the onset of the opening of the North Atlantic from Late Cretaceous to Early Eocene, the area experienced extensive magmatic activity (Saunders et al., 1997; Eldholm et al., 2000; Torsvik et al., 2001; Meyer et al., 2007; Hansen et al., 2009; Ganerød et al., 2010). This study uses the depth-converted and interpreted seismic profile by Fjeldskaar et al. (2008), which crosses the Vøring Basin from SE to NW, from the Dønna Terrace to the volcanic Vøring Marginal High (Fig. 1).

Three main rifting episodes are identified in this area, which generated grabens, basins and structural highs. The first occurred in the Carboniferous-Permian and coincided with the onset of rifting in the North Atlantic (Bukovics et al., 1984; Gabrielsen et al., 1984; Price and Rattey, 1984; Surlyk et al., 1984; Brekke and Riis, 1987; Blystad et al., 1995; Doré and Lundin, 1996). The next took place in the Late-Mid Jurassic to Early Cretaceous and led to subsidence and development of accommodation space for the thick Cretaceous sedimentary sequence consisting mainly of shales (Swiecicki et al., 1998; Scheck-Wenderoth et al., 2007). The third and last episode occurred from Late Cretaceous to Early Eocene and coincided with the opening of the North Atlantic, development of the Vøring Marginal High, and intrusion of numerous sills in the Cretaceous basin fill (Mjelde et al., 1997; Brekke, 2000). Abdelmalak et al. (2016) describe four tectono-volcanic stages of the magmatism of the Vøring Margin. The first stage of basaltic andesitic flows was emplaced into subaqueous sediments as dykes and sills, followed by subaerial dacitic flows in stage two. Finally, ocean-breakup and emplacement of volcanic flows over the Vøring Marginal High in stages three and four.

The stratigraphic column of the area consists mainly of marine to deep marine deposits (mainly shale) with intercalations of shallow marine sediments (mainly sandstone) in the Upper Jurassic and Cretaceous (Fig. 2). The Paleocene consists of chalk deposits in some areas, and the Lower Eocene has volcanic intrusions within the shales. Oligocene, Neogene and Quaternary deposits are mainly shales with some ice rafted debris in the Plio-Pleistocene (Fig. 2). The studied 2D transect is 230 km long and holds ~40 interpreted sills located at 2.5–7 km depth with lateral extension of the sills varying from 3 to 40 km (Fig. 3). The time of intrusion is ~55 Ma, which is supported by ages derived from zircon dating of magmatic sills in the Vøring area (55.6 ± 0.3 Ma and 56.3 ± 0.4 Ma, 6607/5-2 and Utgard wells; Svensen et al., 2010).

3. Methodology and model set up

The software BMT (Basin Modelling Toolbox, Tectonor AS) was used to model the geological, structural, thermal and maturation history of the studied profile and well. BMT is a high-resolution system with the ability to model complex tectonic processes such as igneous intrusions and their related heat flow (Lander et al., 1994; Fjeldskaar, 2003).

The starting point is the present day geometry obtained by the interpreted and depth converted 2D seismic section (Fig. 3a–b) after Fjeldskaar et al. (2008). All digitized layers in the section are assigned a lithology with regard to porosity/depth trend, thermal conductivity and specific heat capacity (Table 1).

For every timestep, one by one layer is removed and the underlying sequences are decompacted (Fig. 3c), a process that is based on the defined porosity/depth trend for each assigned lithology. The porosity/depth trends are exponential functions as described by Sclater and Christie (1980). Furthermore, folds and faults are restored using vertical shear, which is a reasonable model for extensional settings (Gibbs, 1983). Vertical shear keeps track of the rock mass, which is fundamental for the temperature and maturation modeling, and it simplifies and accelerates the calculation of compaction (Fjeldskaar, 2003). If magmatic intrusions are present at a specific timestep, these polygons are assigned magmatic intrusion lithology with related physical properties acting from the time of emplacement. Palaeo-water depths are not included. Eroded material is added to the western part of the section at timesteps 74 Ma and 66 Ma, since unconformities interpreted on the profile imply that the sedimentary sequence was eroded at these stages. The impact of erosion on the resulting temperatures and maturation in the basin is only local and limited to the eroded area and does not influence the larger area of interest here.

When the geohistory for the whole section has been modeled, the basin thermal development is calculated using a transient finite difference model (see Fjeldskaar et al., 2008; Fjeldskaar et al., 2017 for further details). The finite difference grid consists of minimum 400 × 400 cells of varying sizes with an average size of 576 m × 25 m (width and height). The grid size however, depends on the complexity

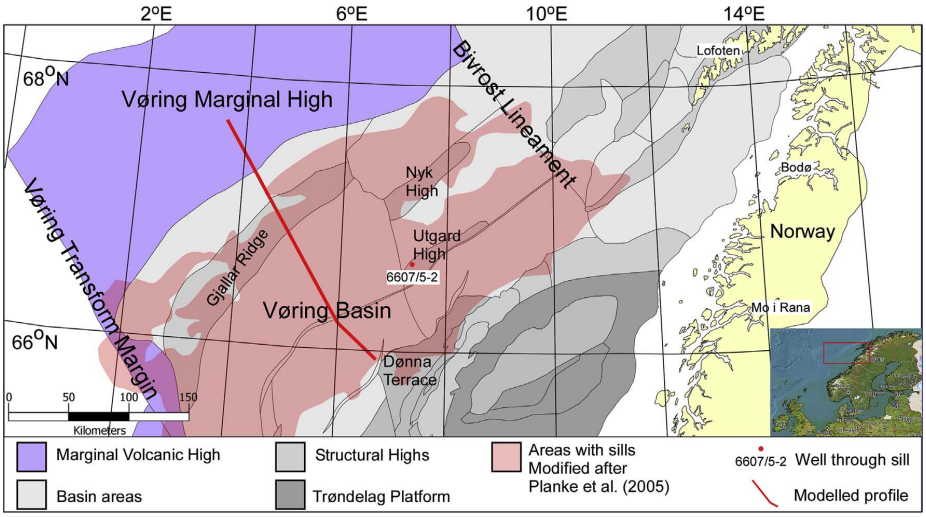

Fig. 1. Location of the modeled 2D transect extending SE-NW across the Vøring Basin in the Norwegian Sea, offshore mid-Norway (red line). Map base is from the Norwegian Petroleum Directorate Map Server. (For interpretation of the references to color in this figure legend, the reader is referred to the web version of this article.)

of structures, and around magmatic sills it is especially small to ensure good temperature calculations. Fjeldskaar et al. (2008) modeled the temperature effect of sill emplacement with the numerical BMT model versus an analytical model, and demonstrated that the numerical code works well for high-resolution modeling, both spatially and temporally.

The temperature history is calculated by conduction and controlled by the thermal conductivity and specific heat capacity of the lithological units in the basin. The palaeo-temperature regime of the sediments is a result of the heat flow from the base of the lithosphere (lower boundary condition) and the sediment-water temperature (upper boundary condition). As the lower boundary condition we assume constant heat flow of 44 mWm^{-2} over time and palaeo-surface temperature is set to 7 °C (upper boundary condition). This is done to keep the model as general as possible. Convection is not included in the model. The temperature regime in the host rock before sill intrusions are calculated, and at time of intrusion the sills heat supply is included in the thermal calculations. To obtain a correct maturation history it is crucial that the sill intrusions are modeled with a realistic temperature history of the basin also before the emplacement. If the background temperature history of the basin has errors so will the modeled maturation history. Intrusion temperature is set to 1000 °C, which is within the normal magma temperature range (Gudmundsson and Løtveit, 2012). No latent crystallization heat is considered.

Temperature is the most important factor influencing the maturation of source rocks (Tissot et al., 1987). Thus, temperature modeling is the foundation for maturation modeling and the resulting conversion of kerogen to hydrocarbons. Different kerogen types respond dissimilarly to thermal influence, and the kerogen type is therefore an important parameter to specify for the source rock. In our study the whole sedimentary sequence is modeled as source rock with kerogen type II, which is commonly the case for marine shales (Tissot and Welte, 1984). The kerogen maturation model in BMT is based on classical first-order kinetics applicable to decomposition reactions (see Fjeldskaar et al., 2008; Fjeldskaar et al., 2017 for further details).

Based on field observations, sill thickness is likely to be within a few meters to a few hundred meters (Aarnes et al., 2011; Gudmundsson and Løtveit, 2012). The aspect ratio, i.e. the relation between the lateral dimension of a sill and its maximum thickness, is generally in the 150–500 range (Hansen et al., 2011; Gudmundsson and Løtveit, 2012). The lateral dimension in this study is in the 3–40 km range giving a thickness range of ~ 6–270 m. Fjeldskaar et al. (2008) used a sill thickness of 50 m in this area, but data from well 6607/5-2 (Fig. 1) shows that sills up to 100 m thick exist. Results from three sill thicknesses are presented here: 0 m (no sills), 50 m and 100 m all intruding simultaneously at 55 Ma. These thicknesses are within the range of what usually can be separated on seismic (Fig. 4) and would normally be accounted for in temperature modeling. Fig. 3b shows the depth-converted seismic section with the present basin geometry and 100 m thick sills.

In the next set of simulations, the impact of timing of sill emplacement was tested. The sills in the profile were divided in two clusters that intrude at different depths during two pulses. There are several possible scenarios for sill clusters along this profile, but a random distribution was selected based on what seems realistic in relation to the location of faults, as outcrop observations show that faults can be conduits for magma transport (Planke et al., 2005). The sills are grouped into lower sills (turquoise, Fig. 3c), and upper sills (black, Fig. 3c) and three scenarios were modeled: 1) all sills intrude at 55 Ma; 2) the upper sills are emplaced before the lower sills; and 3) the lower sills are emplaced before the upper sills. Scenarios 2 and 3 were tested for two intrusion intervals: 10 kyr apart (at 55 and 54.99 Ma) and 100 kyr apart (at 55 and 54.90 Ma) since these time intervals are within the normal intrusion interval range indicated by other studies (Einsele, 1982; Aarnes et al., 2015).

The modeling described above, concentrate on clusters of sills that are thick enough to be detected on seimic. However, as pointed out, sills may escape detection on seismic but will still contribute to the maturation and induce changes in the vitrinite reflectance, a commonly used indicator for thermal maturity of source rocks. Thus, by studying vitrinite reflectance, sills that are undetectable on seismic may be discovered. Well 7316/5-1 in the Barents Sea gives a unique opportunity to study the effect of sills that are below seismic resolution. This well is situated in the western Barents Sea on the Vestbakken Volcanic Province and holds 9 sills varying in thickness from about 5 to 50 m.

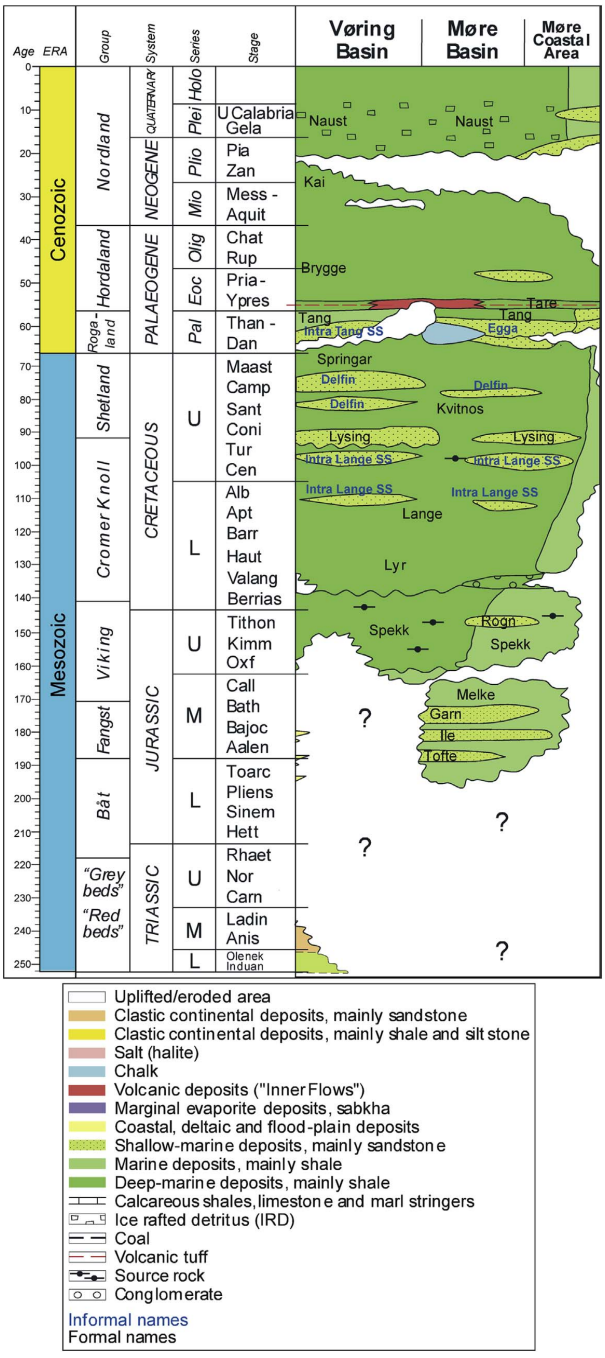

Fig. 2. Lithostratigraphic chart over the Vøring and Møre basins.

Four sills are located at ~2.9–3.1 km and five sills at ~3.6–4.0 km depth, leaving ~500 m of sediments between the two sill clusters. The intrusion of sills in two levels creates a natural division of an upper and a lower group. Vitrinite reflectance data from the well demonstrate when the sills influence the maturation to a significant degree and when they do not. Different intrusion time intervals were tested and various sills were selectively excluded from the calculations to study their influence on the maturation.

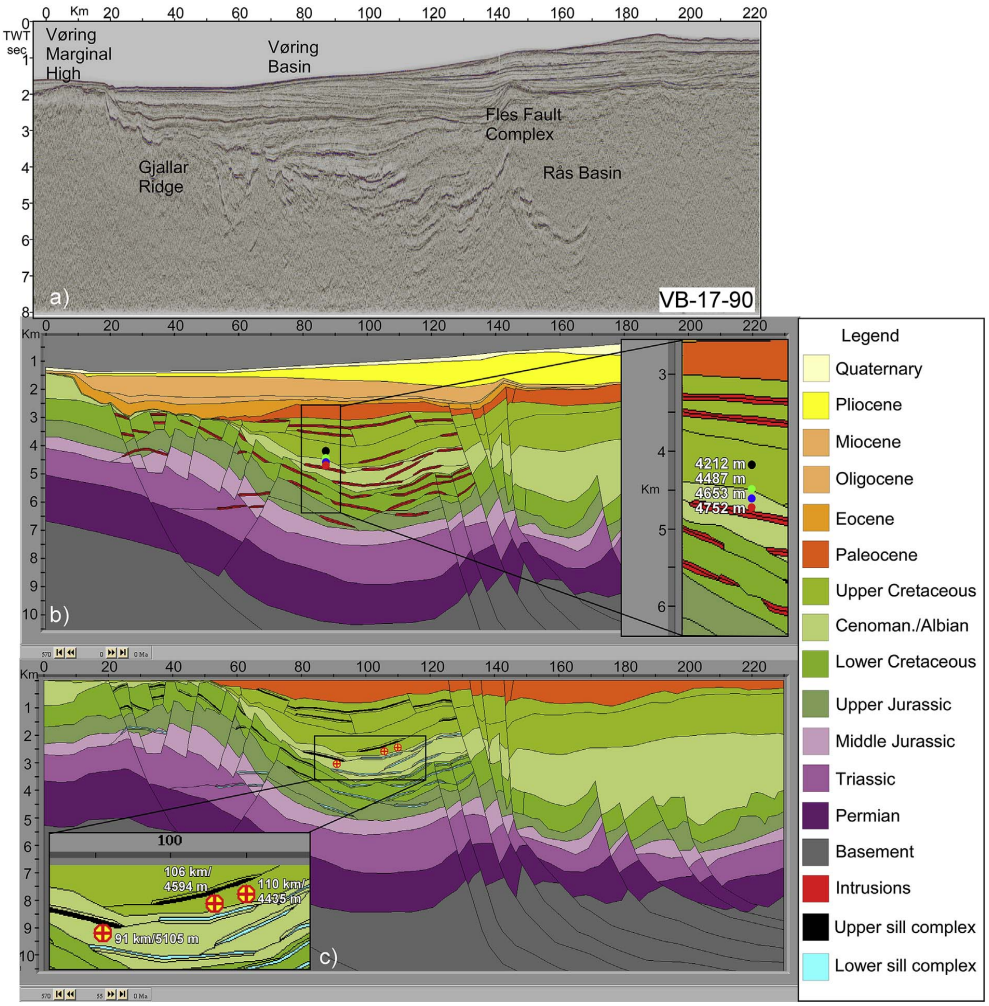

Fig. 3. a) Seismic section VB-17-90 in two-way travel time. b) 2D section showing the present day situation based on interpreted and depth-converted seismic section with 100 m thick sills. c) Restored 2D section at the time of sill intrusion (55 Ma) with 50 m thick sills. Points in Fig. 3b are used in Figs. 6 and 7, points in Fig. 3c are used in Figs. 11 and 12.

Table 1
Lithological parameter values used in the modeling.

Time units	Lithology	Age Ma	Porosity-depth trend		Conductivity (kv) ($Wm^{-1}\ K^{-1}$)		Heat capacity ($Jkg^{-1}\ K^{-1}$)
			Surface Porosity	Exponential constant (km^{-1})	Low porosity	High porosity	
Quaternary	Shale	0–3	0.63	0.51	2.35	1.50	1190
Pliocene	Shale	3–5	0.63	0.51	2.35	1.50	1190
Oligocene	Shale	5–34	0.63	0.51	2.35	1.50	1190
Eocene	Shale	34–56	0.63	0.51	2.35	1.50	1190
Paleocene	Shale	56–66	0.63	0.51	2.35	1.50	1190
Cretaceous	Shale	66–145	0.63	0.51	2.35	1.50	1190
Jurassic	Shale	145–201	0.63	0.51	2.35	1.50	1190
Triassic	Shale	201–252	0.63	0.51	2.35	1.50	1190
Permian	Shale	252–298	0.63	0.51	2.35	1.50	1190
Basement	Metamorphic		0.04	0.05	3.1	3.1	1100
Sills	Intrusion	55	0.04	0.05	3.1	3.1	1100
Asthenosphere					3.5	3.5	1100

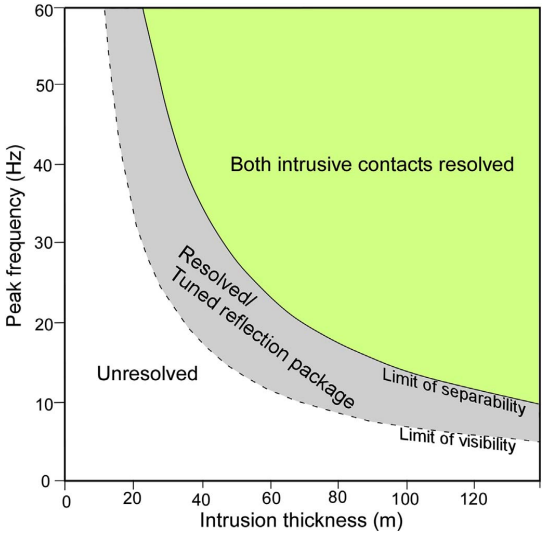

Fig. 4. Relationship between peak frequency and intrusion thickness, and their values needed to identify top and bottom boundaries of sills on seismic. Modified after Osagiede et al. (2014) and Magee et al. (2015). Limit of separability is assumed to be the vertical seismic resolution, it refers to the combination of peak frequency and intrusion thickness where sills top and base can be distinguished. Limit of visibility refers to the minimum combination of peak frequency and intrusion thickness when reflections on seismic confidently can be identified as a sill.

3.1. Limitations to the modeling

Several factors important in the modeling of a real, heterogeneous basin are not considered in this study. These include convection, latent heat of crystallization and variable sill thickness in the lateral dimension.

Convection and thereby any heat advection by fluids is not accounted for in the modeling. Several studies regarding hydrothermal vents in the Vøring area (Svensen et al., 2003, 2004; Planke et al., 2005; Kjoberg et al., 2017) indicate transmission of heat from deeper areas. Therefore the cooling rate in this study may be a minimum estimate.

Permeability is one key factor controlling the intensity and pattern of fluid flow in sedimentary rocks. A basin consisting mainly of shales is normally considered having low permeability. But still in low permeable rocks with intruded sills, fluid flow occurs (Schofield et al., 2010) and influence the thermal evolution (Iyer et al., 2013). Hot fluids at the lower and upper margins of the sill will rise slowly from both tips of the sill, resulting in enhanced maturation in these areas (Iyer et al., 2013, 2017). This also contributes to heat advection from areas where sills are emplaced and thereby faster cooling of the host rock. However, according to Podladchikov and Wickham (1994) conductive heat transfer is a good approximation for magmas containing 10% water or less.

Neglecting latent heat of crystallization is a reasonable assumption for shales where the contents of organic material are only a small fraction of the total rock mass (Aarnes et al., 2015). Some studies incorporate latent crystallization heat by including additional heat at the time sills are allowed to cool (Peace et al., 2017). Here, however, the focus is on the relative difference between the resulting effects of various scenarios of sill thickness and timing of intrusion. Including additional heat from latent heat of crystallization will result in higher peak temperatures, transformation ratios and larger areas affected by the intrusions, but the relative differences between the compared scenarios will remain the same.

In this study, the sills are assumed approximately the same thickness from one lateral end to the other which is often not the case. Modeling the sills with varying thicknesses is more realistic. However, constant lateral sill thickness is a reasonable assumption for comparing the effects of different sill thicknesses.

4. Results

4.1. The effect of sill thickness

In sedimentary basins, temperature generally increases gradually with burial depth (e.g. Fig. 5a) and is related to the geothermal gradient in the area, which is a function of the heat flow and thermal conductivity of the present sediments. Emplacement of magmatic sills delivers additional heat into the basin and disrupts this general temperature distribution. After sill emplacement, the thermal effect is initially located in the immediate vicinity of the sills (Fig. 5b–c), but with time, the heat is dissipated and will affect a larger area around the sills.

There is a clear correlation between the sill thickness and the temperature increase. Thick sills (100 m) result in higher temperatures and larger affected areas than thin sills (50 m) (Fig. 5b–c). This can be illustrated by using four points of increasing depth and decreasing distance to a sill in the central part of the basin (black to red points, Fig. 3b). At these points the peak temperatures drop sharply and continue to decline slowly the first Myr after sill intrusion (Figs. 6 and 7). Around 10 Myr later, all three scenarios show the same temperatures (Fig. 7). From ~40 Ma to the present, the model with 100 m thick sills results in a slightly colder basin temperature than the scenario without sills (Fig. 6). This is related to the higher thermal conductivity of sills in comparison to the sediments.

Maturation of organic material is closely associated with the temperature evolution in the basin. For basins without magmatic sills, the maturation is mainly determined by the geothermal gradient and the transformation ratio increases gradually with depth as the temperatures increases (Fig. 8a). Although the effect of sills may not be detectable in the present-day temperatures (Figs. 6 and 7), it is reflected in the present-day maturation of hydrocarbons (Figs. 6 and 8). Basins holding magmatic sills show area of increased transformation ratios similar to the pattern of increased temperatures around the sills. The area of increased present-day maturation is larger in the model with 100 m thick sills than in the model with 50 m thick sills (Fig. 8b–c).

When the basin maturity with and without 100 m thick sills is compared, it is clear that large parts at 3–5 km depth are much more mature in the first case. In some areas, the difference in maturation is up to 100%, but in general it is between 10 and 50% (Fig. 9a). The trend is the same, but less pronounced when the sill thickness is reduced to 50 m. Maturation differences between the 50 and 100 m thick sills scenarios are around 10–20%. Closer to the sills this difference can be up to 40–60%, and in some smaller areas it can reach 100% (Fig. 9b).

4.2. The effect of timing of sill emplacement

Modeling results of the 2D section show that simultaneous intrusion of several sills impacts the maturation in much the same way as successive intrusion of the same number of sills. This is illustrated in Fig. 10 for 50 m thick sills intruding with a time lapse in both the lower and upper clusters. Similar results were observed for the 100 m thick sills (not presented here). For all intrusion scenarios, the timing of sill emplacement does not influence the maturation of shallow sediments (< 2–3 km). Such sediments were either not present at time of intrusion, or the thermal effects were not significant enough to influence the maturation, which is currently ongoing at these depths. Deep sediments (> 5 km) show high levels of matured organic material. Although sill emplacement increases the temperatures, the thermal impact has conceivable an insignificant influence on the maturation process as these

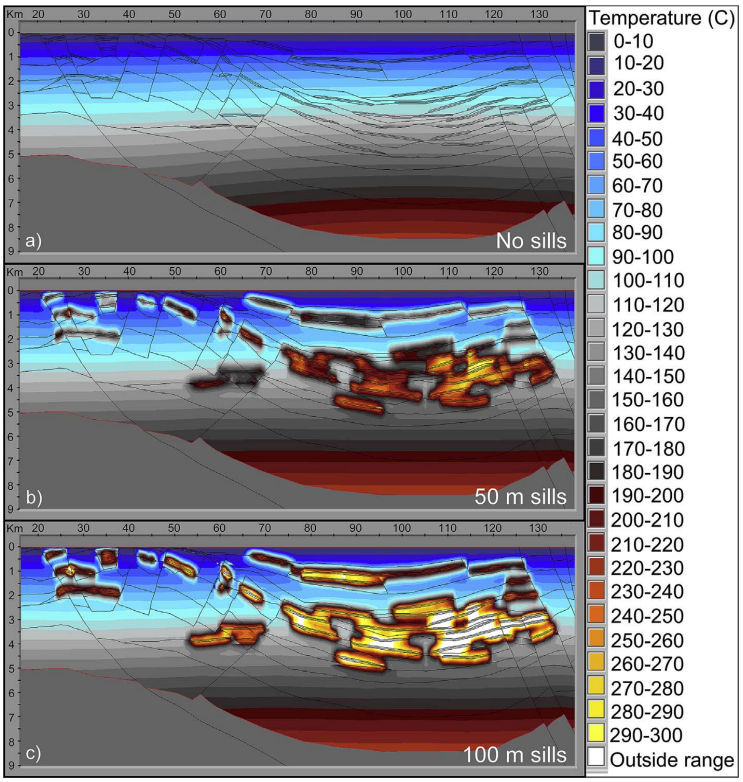

Fig. 5. Calculated temperature at 1 kyr years after intrusion (54.999 Ma) showing a) scenario 1, no sills; b) scenario 2, 50 m thick sills; and c) scenario 3, 100 m thick sills. For scenario 1, temperature increases gradually with depth. For scenarios 2 and 3, abrupt, large temperature increase in the vicinity of emplaced sills is evident. Intrusion temperature is 1000 °C. The areas of high temperatures are marked in yellow to red. (For interpretation of the references to color in this figure legend, the reader is referred to the web version of this article.)

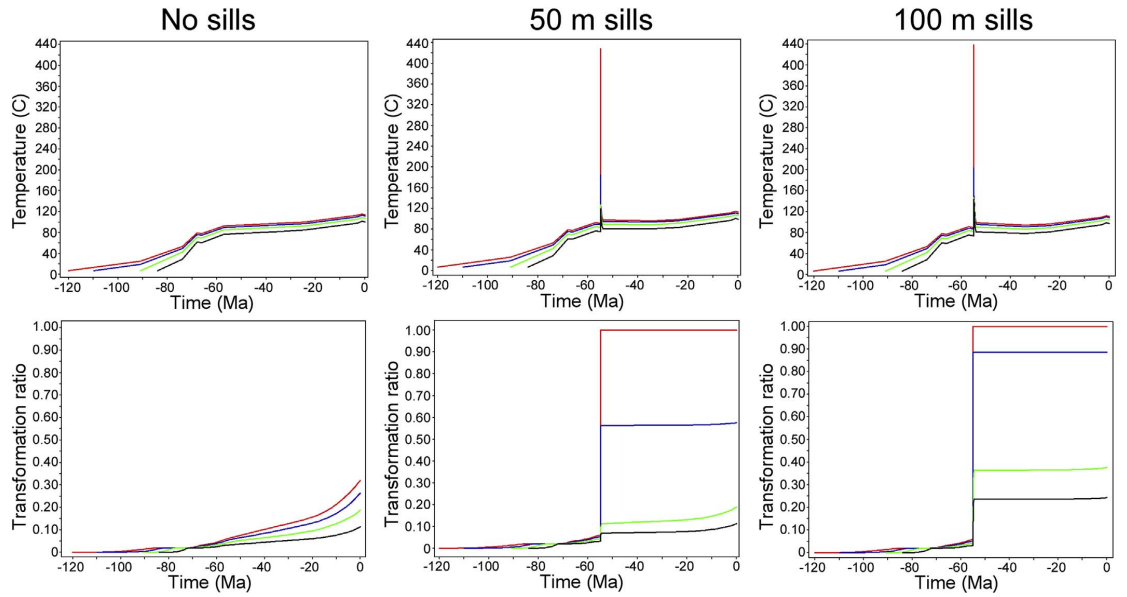

Fig. 6. Temperature and transformation ratio for the four points in the central part of the basin shown in Fig. 3b. The first column corresponds to the scenario with no sills, second column to 50 m sills, and third column to 100 m sills. In all plots, the four lines correspond to the four points and have increasing depth (black, green, blue, red) and decreasing distance to intruded sill. Intrusion temperature is 1000 °C. (For interpretation of the references to color in this figure legend, the reader is referred to the web version of this article.)

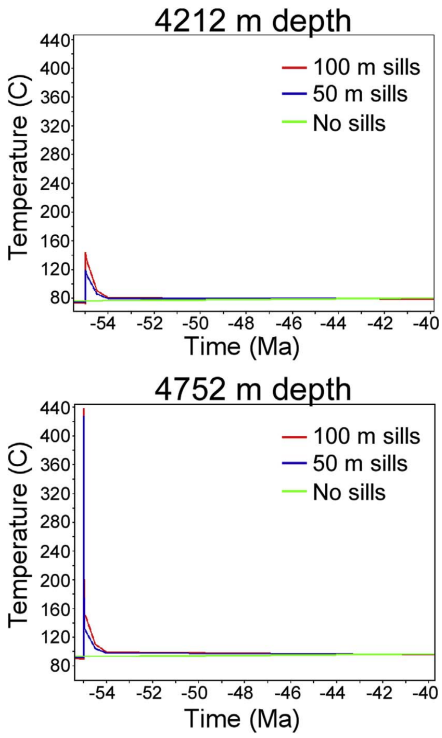

Fig. 7. Temperature evolution for the deepest and shallowest points in the central part of the basin shown in Fig. 3b. Green line corresponds to the scenario with no sills, blue line to 50 m sills and red line to 100 m sills. At both locations, the three thickness scenarios attain the same temperatures around 10 Myr after intrusion. (For interpretation of the references to color in this figure legend, the reader is referred to the web version of this article.)

sediments were already within the oil window at time of intrusion. The maturation is therefore more related to burial depth than the temperature increase caused by sill intrusions. Sediments at 3–5 km depth are the most affected by the emplacement of sills regardless of their timing. The results indicate that modeling the emplacement of sills in one pulse is accurate enough to predict the general influence of sill emplacement on basin maturation provided the intrusion interval between the sills is 10–100 kyr.

There are, however, local effects that must be considered, as they may impact the maturation of source rock between sill clusters of different ages. These local effects are studied at three different locations between the upper and lower sill clusters, with a vertical distance between the sills of ~300 m, at depths of 4–5 km (Fig. 3c) and for a time interval of 100 kyr (results for 10 kyr interval are similar). When all sills are emplaced simultaneously, the full temperature effect occurs instantly resulting in one temperature peak, but when two sill clusters are emplaced at different stages, the temperature effect is distributed over two magma pulses and two temperature peaks (Fig. 11). The question is whether or not the hydrocarbon potential of the source rock placed between the sill clusters would be affected by the order the sills are emplaced.

The highest temperatures are obtained when all sills intrude simultaneously (Fig. 11). When the sills intrude as two pulses at different times, the second magma pulse tends to result in higher temperatures than the first one at the studied locations. Furthermore, higher temperatures are obtained during the second magma pulse when the lower sill cluster intrudes first (Fig. 11), suggesting that the first, deeper pulse of magma thermally affects sediments at shallower depths. This effect is also seen in the temperatures between the two magma pulses, where the sediments affected by the emplacement of deeper sills preserve higher temperatures prior to the emplacement of the upper sills (Fig. 11). A higher host rock background temperature produced by the earlier emplacement of the lower sills allows for a more gradual cooling of these sills, as opposed to lower background temperature and abrupt cooling of the upper sills when they intrude first (Fig. 11). After emplacement of the second sill cluster, the basin strives to achieve temperature equilibrium. Since the model with upper sills intruding first results in less contrasting temperatures between the two magma pulses, it leads to a more gradual cooling of the sill clusters, and equilibrium is reached at higher temperatures than in the model with lower sills intruding first (Fig. 11).

There is a clear correspondence between the highest temperature obtained and the maturation (Fig. 12). The highest transformation ratio for 50 m thick sills is achieved when all sills are emplaced in one pulse. Although there are variations, the results show higher transformation ratios when the lower sills intrude before the upper sills. The exception is the easternmost point at 4.4 km depth for 50 m thick sills (Fig. 12) where the results may have been affected by other neighboring sills. For the 100 m thick sills, there is no significant difference in the resulting transformation ratio, since all scenarios result in ~100% transformation of the organic material. Thus, the timing of sill emplacement may introduce an extra degree of uncertainty when dealing with sill complexes, especially if source rock is situated between the sill clusters.

4.3. Well 7316/5-1

The results from well 7316/5-1 in the Barents Sea are particularly interesting as they show that leaving out both the thin or one of the thick sills in the upper cluster still makes an adequate match with the observed vitrinite reflectance data (Fig. 13). For the lower cluster, however, only the thinnest sill (~5 m) can be left out without significant difference in calculated maturation. Based on these results, it is reasonable to conclude that thin sills between thick sills that are relatively closely spaced, do not significantly influence the maturation in the basin. However, thin sills that are emplaced with no thick sills in the immediate vicinity play an important role in the maturation of organic material (Fig. 13).

Regarding the timing of intrusion, the results for this well show the best match when the lower sill cluster intrudes last with a 10 kyr time interval (Fig. 14). Seemingly, this gives a better match with the observed vitrinite reflectance data than the results for sills intruding simultaneously. In most parts of the well, calculated vitrinite reflectance declines when changing from 10 to 100 kyr intrusion interval, indicating less mature source rock for intrusion intervals of 100 kyr. For a 50 kyr intrusion interval, the results are essentially the same as for 100 kyr interval (not presented here). Well depth between 3300 m and 3525 m and a 100 kyr intrusion interval gives roughly the same calculated vitrinite reflectance as scenario without sills (Fig. 14).

Another interesting observation is the dissymmetry of the calculated vitrinite reflectance between the sill clusters, especially for the 100 kyr intrusion interval. The upper cluster ends at 3100 m depth, and the lower starts at 3600 m. The graph for the 100 kyr intrusion interval (Fig. 14) suggests that the upper sills affect the maturation processes 200 m below the cluster, while the lower sills influence the same processes just some 50 m above the cluster.

5. Discussion

5.1. Sill thickness

Through seismic interpretation and amplitude modeling, Berndt et al. (2000) concluded that the thickness of individual sills in the

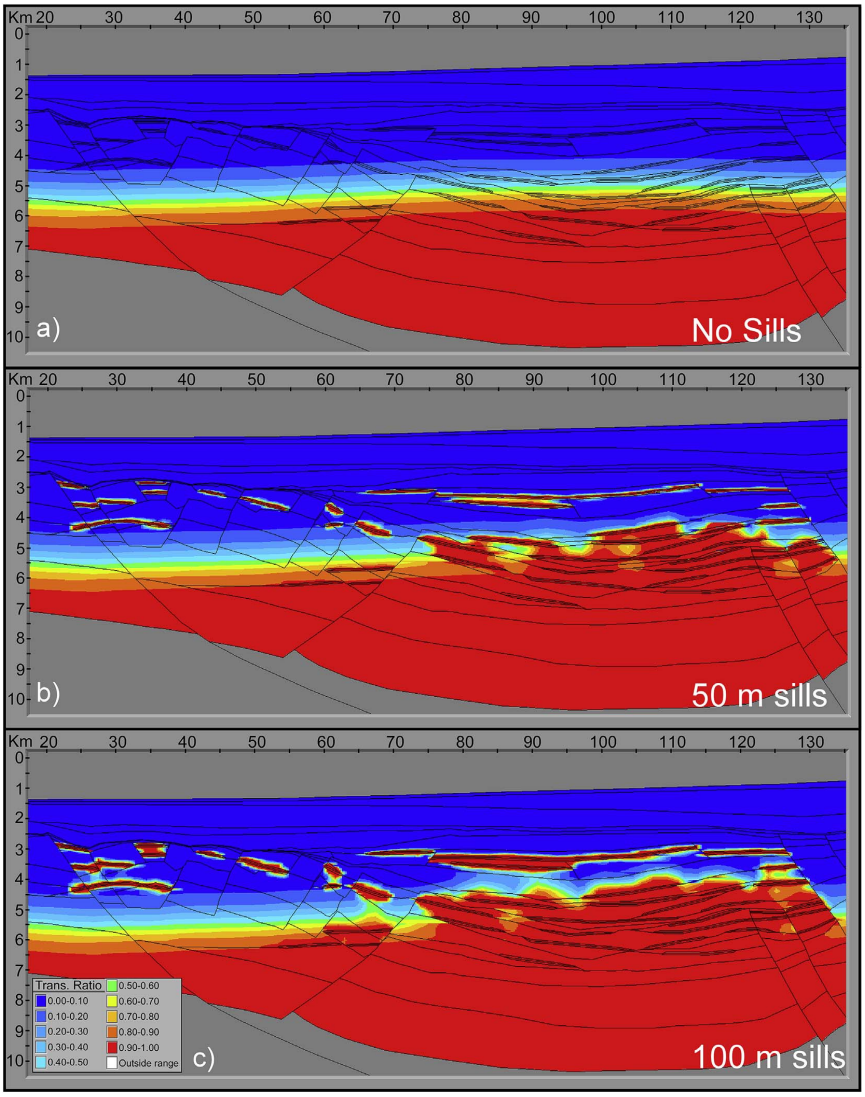

Fig. 8. Present day calculated transformation ratio for the three modeled scenarios: a) no sills, b) 50 m thick sills and c) 100 m thick sills. Maturation increases gradually with depth (a) whereas organic material is matured at shallower depths for scenarios modeled with sill intrusions (b–c). The areas of high transformation ratios are marked in yellow to red. (For interpretation of the references to color in this figure legend, the reader is referred to the web version of this article.)

Vøring Basin, offshore mid-Norway was about 100 m, whereas 2D ray tracing modeling of the same area, indicated sill thicknesses of approximately 200 m (Mjelde et al., 1997). Well 6607/5-2 on the Utgard High, Norwegian Sea (Fig. 1), penetrated two sills, 2 m and 92 m thick, before it stopped some 40 m into a third sill. On seismic, however, only the 92 m thick sill is visible (Planke et al., 2005). Therefore, it is reasonable to assume that only a fraction of existing sills are imaged and interpreted on seismic data. This is supported in a study by Schofield et al. (2015). They found that only two sills in well 205/10-2b, in the Faroe-Shetland Sill Complex, could be clearly interpreted from seismic and these two sills amounted to about 40% of the intruded material in the well. The same study also revealed decreasing limits of visibility and separability of sills in a normal sequence of Cretaceous to Paleocene sediments of the Faroe-Shetland Basin. This indicates that decreasing seismic resolution with depth may leave thick intrusions unresolved in deeper parts of the section.

These studies clearly show that determination of the thickness of intrusions in a basin is sensitive to seismic resolution. Modeling sills too thin leads to an underestimation of the petroleum potential of the basin, while modeling sills too thick results in an overestimation, especially in the depth range 3–5 km. In either case, the ultimate consequence is a wrong estimate of maturation up to 100% in the close vicinity of sills. Sills that are not visible on seismic and not detected by well data will generally not be incorporated in the modeling, thus affecting the predicted basin temperature and maturation. This shows that knowledge about sill thickness is crucial for accurate assessment of the

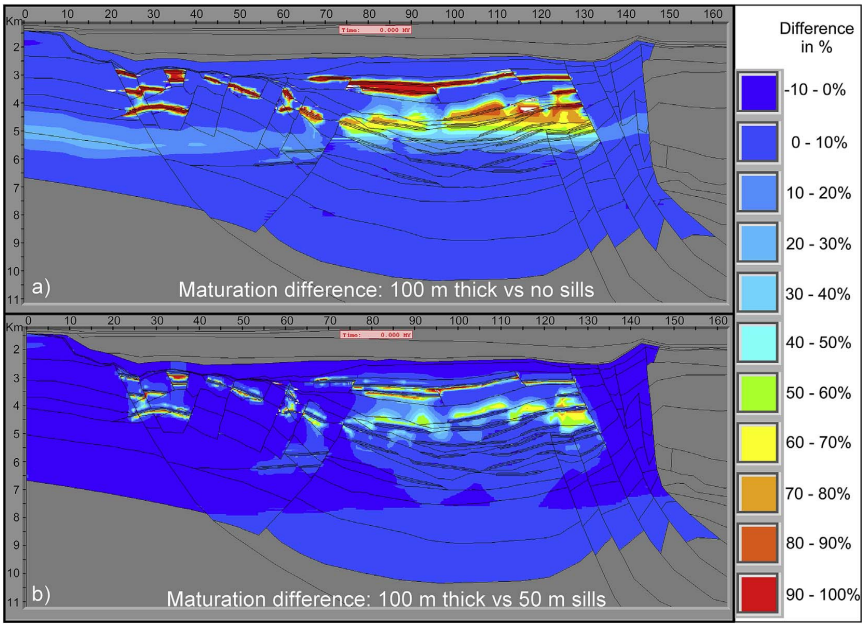

Fig. 9. Differences in transformation ratio between: a) 100 m thick sills versus no sills and b) 100 m thick sills versus 50 m thick sills. Yellow to red colors indicate areas of largest differences in maturation between the compared scenarios. (For interpretation of the references to color in this figure legend, the reader is referred to the web version of this article.)

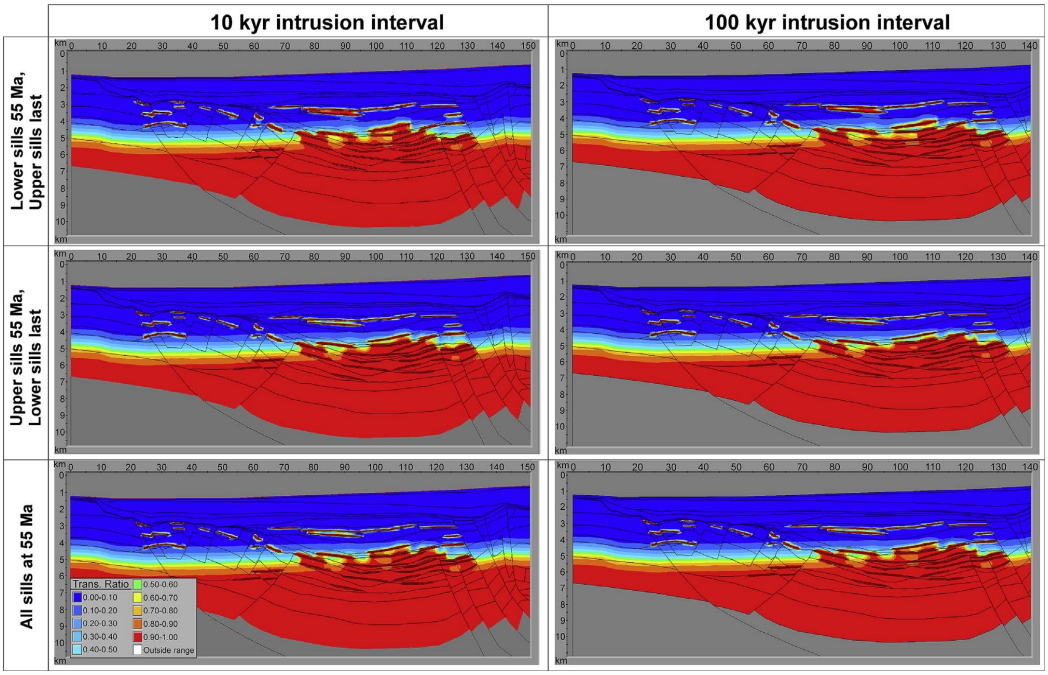

Fig. 10. Transformation ratio for sills intruding 10 and 100 kyr apart. Upper row: lower sills intrude first and upper sills last. Middle row: upper sills intrude first and lower sills last. Bottom row: all sills intrude at 55 Ma. All sills have a thickness of 50 m. The areas of high transformation ratios are marked in yellow to red. (For interpretation of the references to color in this figure legend, the reader is referred to the web version of this article.)

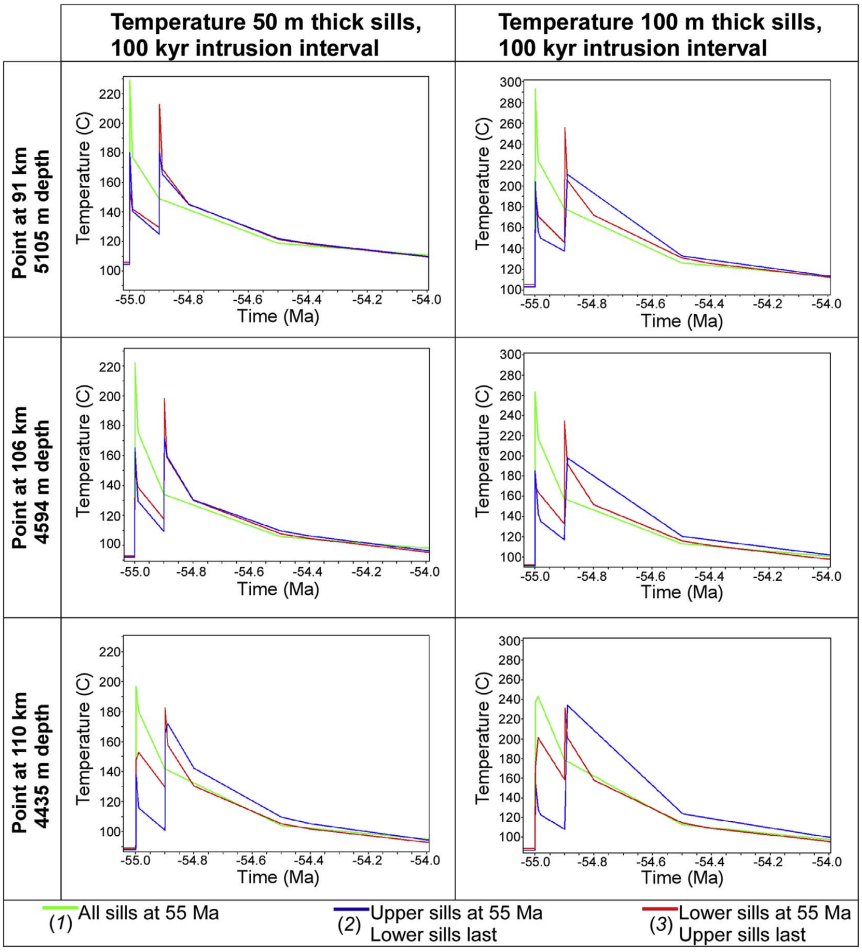

Fig. 11. Temperature histories at the points indicated in Fig. 3c, and for the three scenarios of sill emplacement (green, blue, red). First column is for the 50 m thick sills, and second column is for 100 m thick sills. Time interval between sill clusters is 100 kyr. Notice that the temperature scale is different between the 50 and 100 m thick sills plots. (For interpretation of the references to color in this figure legend, the reader is referred to the web version of this article.)

hydrocarbon prospectivity of sedimentary basins in volcanic provinces. However, it is important to keep in mind that the degree of hydrocarbon maturation depends on the location of potential source rocks in the basin in relation to the emplaced sills.

Well 7316/5-1 in the Barents Sea is a good example of sill clusters where a large fraction of the present sills would be neither detected (visible) nor resolved (separated) (Fig. 4) on seismic and therefore be left out of the temperature and maturation calculations. Thin sills encountered by wells are discovered, but may not be visible on seismic which makes it difficult to determine its horizontal extent and three-dimensional geometry. Data from this well show that vitrinite reflectance (Figs. 13 and 14) is influenced by sills of various thicknesses.

Our modeling shows that even one of the thicker sills in the upper part of well 7316/5-1 can be left out and still the calculated vitrinite reflectance have an adequate match with the observed data (Fig. 13). However, in the lower part of the well, even thin sills left out of the calculations result in poor correlation between observed and calculated vitrinite reflectance. The results from this well are closely tied to the distance between sills and the possibility of heat exchange between neighboring sills, which is related to the vertical distribution of the intruded material. This is in accordance with Aarnes et al. (2011) who show that the interaction between sills becomes stronger with decreasing vertical distance between sills. At a vertical distance of seven sill thicknesses the sills will interact thermally, and for thin sills (10 m) a vertical distance of four sill thicknesses gives an optimal output regarding the total hydrocarbon potential (Aarnes et al., 2015). The upper interval (200 m) of well 7316/5-1 consists of 50% intruded material, whereas the lower interval (400 m) contains 13% sill material (Fig. 13). Based on these results, it is reasonable to conclude that thin sills between thick sills in basins can safely be left out of the temperature and maturation calculations, whereas in basins or parts of basins with only thin sills, every sill counts in the calculations.

The age of the sills is, in our case, 55 Ma. In other areas the age of the sills can be different. However, the modeled effect of sill emplacement is not, to a significant degree, affected by the emplacement age of the sills because of the short-lived significant temperature increase, as shown in Figs. 11 and 12. A geothermal gradient different from our case can lead to small changes in maturation from the results reported here.

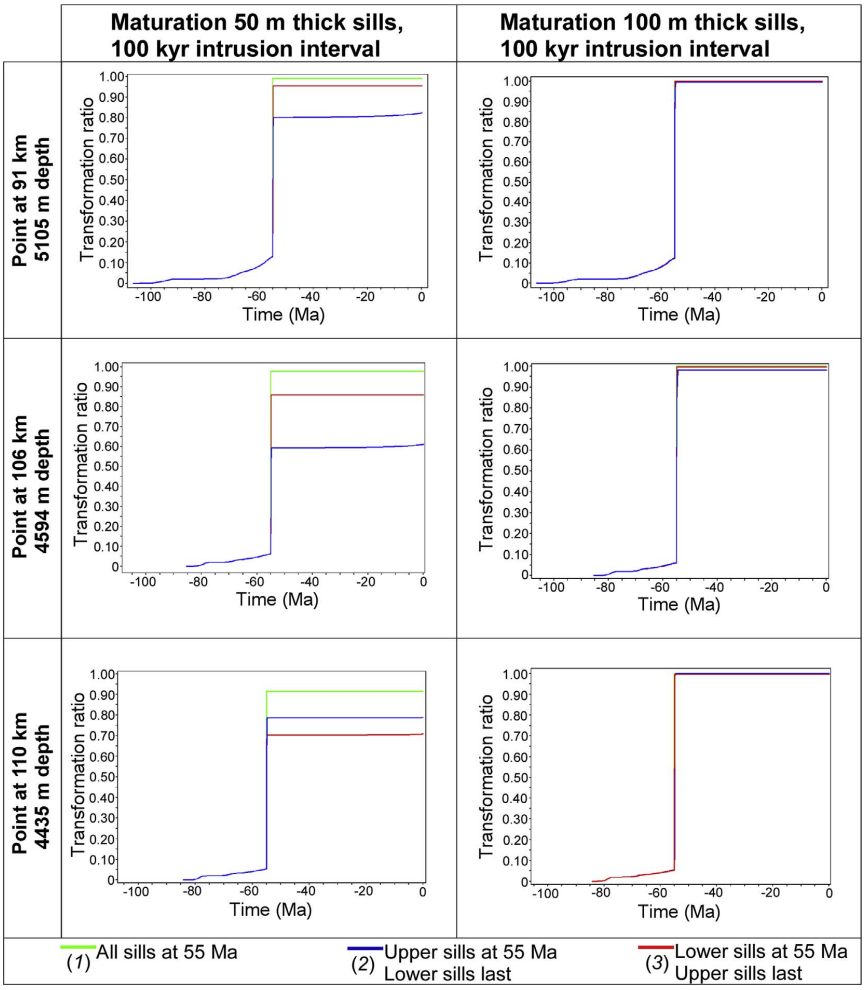

Fig. 12. Transformation ratio at the points indicated in Fig. 3c, and for the three scenarios of sill emplacement (green, blue, red). First column is for the 50 m thick sills, and second column is for 100 m thick sills. Time interval between sill clusters is 100 kyr. (For interpretation of the references to color in this figure legend, the reader is referred to the web version of this article.)

5.2. Timing of sill emplacement

Outcrop observations show that many sills are emplaced as clusters (Planke et al., 2005; Aarnes et al., 2011; Svensen et al., 2012; Eide et al., 2016). Based solely on seismic, it may be impossible to determine if the sills intruded simultaneously or as clusters at different times. Magee et al. (2014) concluded that radiometric or seismic-stratigraphic data from one or more sills in a cluster are not sufficient to characterize the timing of emplacement of the entire sill network.

Aarnes et al. (2015) studied the impact of two 100 m thick sills, where the upper sill intruded last with increasing time interval up to 100 kyr apart. They concluded that two sills intruding with a time interval < 50 kyr show a positive effect on the total methane production potential. Hanson and Barton (1989) also found a positive effect for intrusions emplaced simultaneously as opposed to when complete cooling was allowed between magmatic pulses. A time interval of 10–100 kyr between sill intrusions will not be detected with current dating methods. Based on these facts, the sills in this study were divided into upper and lower sill complexes to study the effect different timing of sill emplacement has on the temperature and maturation of source rock between sill clusters. The resulting maturation shows insignificant differences regarding timing of emplacement for the 100 m thick sills and only small differences for the 50 m thick sills. Overall, modeling the sills as contemporary gives a good first approximation to the petroleum potential of the basin (Fig. 10). However, the presence and the type of source rock between the sill clusters are key factors in the prospectivity assessment.

Aarnes et al. (2015) also found that simultaneous sill emplacement may lead to 25% higher total hydrocarbon potential than if the emplacement occurs in two separate events (intrusion interval $>$ 50 kyr). Our results show similar local effects for the 50 m thick sills and 100 kyr intrusion interval, which show up to 40% higher maturation when all sills intrude simultaneously as opposed to in two pulses. The 100 m thick sills show no differences in maturation regardless of timing of intrusion, all scenarios show approximately 100% matured organic material (Fig. 12). Aarnes et al. (2015) use a vertical spacing of 760 m

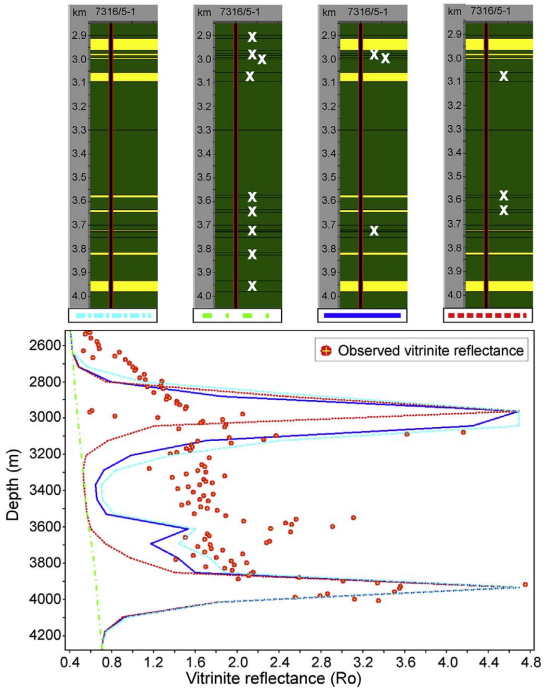

Fig. 13. Calculated and observed vitrinite reflectance in well 7316/5-1 in the Barents Sea for various modeling scenarios. The upper part show intruded sills (in yellow) and host rock (in green). The white Xs highlight the sills left out in the calculations. (For interpretation of the references to color in this figure legend, the reader is referred to the web version of this article.)

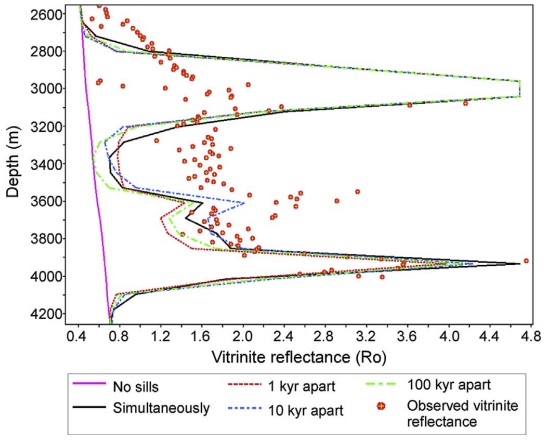

Fig. 14. Calculated vitrinite reflectance for different intrusion intervals plotted against observed vitrinite reflectance in well 7316/5-1 in the Barents Sea. All nine sills in the well were included, but the four sills of the upper level (2.9–3.1 km) are assumed to have intruded first.

between the modeled sills, while in our study, the spacing between the upper and lower sills in the area of the monitored points is ~300 m (Fig. 3c). There is a critical vertical distance between neighboring sills at which the sills thermal aureoles start to interact (Aarnes et al., 2011). This critical distance is related to the thickness of the sills, because the thermal aureole increases with sill thickness. For thick sills, the vertical spacing between neighboring sills must be relatively large to avoid interaction between their thermal aureoles. Thus, it is reasonable to expect that with increasing vertical distance between the upper and lower sills, the results for the 100 m thick sills will approach those of the 50 m thick sills. Nevertheless, if the sill clusters are closely spaced (< 300 m vertically), the timing of sill emplacement has insignificant influence on the resulting maturation of source rock between two complexes of thick (100 m) sills.

The best match between observed and calculated vitrinite reflectances for well 7316/5-1 is achieved when the lower sills intrude last with an intrusion interval of 10 kyr (Fig. 14). This observed time interval is in accordance with results from other studies (Einsele, 1982; Aarnes et al., 2015). Furthermore, this result is also in keeping with work reported by Barnett and Gudmundsson (2012), which indicates that the upper sill tends to be the oldest for sill complexes intruding over a relatively short period of time. Therefore, as a first approximation in predicting the transformation ratio of a basin, it is recommended to consider the upper sills to be the oldest unless there are good indications to assume otherwise. Further, the results from timing of intrusion in well 7316/5-1 show that intervals > 50 kyr can be considered as two separate events. This is in accordance with observations by Aarnes et al. (2015). However, our results also show that the upper sill cluster consisting of a much larger fraction of intruded material as well as thicker sills, influence the maturation processes and thereby the vitrinite reflectance further downwards (200 m) than the lower sill cluster with relatively thin sills affects the same process upwards (50 m). This is in agreement with our results regarding sill thicknesses from the modeling of the 2D transect in the Vøring Basin (Figs. 5–9).

A potentially significant consequence of sill intrusions in a basin is a change from kinetic to thermodynamic control of the chemical reactions modifying the source rock. Due to the temperature increase, energetically more demanding transformations can take place (De Paula and Atkins, 2014). In general, these transformations are oxidative and lead to formation of more CO_2 and a type of kerogen that is less prone to form hydrocarbons (Tissot and Welte, 1984; Michelsen, 2017). Such development has been supported by laboratory simulations (Goodarzi and Gentzis, 1990) and can clearly be seen in the variation of the observed vitrinite reflectance in well 7316/5-1 (Figs. 13 and 14).

6. Conclusions

In general this study shows that the thickness of sills has a large impact on the temperature and maturation of sedimentary basins, especially at 3–5 km depth. It advocates for thorough interpretation of sill thickness to correctly assess the petroleum potential of volcanic basins. For areas with source rocks between sill complexes, considering the timing of sill emplacement can be necessary to estimate the range of expected transformation ratios. This is especially important if sills are thin, or thick but with large (> 300 m) vertical spacing. There is a positive effect on temperature and maturation when upper sill clusters intrude last. As presumably many sills are left out, due to their non-visibility and separability on seismic, the amount of interpreted sills in the basin is perhaps the largest uncertainty when modeling and assessing sills effect on the petroleum system. For intervals with low frequency of intruded material, every sill influences the maturation. However, for intervals with high frequency of intruded material, thin sills have no significant influence on the maturation.

A good representation of the structural development of the basin is fundamental for proper thermal modeling as it affects the heat flow in the basin. In BMT, fault restoration is based on a vertical shear model but other restoration methods exist, e.g. inclined shear. Sensitivity modeling on fault restoration methods will determine to what degree different restoration methods influence the modeled heat flow and best represents the observed heat flow in the basin. This is the subject of future work.

Acknowledgements

This study was funded by the Research Council of Norway and Tectonor AS as part of the industrial PhD 'Effects of magmatic intrusions on temperature history and diagenesis in sedimentary basins', RCN project number 257492. We would like to thank reviewers Nick Schofield and Sverre Planke, and two anonymous reviewers, for constructive and useful comments that substantially improved the content of this paper.

References

Aarnes, I., Svensen, H., Connolly, J.A.D., Podladchikov, Y.Y., 2010. How contact metamorphism can trigger global climate changes: modeling gas generation around igneous sills in sedimentary basins. Geochimica Cosmochimica Acta 74, 7179–7195.
Aarnes, I., Svensen, H., Polteau, S., Planke, S., 2011. Contact metamorphic devolatilization of shales in the Karoo Basin, South Africa, and the effects of multiple sill intrusions. Chem. Geol. 281, 181–194.
Aarnes, I., Planke, S., Trulsvik, M., Svensen, H., 2015. Contact metamorphism and thermogenic gas generation in the Vøring and Møre basins, offshore Norway, during the Paleocene-Eocene thermal maximum. J. Geol. Soc. 172, 588–598.
Abdelmalak, M.M., Meyer, R., Planke, S., Faleide, J.I., Gernigon, L., Frieling, J., Sluijs, A., Reichart, G.-J., Zastrozhnov, D., Theissen-Krah, S., Said, A., Myklebust, R., 2016. Pre-breakup magmatism on the Vøring margin: insight from new sub-basalt imaging and results from ocean drilling program hole 642E. Tectonophysics 675, 258–274.
Barnett, Z., Gudmundsson, A., 2012. Field Data and Numerical Models on the Emplacement of Sill Complexes. EGU General Assembly, 22-27 April, Vienna, Austria. pp. 365.
Berndt, C., Skogly, O.P., Planke, S., Eldholm, O., Mjelde, R., 2000. High-velocity breakup-related sills in the Vøring basin, off Norway. J. Geophys. Res. 105, 28443–28454.
Blystad, P., Brekke, H., Færseth, R.B., Larsen, B.T., Skogseid, J., Tørudbakken, B., 1995. Structural Elements of the Norwegian Continental Shelf, Part II: the Norwegian Sea Region. The Norwegian NPD-Bulletin. pp. 8.
Brekke, H., Riis, F., 1987. Tectonics and basin evolution of the Norwegian shelf between 62°N and 72°N. Nor. Geol. Tidsskr. 67, 295–322.
Brekke, H., 2000. The tectonic evolution of the Norwegian Sea continental margin with emphasis on the Vøring and Møre basins. In: In: Nøttvedt, A. (Ed.), Dynamics of the Norwegian Margin, vol 167. Geological Society, London, pp. 327–378 Special Publications.
Brown, A.R., 2004. sixth ed. Interpretation of Three-dimensional Seismic Data, vol 42. American Association of Petroleum Geologists Memoir, pp. 534.
Bukovics, C., Cartier, E.G., Shaw, N.D., Ziegler, P.A., 1984. Structure and development of the mid-Norway continental margin. In: Spencer, A.M. (Ed.), Petroleum Geology of the North European Margin. Norwegian Petroleum Society, Graham and Trotman, pp. 407–423.
Burchardt, S., 2008. New insights into the mechanics of sill emplacement provided by field observations of the Njardvik Sill, Northeast Iceland. J. Volcanol. Geotherm. Res. 173, 280–288.
Button, A., Cawthorn, R.G., 2015. Distribution of mafic sills in the Transvaal Supergroup, northeastern South Africa. J. Geol. Soc. 172, 357–367.
Caineng, Z., Guangya, Z., Rukai, Z., Xuanjun, Y., Xia, Z., Lianhua, H., Baihong, W., Xiaozhi, W., 2012. Volcanic Reservoirs in Petroleum Exploration. Petroleum Industry Press. Elsevier Inc.
Chevallier, L., Woodford, A., 1999. Morpho-tectonics and mechanism of emplacement of the dolerite rings and sills of the western Karoo, South Africa. South Afr. J. Geol. 102, 43–54.
Cukur, D., Horozal, S., Kim, D.C., Lee, G.H., Han, H.C., Kang, M.H., 2010. The distribution and characteristics of the igneous complexes in the northern East China Sea Shelf Basin and their implications for hydrocarbon potential. Mar. Geophys. Res. 31, 299–313.
De Paula, J., Atkins, P., 2014. Atkins' Physical Chemistry. Oxford University Press, Oxford, UK.
Doré, A.G., Lundin, E.R., 1996. Cenozoic compressional structures on the NE Atlantic margin: nature, origin and potential significance for hydrocarbon exploration. Pet. Geosci. 2, 299–311.
Eide, C.H., Schofield, N., Jerram, D.A., Howell, J.A., 2016. Basin-scale architecture of deeply emplaced sill complexes: Jameson Land, East Greenland. J. Geol. Soc. 174, 23–40.
Einsele, G., 1982. Mechanism of Sill Intrusion into Soft Sediment and Expulsion of Pore Water. Deep Sea Drilling Project, Initial report, 64, part VIII, no. 56. .
Eldholm, O., Gladczenko, T.P., Skogseid, J., Planke, S., 2000. Atlantic volcanic margins: a comparative study. In: In: Nøttvedt, A.E.A. (Ed.), Dynamics of the Norwegian Margin, vol 167. Geological Society, London, pp. 411–428 Special Publications.
Fjeldskaar, W., 2003. BMT™ - Exploration Tool Combining Tectonic and Temperature Modeling: Business Briefing: Exploration & Production. The Oil and Gas Review. pp. 1–4.
Fjeldskaar, W., Helset, H.M., Johansen, H., Grunnaleite, I., Horstad, I., 2008. Thermal modelling of magmatic intrusions in the Gjallar Ridge, Norwegian Sea: implications for vitrinite reflectance and hydrocarbon maturation. Basin Res. 20, 143–159.
Fjeldskaar, W., Andersen, Å., Johansen, H., Lander, R., Blomvik, V., Skurve, O., Michelsen, J.K., Grunnaleite, I., Mykkeltveit, J., 2017. Bridging the gap between basin modelling and structural geology. Accepted for publication in Regional Geology and Metallogeny. (in press). .
Gabrielsen, R.H., Færseth, R., Hamar, G., Rønnevik, H., 1984. Nomenclature of the main structural features on the Norwegian Continental Shelf north of the 62nd parallel. In: Spencer, A.M. (Ed.), Petroleum Geology of the North European Margin. Norwegian Petroleum Society, Graham and Trotman, pp. 41–60.
Galerne, C.Y., Neumann, E.-R., Aarnes, I., Planke, S., 2010. Magmatic differentiation processes in saucer-shaped sills: evidence from the golden valley sill in the Karoo basin, South Africa. Geosphere 6, 163–188.
Galerne, C.Y., Galland, O., Neumann, E.-R., Planke, S., 2011. 3D relationships between sills and their feeders: evidence from the golden Valley Sill Complex (Karoo Basin) and experimental modeling. J. Volcanol. Geotherm. Res. 202, 189–199.
Galushkin, Y.I., 1997. Thermal effects of igneous intrusions on maturity of organic matter: a possible mechanism of intrusion. Org. Geochem. 26, 645–658.
Ganerød, M., Smethurst, M.A., Torsvik, T.H., Prestvik, T., Rousse, S., McKenna, C., Van Hinsbergen, D.J.J., Hendriks, B.W.H., 2010. The North Atlantic igneous province reconstructed and its relation to the plume generation zone: the Antrim lava group revisited. Geophys. J. Int. 182, 183–202.
Gibbs, A.D., 1983. Balanced cross-section construction from seismic sections in areas of extensional tectonics. J. Struct. Geol. 5, 153–160.
Gleadow, A.J.W., Brooks, C.K., 1979. Fission track dating, thermal histories and tectonics of igneous intrusions in East Greenland. Contributions Mineralogy Petrology 71, 45–60.
Goodarzi, F., Gentzis, T., 1990. The lateral and vertical reflectance and petrological variation of a heat-affected bituminous coal seam from southeastern British Columbia, Canada. Int. J. Coal Geol. 15, 317–339.
Gudmundsson, A., Løtveit, I.F., 2012. Sills as Hydrocarbon Reservoirs: Examples and Models, vol 374. Geological Society, London, pp. 251–271 Special Publications.
Hansen, D.M., Cartwright, J., 2006. Saucer-shaped sill with lobate morphology revealed by 3D seismic data: implications for resolving a shallow-level sill emplacement mechanism. J. Geol. Soc. 163, 509–523.
Hansen, J., Jerram, D.A., McCaffrey, K., Passey, S.R., 2009. The onset of the North Atlantic igneous province in a rifting perspective. Geol. Mag. 146, 309–325.
Hansen, J., Jerram, D.A., McCaffrey, K., Passey, S.R., 2011. Early Cenozoic saucer-shaped sills of the Faroe Islands: an example of intrusive styles in basaltic lava piles. J. Geol. Soc. 168, 159–178.
Hanson, R.B., Barton, M.D., 1989. Thermal development of low-pressure metamorphic belts: results from two-dimensional numerical models. J. Geophys. Res. 94, 10363–10377.
Hart, B.S., 2000. 3-D Seismic Interpretation: a Primer for Geologists. Society for Sedimentary Geology Special Publication, pp. 48 Short Course.
Inam, R.H., Asif, A.A., Shoaib, K., Anjum, A.G., Faizan, M., 2014. Igneous Intrusion and its Impact on Petroleum Play of Lower Goru Formation in Jati Blok, Southern Indus Basin, Pakistan. PAPG-SPE Annual technical Conference, 25–26 November 2014, Conference paper.
Iyer, K., Rüpke, L., Galerne, C.Y., 2013. Modeling fluid flow in sedimentary basins with sill intrusions: implications for hydrothermal venting and climate change. Geochem. Geophys. Geosystems 14, 5244–5262.
Iyer, K., Schmid, D.W., Planke, S., Millett, J., 2017. Modelling hydrothermal venting in volcanic sedimentary basins: impact on hydrocarbon maturation and paleoclimate. Earth Planet. Sci. Lett. 467, 30–42.
Kjoberg, S., Schmiedel, T., Planke, S., Svensen, H.H., Millett, J.M., Jerram, D.A., Galland, O., Lecomte, I., Schofield, N., Haug, Ø.T., Helsem, A., 2017. 3D structure and formation of hydrothermal vent complexes at the Paleocene-Eocene transition, the Møre Basin, mid-Norwegian margin. Interpretation 5, 65–81.
Lander, R.H., Langfeldt, M., Bonnell, L., Fjeldskaar, W., 1994. BMT User's Guide. Tectonor AS proprietary publication.
Magee, C., Jackson, C.A.-L., Schofield, N., 2014. Diachronous sub-volcanic intrusion along deep-water margins: insights from the Irish Rockall Basin. Basin Res. 25, 85–105.
Magee, C., Maharaj, S.M., Wrona, T., Jackson, C.A.-L., 2015. Controls on the expression of igneous intrusions in seismic reflection data. Geosphere 11, 1024–1041.
Meyer, R., van Wijk, J., Gernigon, L., 2007. The North Atlantic Igneous Province: a Review of Models for its Formation. vol 430. Geological Society of America, pp. 525–552 Special Paper.
Michelsen, J.K., 2017. Personal Communication.
Mjelde, R., Kodaira, S., Shimamura, H., Kanazawa, T., Shiobara, H., Berg, E.W., Riise, O., 1997. Crustal structure of the central part of the Vøring Basin, mid- Norway margin, from ocean bottom seismographs. Tectonophysics 277, 235–257.
Moore, J.G., Fleming, H.S., Phillips, J.D., 1974. Preliminary model for extrusion and rifting at the Axis of the Mid-Atlantic Ridge, 36°48′ north. Geology 2, 437–440.
Osagiede, E.E., Duffy, O.B., Jackson, C.A.-L., Wrona, T., 2014. Quantifying the growth history of seismically imaged normal faults. J. Struct. Geol. 66, 382–399.
Othman, R., Arouri, K.R., Ward, C.R., McKirdy, D.M., 2001. Oil generation by igneous intrusions in the northern Gunnedah Basin, Australia. Org. Geochem. 32, 1219–1232.
Peace, A., McCaffrey, K., Imber, J., Hobbs, R., van Hunen, J., Gerdes, K., 2017. Quantifying the influence of sill intrusion on the thermal evolution of organic-rich sedimentary rocks in nonvolcanic passive margins: an example from ODP 210-1276, offshore Newfoundland, Canada. Basin Res. 29, 249–265.
Planke, S., Rasmussen, T., Rey, S.S., Myklebust, R., 2005. Seismic characteristics and distribution of volcanic intrusions and hydrothermal vent complexes in the Vøring and Møre basins. In: Dorè, A.G., Vining, B.A. (Eds.), Petroleum Geology: North-West Europe and Global Perspectives, pp. 833–844 Proceedings of the 6th Petroleum Geology Conference.
Podladchikov, Y.Y., Wickham, S.M., 1994. Crystallization of hydrous magmas: calculation of associated thermal effects, volatile fluxes, and isotopic alteration. J. Geol. 102, 25–45.

Polteau, S., Ferré, E.C., Neumann, E.-R., Chevallier, L., 2008. How are saucer-shaped sills emplaced? Constraints from the Golden Valley Sill, South Africa. J. Geophys. Res. 113, 1–13.
Polyansky, O.P., Reverdatto, V.V., 2006. Contact metamorphism and metasomatism near the talnakh intrusion: fluid convection and heat transfer modeling on the basis of the finite-difference method. Geochemistry 411A, 1480–1484.
Price, I., Rattey, R.P., 1984. Cretaceous tectonics off mid-Norway: implications for the Rockall and Faeroe-Shetland troughs. J. Geol. Soc. 141, 985–992.
Quinn, D., Meere, P.A., Wartho, J.-A., 2005. A chronology of foreland deformation: ultra violet laser $^{40}AR/^{39}AR$ dating of syn/late-orogenic intrusions from the Variscides of southwest Ireland. J. Struct. Geol. 27, 1413–1425.
Saunders, A.D., Fitton, J.G., Kerr, A.C., Norry, M.J., Kent, R.W., 1997. The North Atlantic igneous province. In: In: Mahoney, J.J., Coffin, M.F. (Eds.), Large Igneous Provinces: Continental, Oceanic, and Planetary Flood Volcanism, vol 100. pp. 45–93 AGU Geophysical Monograph Series.
Scheck-Wenderoth, M., Raum, T., Faleide, J.I., Mjelde, R., Horsfield, B., 2007. The transition from the continent to the ocean: a deeper view on the Norwegian margin. J. Geol. Soc. 164, 855–868.
Schofield, N., Stevenson, C., Reston, T., 2010. Magma fingers and host rock fluidization in the emplacement of sills. Geology 38, 63–66.
Schofield, N., Holford, S., Millett, J., Brown, D., Jolley, D., Passey, S.R., Muirhead, D., Grove, C., Magee, C., Murray, J., Hole, M., Jackson, C.A.-L., Stevenson, C., 2015. Regional magma plumbing and emplacement mechanisms of the Faroe-Shetland Sill Complex: implications for magma transport and petroleum systems within sedimentary basins. Basin Res. 1–23.
Schofield, N., Jolley, D., Holford, S., Archer, S., Watson, D., Hartley, A., Howell, J., Muirhead, D., Underhill, J., Green, P., 2017. Challenges of future exploration within the UK Rockall basin. In: Petroleum Geology of NW Europe: 50 Years of Learning – Proceedings of the 8th Petroleum Geology Conference. Geological Society, London.
Sclater, J.G., Christie, P.A.F., 1980. Continental stretching: an explanation of the post-mid-cretaceous subsidence of the central North Sea basin. J. Geophys. Res. 85, 3711–3739.
Senger, K., Planke, S., Polteau, S., Ogata, K., Svensen, H., 2014. Sill emplacement and contact metamorphism in a siliciclastic reservoir on Svalbard, Arctic Norway. Nor. J. Geol. 155–169.
Senger, K., Millett, J., Planke, S., Ogata, K., Eide, C.H., Festøy, M., Galland, O., Jerram, D.A., 2017. Effects of igneous intrusions on the petroleum system: a review. First Break 35, 47–56.
Smallwood, J.R., Maresh, J., 2002. The properties, morphology and distribution of igneous sills: modelling, borehole data and 3D seismic from the Faroe-Shetland area. In: In: Jolley, D.W., Bell, B.R. (Eds.), The North Atlantic Igneous Province: Stratigraphy, Tectonic, Volcanic and Magmatic Processes, vol 197. Geological Society, London, pp. 271–306 Special Publications.
Surlyk, F., Piasecki, S., Rolle, F., Stemmerik, L., Thomsen, E., Wrang, P., 1984. The permian base of East Greenland. In: Spencer, A.M. (Ed.), Petroleum Geology of the North European Margin. Norwegian Petroleum Society, Graham and Trotman, pp. 303–315.
Svensen, H., Planke, S., Jamtveit, B., Pedersen, T., 2003. Seep carbonate formation controlled by hydrothermal vent complexes: a case study from the Vøring Basin, the Norwegian Sea. Geo-Marine Lett. 23, 351–358.
Svensen, H., Planke, S., Malthe-Sørenssen, A., Jamtveit, B., Myklebust, R., Eidem, T.R., Rey, S.S., 2004. Release of methane from a volcanic basin as a mechanism for initial Eocene global warming. Nature 429, 542–545.
Svensen, H., Planke, S., Corfu, F., 2010. Zircon dating ties NE Atlantic sill emplacement to initial Eocene global warming. J. Geol. Soc. 167, 433–436.
Svensen, H., Corfu, F., Polteau, S., Hammer, Ø., Planke, S., 2012. Rapid magma emplacement in the Karoo large igneous province. Earth Planet. Sci. Lett. 325–326, 1–9.
Swiecicki, T., Gibbs, P.B., Farrow, G.E., Coward, M.P., 1998. A tectonostratigraphic framework for the Mid-Norway region. Mar. Petroleum Geol. 15, 245–276.
Torsvik, T.H., Mosar, J., Eide, E.A., 2001. Cretaceous-tertiary geodynamics: a North Atlantic exercise. Geophys. J. Int. 146, 850–866.
Tissot, B.P., Welte, D.H., 1984. Petroleum Formation and Occurrence, second ed. Springer-Verlag.
Tissot, B.P., Pelet, R., Ungerer, P., 1987. Thermal history of sedimentary basins, maturation indices, and kinetics of oil and gas generation. Am. Assoc. Petroleum Geol. Bull. 71, 1445–1466.
Trude, J., Cartwright, J., Davies, R.J., Smallwood, J., 2003. New technique for dating igneous sills. Geology 31, 813–816.
Wang, D., 2012. Comparable study on the effect of errors and uncertainties of heat transfer models on quatitative evaluation of thermal alteration in contact metamorphic aureoles: thermophysical parameters, intrusion mechanism, pore-water volatilization and mathematical equations. Int. J. Coal Geol. 95, 12–19.
Wang, D., Zhao, M., Qi, T., 2012. Heat-transfer-model Analysis of the thermal effect of intrusive sills on organic-rich host rocks in sedimentary basins. In: Dar, I.A. (Ed.), Earth Sciences. InTech.
Wang, D., Song, Y., Xu, H., Ma, X., Zhao, M., 2013. Numerical modeling of thermal evolution in the contact aureole of a 0.9 m thick dolerite dike in the Jurassic siltstone section from Isle of Skye, Scotland. J. Appl. Geophys. 89, 134–140.
Zhong, H., Campbell, I.H., Zhu, W.-G., Allen, C.M., Hu, R.-Z., Xie, L.-W., He, D.-F., 2011. Timing and source constraints on the relationship between mafic and felsic intrusions in the Emeishan large igneous province. Geochem. Cosmochimica Acta 75, 1374–1395.

Paper 2: Transient Thermal Effects in Sedimentary Basins with Normal Faults and Magmatic Sill Intrusions – A Sensitivity Study

Magnhild Sydnes, Willy Fjeldskaar, Ivar Grunnaleite, Ingrid Fjeldskaar Løtveit, Rolf Mjelde

Published in Geosciences, 9, 160, Special Issue "Future Advances in Basin Modeling: Suggestions from Current Observations, Analyses and Simulations"

2

geosciences

MDPI

Article

Transient Thermal Effects in Sedimentary Basins with Normal Faults and Magmatic Sill Intrusions—A Sensitivity Study

Magnhild Sydnes [1,2,*], Willy Fjeldskaar [1], Ivar Grunnaleite [1], Ingrid Fjeldskaar Løtveit [1] and Rolf Mjelde [2]

[1] Tectonor AS, P.O. Box 8034, NO-4068 Stavanger, Norway; wf@tectonor.com (W.F.); ig@tectonor.com (I.G.); ifl@tectonor.com (I.F.L.)

[2] Department of Earth Science, University of Bergen, Box 7803, 5020 Bergen, Norway; Rolf.Mjelde@uib.no

* Correspondence: ms@tectonor.com

Received: 13 March 2019; Accepted: 2 April 2019; Published: 5 April 2019

Abstract: Magmatic intrusions affect the basin temperature in their vicinity. Faulting and physical properties of the basin may influence the magnitudes of their thermal effects and the potential source rock maturation. We present results from a sensitivity study of the most important factors affecting the thermal history in structurally complex sedimentary basins with magmatic sill intrusions. These factors are related to faulting, physical properties, and restoration methods: (1) fault displacement, (2) time span of faulting and deposition, (3) fault angle, (4) thermal conductivity and specific heat capacity, (5) basal heat flow and (6) restoration method. All modeling is performed on the same constructed clastic sedimentary profile containing one normal listric fault with one faulting event. Sills are modeled to intrude into either side of the fault zone with a temperature of 1000 °C. The results show that transient thermal effects may last up to several million years after fault slip. Thermal differences up to 40 °C could occur for sills intruding at time of fault slip, to sills intruding 10 million years later. We have shown that omitting the transient thermal effects of structural development in basins with magmatic intrusions may lead to over- or underestimation of the thermal effects of magmatic intrusions and ultimately the estimated maturation.

Keywords: normal faulting; sill intrusions; transient thermal effects; steady state; basin modeling; volcanic basins

1. Introduction

Hydrocarbon discoveries associated with magmatic intrusions are common in many sedimentary basins throughout the world [1–3], and these intrusions may potentially affect all parts of the petroleum system [4]. The impact of magmatic intrusions has been studied in several basins worldwide, e.g., Vøring Basin, Norway (e.g., [5–7]), Karoo Basin, South Africa (e.g., [8–10]), Gunnedah Basin, Australia [11], Neuquén Basin, Argentina (e.g., [12,13]), Bohai Bay Basin, China (e.g., [14,15]). All these studies conclude that magmatic intrusions significantly influence the basin thermal history and thus the maturation of organic material in their vicinity.

Several studies have identified the pre-intrusion temperature of the host rock as an important variable for the ultimate thermal and maturation levels of sedimentary basins with magmatic intrusions [8,10,13,16–18]. However, this variable is one of the most difficult parameters to constrain, as the traces of pre-intrusion temperature and maturation are erased instantly in the thermal aureole of magmatic intrusions when magmatic emplacement occurs [19] and the basin has been subject to later geological development. As magmatic intrusions often are emplaced into structurally complex sedimentary basins, it is crucial to understand how the basin's structural evolution affects the

temperature development. With such knowledge it should be possible to discern temperature effects of the structural development from temperature effects of magmatic intrusions. This is important as the pre-intrusion temperatures have implications for the magnitude of the thermal effect of sills, i.e., size and temperatures of the thermal aureole, which eventually will have implications for the estimated maturation of the basin.

Magmatic intrusions and their effect on temperature and maturation in the surrounding host rocks have been subject of several studies (e.g., [8,13,19–24]). Only a few studies model sills intruding into structurally complex basins under development, while taking the temporary host-rock temperature and maturation into consideration (e.g., [7,25]). Structurally complex basins are characterized by numerous faults, changing lithologies with different physical properties and area specific heat flow. To estimate the basin's thermal development as a function of time, the geohistory of the basin must first be established by reconstruction. In standard basin modeling, the impact of the structural development on the temperature history is seldom taken into account and this may give incorrect thermal and maturation predictions [26].

Several studies exist on temperature modeling in fault zones, but many of these focus on the effects related to uplift and erosion observed in the footwall part of the fault zone and not on the thermal transients in the hanging wall section (e.g., [27–34]). To our knowledge no studies includes magmatism in a fault setting. In our study the main focus is on the transient thermal effects of normal faults with syn- and post-rift deposits, and the influence such structural development has on the thermal effects of sills. Possible transient thermal effects due to erosion have not been pursued in this study.

The calculated pre-intrusion temperatures are dependent on the representation of the basin's structural development [13,25,26]. The purpose of this study is to quantify the thermal effects of the most important factors affecting the thermal history in structurally complex sedimentary basins with magmatic sill intrusions. We do this by running a series of simple models. A more realistic model would require higher structural resolution with variation of lithological and geometrical properties in space and time. However, many simultaneously varying factors affecting the thermal evolution would obscure the magnitude and impact of the individual factors. We therefore first study the thermal effects on structural complex basin on a simple, synthetic profile followed by analysis of the subsequent sensitivity sets: (1) fault displacement, (2) time span of faulting and deposition, (3) fault angle, (4) thermal conductivity and specific heat capacity, (5) basal heat flow and (6) restoration method. The overall goal is to test the sensitivity of faulting, physical properties of the lithologies and choice of fault restoration method on the thermal effect of magmatic intrusions in complex sedimentary basins. We aim for some general conclusions that are applicable to sedimentary basins with normal faults and magmatic sill intrusions.

2. Methods

Our study investigates the relative effect faulting, different physical properties and choice of restoration method have on the resulting thermal and maturation history in structurally complex sedimentary basins intruded by sills. A simple, synthetic profile containing one listric fault and a number of horizons, including syn- and post-rift deposits, is used as the basis for this study (Figure 1). Throughout the simulations, one parameter is changed at a time which allows for evaluating the impact each parameter has on the modeling results. Table 1 shows the different modeling sets, the tested parameter values and default values of non-changing parameters. Shale and sandstone are the applied lithologies as these are common in sedimentary basins worldwide.

Table 1. Input parameters for the modeling. w = with, sh = shale, sst = sandstone, ant = antithetic, inc = inclined, synth = synthetic, kyr = thousand years.

Simulation Set	Tested Parameter	Tested Values	Fault Displacement	Time Span of Faulting and Deposition	Fault Angle	Thermal Conductivity/ Heat Capacity	Basal Heat Flow	Restoration Method
Set 1	Fault displacement	1200 m 500 m 1000 m 2000 m 3000 m	X	10 kyr	Original	All shale	47 $mW \cdot m^{-2}$	Vertical shear
Set 2	Time span of faulting and deposition	10 kyr 1 Myr 5 Myr 10 Myr 20 Myr	1200 m	X	Original	All shale	47 $mW \cdot m^{-2}$	Vertical shear
Set 3	Fault angle	Original Steepest Less steep Least steep	1200 m	10 kyr	X	All shale	47 $mW \cdot m^{-2}$	Vertical shear
Set 4	Thermal conductivity/ Heat capacity	All shale All sandstone Sh basin w/sst layer Sst basin w/sh layer	1200 m	10 kyr	Original	X	47 $mW \cdot m^{-2}$	Vertical shear
Set 5	Basal heat flow	47 $mW \cdot m^{-2}$ 40 $mW \cdot m^{-2}$ 60 $mW \cdot m^{-2}$ 80 $mW \cdot m^{-2}$	1200 m	10 kyr	Original	All shale	X	Vertical shear
Set 6	Restoration method	Vertical shear No fault restoration 10° ant. inc. shear 20° ant. inc. shear 30° ant. inc. shear 10° synth. inc. shear	1200 m	10 kyr	Original	All shale	47 $mW \cdot m^{-2}$	X

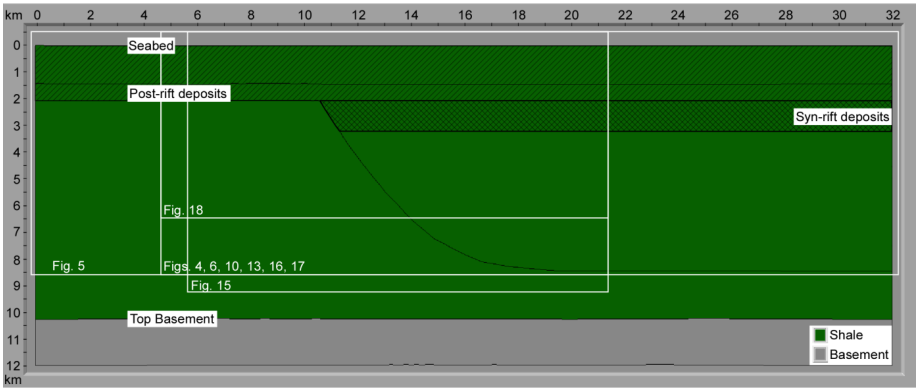

Figure 1. The synthetic profile with one active, listric fault used in the modeling. The green color (in this case) represents shale lithology. White squares indicate the blow-up area of following figures.

2.1. Thermal and Maturation Modeling

The geological, structural, thermal, and maturation history of the studied synthetic profile is performed with BMT (Basin Modelling Toolbox, Tectonor AS), a high-resolution 2D basin modeling software [26,35,36]. All thermal and maturation modeling simulations starts with present day geometry, where every horizon is given a specific age and all polygons are assigned a lithology with related porosity/depth trend, thermal conductivity and specific heat capacity (Table 2, upper part).

Table 2. Lithological parameters used in the modeling, based on standard values published in the literature (e.g., [37,38]).

	Porosity-Depth Trend		Conductivity (kv) ($W \cdot m^{-1} \cdot K^{-1}$)		Heat Capacity
Lithology	**Surface Porosity**	**Exponential Constant (km^{-1})**	**Low Porosity**	**High Porosity**	**($J \cdot kg^{-1} \cdot K^{-1}$)**
Shale (Default)	0.63	0.51	3.00 (6%)	2.80 (60%)	1190
Sandstone (Default)	0.45	0.27	3.30 (6%)	1.50 (40%)	1080
Basement, metamorphic			3.10	3.10	1100
Magmatic intrusions			3.10	3.10	1100
Asthenosphere			3.50	3.50	1100
Shale, average conductivity	0.63	0.51	1.98 (6%)	1.19 (60%)	1190
Shale, max. conductivity	0.63	0.51	4.08 (6%)	2.08 (60%)	1190
Sandstone, average conductivity	0.45	0.27	2.36 (6%)	1.72 (40%)	1080
Sandstone, max. conductivity	0.45	0.27	6.24 (6%)	4.20 (40%)	1080
Shale, min. heat capacity	0.63	0.51	3.00 (6%)	2.80 (60%)	840
Shale, max. heat capacity	0.63	0.51	3.00 (6%)	2.80 (60%)	1420
Sandstone, min. heat capacity	0.45	0.27	3.30 (6%)	1.50 (40%)	760
Sandstone, max. heat capacity	0.45	0.27	3.30 (6%)	1.50 (40%)	3350

The first modeling step is a backstripping process, where one horizon at a time is removed, faults are restored and underlying deposits are decompacted. This process is repeated all the way down to top basement and in this way the section's geohistory is built. All elements that characterize the basin, such as faults, horizons, and lithologies, are parts of the geohistory process, and must be carefully defined. For the geohistory reconstruction a special type of grid was developed in BMT [26]. The grids are vertical line segments that are connected to the base of a polygon. A grid is always created at each digitized point in the present-day polygon. Additional grid columns are added to the section automatically. The number of inserted grid points can be controlled by the user (the default is 70). The foundation for thermal and maturation modeling is established during the geohistory process, and it is therefore important that the geological reconstruction of the basin is accurate.

The next step in the modeling process is the thermal development of the basin. BMT utilizes finite difference calculations by conduction with a rectangular finite difference grid of varying sizes (cf., [7,26]). For every reconstructed timestep in the geohistory, BMT builds a new high-resolution thermal modeling grid. Where needed, grid lines are automatically inserted so that the geometry is accurately represented. Around small features, like sills, the grid size is especially fine to ensure realistic calculations. The finite difference grid in this study consists of minimum 400 × 400 cells of varying sizes with an average size of 80 m × 30 m (width and height). The spatial variation in rock properties and possible differences from one timestep to the next are adjusted for so that appropriate finite difference calculations are maintained.

The finite difference calculation by conduction is controlled by the temperatures from the previous timestep, thermal conductivity (vertical and horizontal) and specific heat capacity of the basin's lithology/lithologies (see Appendix A for details on the numerical temperature model from Fjeldskaar et al. [7]). Temperature-dependent thermal conductivity is used, which commonly leads to reduction of the conductivity with increasing temperature. However, compared to conduction variations derived from differences in porosity and lithology, the temperature dependent variations are considered to be modest [35]. The lower boundary condition of the temperature calculations is the basal heat flow from the mantle, and the upper boundary condition is the paleo-surface temperature. The surface temperature is kept constant at 7 °C, and the heat flow is constant over the profile. Fjeldskaar et al. [7] tested BMT's numerical model versus an analytical model on the temperature effect of sill emplacement, and documented good performance for high-resolution modeling, both spatially and temporally.

Maturity modeling is completed in BMT and all calculations in this study assume kerogen type II, the most common in marine shales [39]. Classical first-order kinetics for the decomposition reactions is the basis for the maturation model in BMT (see [7,26]). In this study the whole basin is set as source rock in order to study the potential maturation effect of magmatic sill intrusions. However, for a case study, only the potential source rock would be defined as such a sequence.

2.2. Restoration of Faults

Several algorithms exist for restoring the structural evolution of basins. The different algorithms result in different basin and fault geometries, which again impact the calculated thermal history. Commonly, basin modeling simplifies the structural reconstruction of basins, e.g., by not reconstructing the faults through time, regardless the fact that hydrocarbons often accumulate in complex geological structures associated with faults [26]. According to Dula [40] reconstruction with simple inclined antithetic shear of 20° is one of the methods that best represents the observed fault shape, but all tested reconstruction methods in that study gave adequate results.

The present study utilizes vertical shear as a standard fault reconstruction method. However, different segments of simple shear, including inclined antithetic and synthetic shear are explored (Figure 2). Furthermore, we investigate how the different resulting geometries impact the thermal history. Because BMT restore faults solely by vertical shear, and the software Move (Petex Ltd.) does not have the ability to perform thermal and maturation modeling, both Move and BMT were used to model the structural development of the section. In the restoration process BMT and Move both use the backstripping process, which removes layers one by one and decompact the underlying sequences based on the given porosity-depth trend for the assigned lithology/lithologies. The porosity calculations are based on exponential functions (cf., [37]) and the same values are used in both softwares (Table 2). Move is a commercial software restoring geological cross sections by kinematic algorithms. Six algorithms are available for fault restoration, these are: simple shear, fault parallel flow, fault bend fold, fault propagation fold, trishear, and detachment fold. BMT is a non-commercial basin modeling software with the ability to perform fault restoration (by vertical simple shear) so that structural effects on temperature estimates are accounted for (cf., [26]).

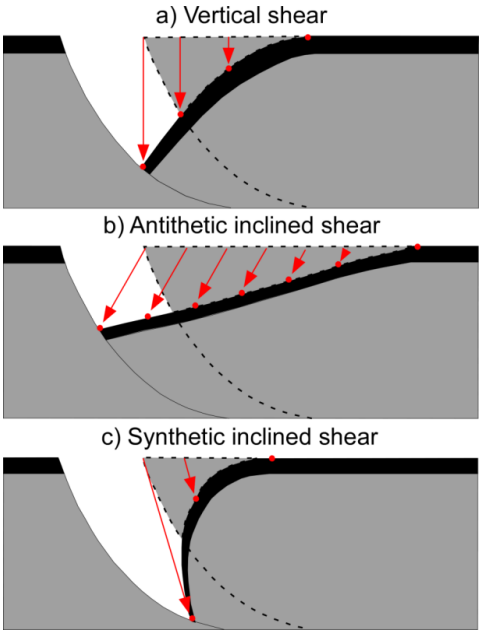

Figure 2. Illustration of the technique of (**a**) vertical simple shear, (**b**) antithetic inclined simple shear and (**c**) synthetic inclined simple shear. Antithetic simple shear results in a broader basin compared to for instance synthetic shear. Modified after Fossen [41].

In our study Move was used to restore the fault by antithetic and synthetic inclined shear. The tested angles for inclined shear are summarized in Table 1. The resulting reconstructions from Move are replicated in BMT by utilizing a "volume editing" function (cf., [26]). This method enables calculations of the thermal histories for the different restoration methods. All models have the same starting geometry. However, through restoration by different algorithms the paleo geometries will differ and so will the temperature histories.

2.3. Thermal Effects of Sills

On reflection seismic data, upper and lower boundaries of sills can be difficult to discern due to limited vertical resolution (cf., [42–45]). Many sills may therefore be left out in seismic interpretations due to sill thicknesses below the detection limit of the data (e.g., [44,45]). Sill thickness, both when sills intrude individually or as clusters, has a large impact on the temperature and maturation in sedimentary basins (e.g., [8,25]). The relative timing between sills emplaced as clusters is especially important if potential source rocks are located between sills [25]. Reported sill thicknesses from the literature vary from ~10 cm to >400 m (e.g., [44,46–55]). In our study a modest sill thickness of ~50 m has been chosen for the modeled sills and we assume the sills to intrude during one pulse with a magma temperature of 1000 °C. In BMT this is done by changing the lithology in sill polygon from shale to sill lithology, with related physical properties at time of intrusion. The sills have been modeled to intrude at various times relative to fault slip. This is done to study the interaction of two transient thermal effects simultaneously. As the largest thermal and maturation impact of sill intrusions are found at 3–5 km depths [25], the sills are modeled to intrude within this depth range. Commonly magmatic sills observed in the field and on seismic images (e.g., [7,52]) are layer concordant. Therefore, the sills in the study are modeled accordingly.

Latent crystallization heat introduces an extra source of heat when magma cools and starts to crystallize [56,57]. This extra heat source is not taken into account, as it is the relative differences between scenarios that are of interest in our study. Heat advection by fluids in relation to magmatic intrusions is common (e.g., [5,58–61]). However, convection is not accounted for in our modeling, as convection is considered insignificant in low permeability rocks (e.g., [7,8,13,25,62]) and is beyond the scope of this study.

3. Modeling Strategy and Results

A basin not subjected to tectonic deformation undergoes a slow rate of erosion or sedimentation and has a gradual temperature increase with burial depth. Such a basin is in steady state [63]. On the other hand, structurally active basins may undergo sudden erosion or high influx of sediments, e.g., due to increased accommodation space during faulting, leading to abrupt changes in the geothermal gradient. When magmatic intrusions are emplaced into such active basins, the temporary, local change in temperature is not solely an effect of the hot magma intruding the system, but also due to transient thermal effects caused by structural development. Figure 3 shows the studied synthetic profile assuming thermal steady state with input parameters as given in Table 2.

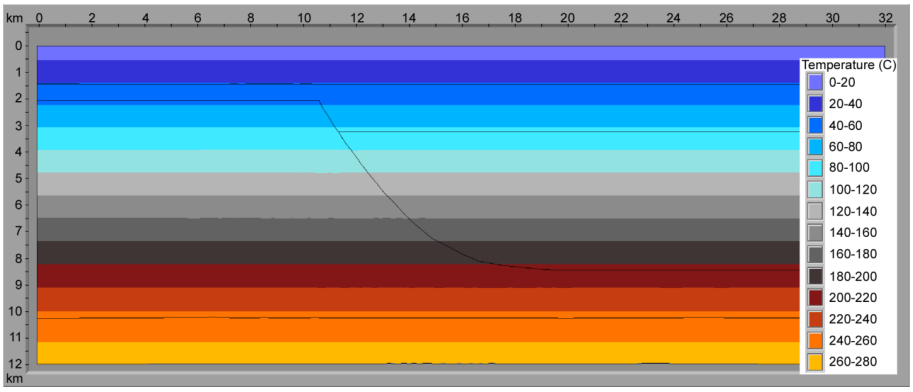

Figure 3. Temperature regime for the modeled basin in steady state solution.

Emplacement of sills and significant structural development may occur within the same timeframe (e.g., [30,64,65]). Therefore, we want to investigate the combined transient thermal contributions from the structural development and magmatic intrusions. The results should be considered as trends, not absolute values, as the study aim to give some general conclusions. The models are considered to have arrived at steady state when the whole basin show transient temperatures <1 °C from the steady state temperatures. However, for some cases exact steady state conditions are obtained right after reaching this limit, for other cases several million years (Myr) are required before actual steady state is obtained.

3.1. Thermal Effect of Slip along a Single, Normal Fault

Normal faulting causes downward displacement of sediments and generally deposition of syn-rift sediments (ref., Figure 1) in the hanging wall section of the fault zone. These down faulted sediments in the hanging wall are initially colder than the sedimentary rocks at the same depth in the footwall part, which result in transient thermal effects mostly in the hanging wall part (Figure 4). The basin is thermally unstable and results in a temperature difference up to 40 °C from one side of the fault zone to the other at the time of fault slip (Figure 4). Post-rift sediments deposited over the whole basin leads to thermal transient effects also in the foot wall section. However, these temperature differences will vary depending on physical properties and geometry of the basin. In the event of extension and normal faulting, the footwall temperatures are hardly influenced at time of fault slip. At 1000 years after the fault

movement the isotherms in the footwall show a small downward bend towards the fault zone, indicating a small thermal influence by the neighboring colder sediments in the hanging wall (Figure 4).

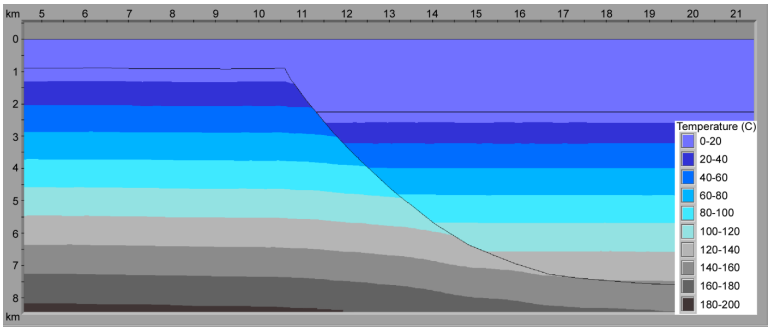

Figure 4. Temperature regime in the uppermost 8 km of the basin 1000 years after fault movement and sediment deposition. Fault slip is 1200 m.

The main temperature effect of magmatic sills lasts only some thousand years (see e.g., [25]). In accordance with this, we have here assumed that the syn- and post-rift sediments (Figure 1) of the timestep with fault movement are deposited over a period of only some thousand years. Deposition of these sediments leads to thermal instability in the basin. Figure 5 shows the temperature difference between steady state and transient models for deposition of these sediments at 10,000 years (10 kyr) and 500 kyr after fault slip. This causes larger parts of the basin to have transient temperatures up to 20 °C lower than under steady state conditions even up to 500 kyr after fault slip (Figure 5). Around 10 Myr is required for the basin to reach steady state temperatures.

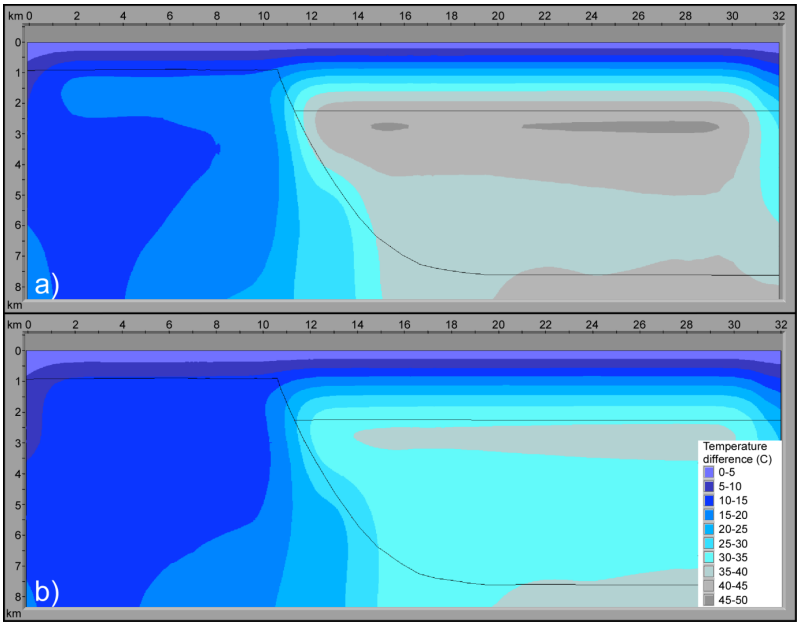

Figure 5. Temperature difference between steady state and transient model of the studied synthetic profile at 10 kyr (**a**) and 500 kyr (**b**) after fault displacement.

3.1.1. Fault Displacement

The original model has a fault displacement of 1200 m with syn-rift deposits of the same thickness and about 600 m of post-rift deposits, taking place over one timestep (Figure1). These post-rift deposits are kept unchanged in all tested scenarios. Additional four fault displacement models were tested; 500 m, 1000 m, 2000 m, and 3000 m (Table 1). As expected, temperature differences across the fault zone increases with the fault displacement. With 3000 m fault slip there is a temperature difference of more than 50 °C across the fault zone immediately after fault slip (Figure 6a). In the footwall part, the isotherms make a gentle downward bend towards the fault zone. As time passes, a gradual heating of the sediments in the hanging wall section occurs and the bend of the isotherms from the footwall side ties with those of the hanging wall (~10 kyr after faulting) creating continuous isotherms (Figure 6b,c). There is also a slight temperature change in the footwall part due to the deposition of cold post-rift sediments over that area.

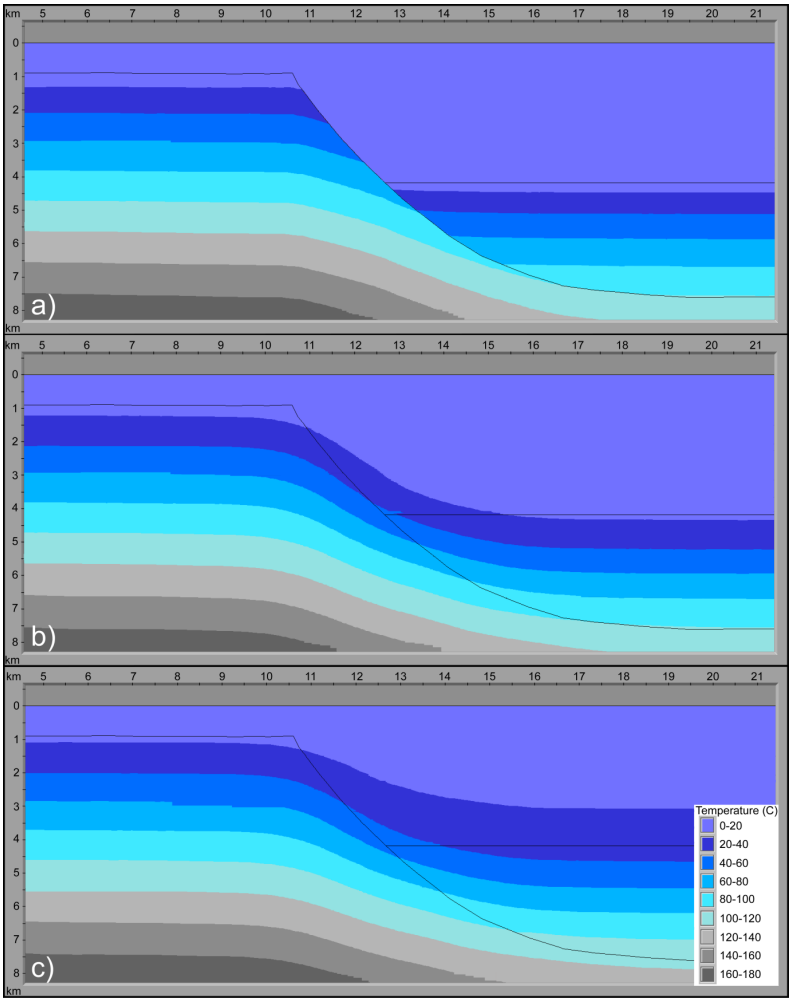

Figure 6. Temperature development in a basin with 3000 m fault slip: temperatures at 1 kyr (**a**), 500 kyr (**b**), and 5 Myr (**c**) after fault slip.

With increasing fault slip but within the same timeframe, the volume of deposited sediments and time needed for basin to regain steady state increases. For the modeled basin with 500 m of fault slip, large parts of the basin differ ~20 °C from the steady state basin 10 kyr after displacement (Figure 7a). Around 9 Myr later the basin obtains steady state. When fault displacement is 3000 m, large parts of the hanging wall section differ more than 50 °C from the steady state basin at 10 kyr after fault slip (Figure 7b). Steady state is achieved approximately 11 Myr after fault slip. As expected a basin with larger fault slip and higher influx of sediments requires more time to regain steady state, compared to a basin with smaller fault slip and less sediment deposits.

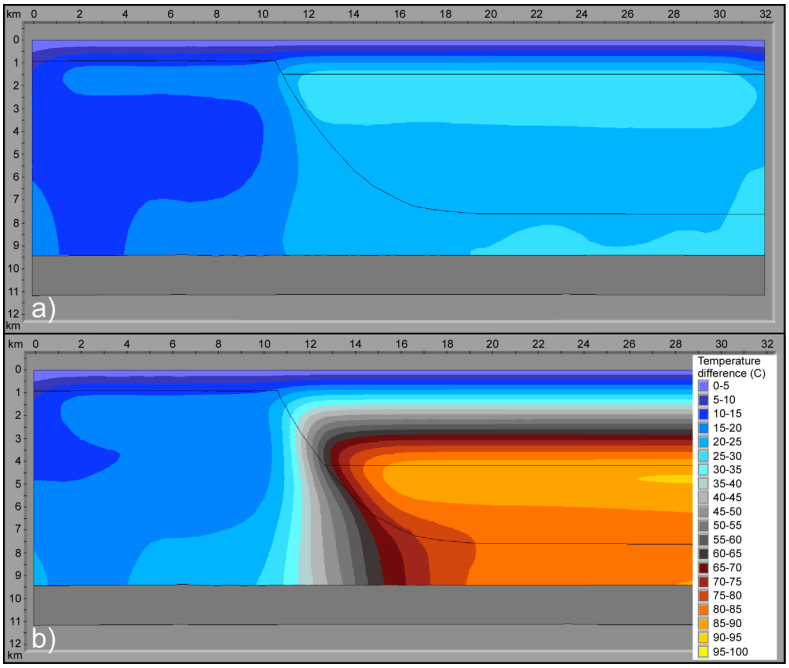

Figure 7. Temperature difference between steady state and transient temperatures for fault slip of 500 m (**a**) and 3000 m (**b**) at 10 kyr after fault slip.

3.1.2. Time Span of Faulting and Deposition

So far the modeling assumes the fault slip to be almost instantaneous (taking place over 10 kyr). The next set of models explores four different time spans of faulting and deposition of the same amount of sediments: 1, 5, 10, and 20 Myr. The results show that slower faulting and deposition rates, as expected, keep the basin closer to a steady-state condition compared to high rates (Figure 8a,b). Adding 10 Myr to the faulting and deposition time results in a basin with transient temperatures much closer to those of steady state throughout the whole period. For a faulting and deposition rate over 20 Myr, the basin is never in a state of thermal instability. The resulting trend show that basins with the same amount of sediment input and faulting and deposition time up to 10 Myr regains steady state approximately 10 Myr after faulting initiated (Figure 8c). This means that from time of faulting and deposition to the process is finalized, more time is required for a basin with rapid fault slip and deposition to regain steady state compared to a basin with slow fault slip and deposition. It emphasizes how crucial the time relation is for faulting and deposition and basin's thermal development after fault slip.

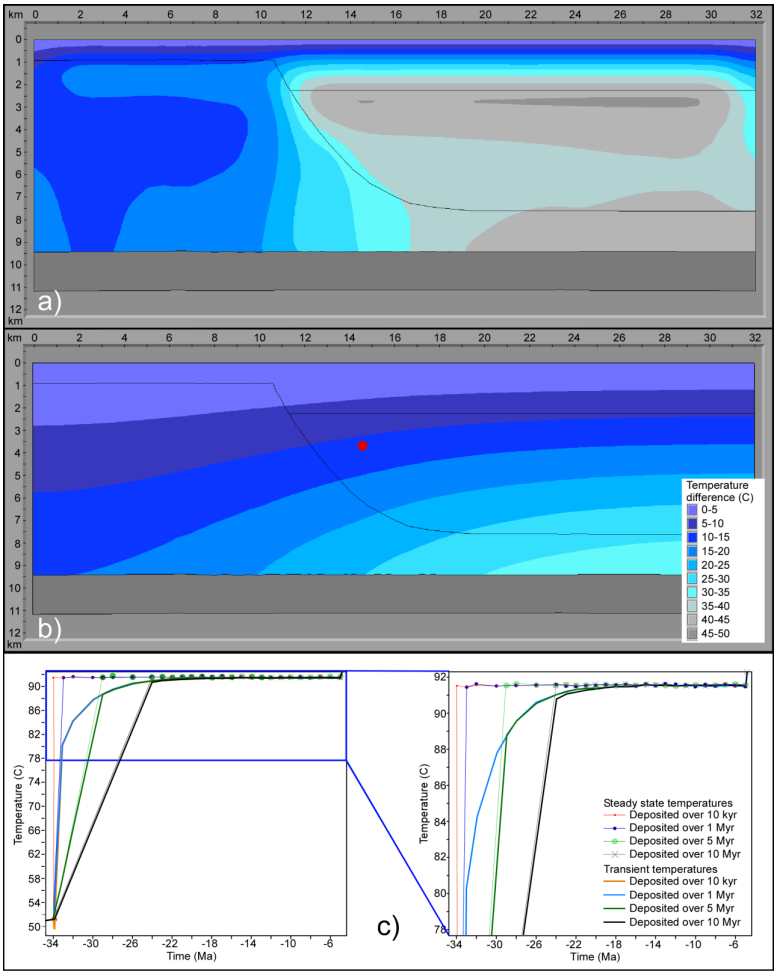

Figure 8. (**a**) Temperature difference between steady state and transient temperatures with fault slip and deposition over 10 kyr. (**b**) Temperature difference between steady state and transient temperature with fault slip and deposition over 1 Myr. Temperatures in (**a**,**b**) are from the same timestep, 10 kyr and 1.01 Myr respectively after faulting started. The red point in (**b**) indicates location of point plot in (**c**). (**c**) Resulting temperatures for four tested time spans of deposition of syn- and post-rift sediments.

3.1.3. Fault Angle

The previous results show that the largest thermal differences between steady state and transient temperatures are found in the hanging wall part of the basin. For all the tested fault angles the results are broadly similar, but the temperature effect will change with the fault angle. As the fault angle is changed, so is the affected area of the hanging wall. With a steeper fault angle a smaller part of the basin experiences the largest thermal instabilities (Figure 9a). The opposite is the case for lower fault angles, a larger part of the basin will then experience higher thermal instabilities before the basin regain steady state (Figure 9b). Five different fault angles have been tested (Figure 9a,b). All scenarios show temperature differences up to 45 °C between transient and steady state models. Around 10 Myr after fault slip all scenarios regain steady state temperatures.

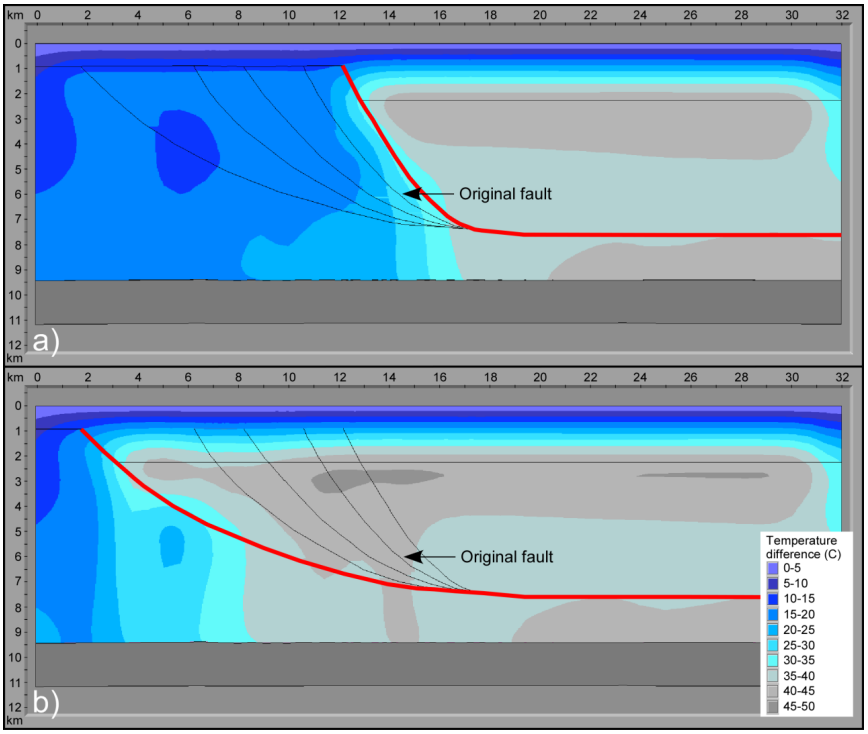

Figure 9. Temperature difference between steady state and transient model 10 kyr after fault slip for the steepest (**a**) and the least steep (**b**) studied listric fault.

3.1.4. Thermal Conductivity and Specific Heat Capacity

The thermal conductivity ($W \cdot m^{-1} \cdot K^{-1}$) of a lithology relates to the rock's ability to transfer heat. Rocks with low thermal conductivity result in warm basins, while high thermal conductivity rocks give colder basins. A lithology's specific heat capacity ($J \cdot kg^{-1} \cdot K^{-1}$) is the physical property crucial for the time frame needed to transfer heat through the stratum and thus for the time needed for basins to regain steady state after sediment deposition or erosion. So far the section has been modeled as all shale with properties as listed in Table 2. Commonly, basins consist of altering layers of different lithology types, often shale and sandstone. Therefore, the following four scenarios have been compared: all shale, all sandstone, all shale with one sandstone layer, and all sandstone with one shale layer.

Thermal conductivities and specific heat capacities of shale and sandstone show a large variation (e.g., values in Table 2). The default values are given in Table 2 and to illustrate the span of values within the same lithology segment, we refer to Čermác and Rybach [38]. Their minimum and maximum specific heat capacities and the average and maximum thermal conductivities of sandstone and shale are used in this study (Table 2). In order to determine the thermal conductivity values based on the rock's porosity, the mixing law arithmetic mean model [66] has been used:

$$k = \Phi \cdot k_f + (1 - \Phi) k_s, \quad (1)$$

where the thermal conductivity (k) is obtained on the basis of the rock porosity (Φ) by combining the thermal conductivity of rock matrix (k_s) with that of the pore fluid (k_f).

Generally, sandstones have higher thermal conductivities than shales, resulting in colder basins where they are abundant. The results from the homogeneous basins, either all shale or sandstone,

coincide with this, showing high temperatures in the basin when the thermal conductivity is low, and lower temperatures when the thermal conductivities are high. A comparison between two basins with the same fixed specific heat capacity, but with one basin modeled with average shale conductivity, to another basin modeled with default shale conductivity, shows up to 140 °C difference between the two models shortly after fault slip (Figure 10a). With fixed specific heat and changing conductivity the results show that the basin needs longer time to regain steady state in basins with low thermal conductivity values due to the higher temperatures obtained in these basins (Figure 10b). This applies for both scenarios with all shale and all sandstone of varying thermal conductivity. Steady state is regained from 3–22 Myr after fault slip and the quickest scenario to regain steady state is the sandstone basin with maximum thermal conductivity.

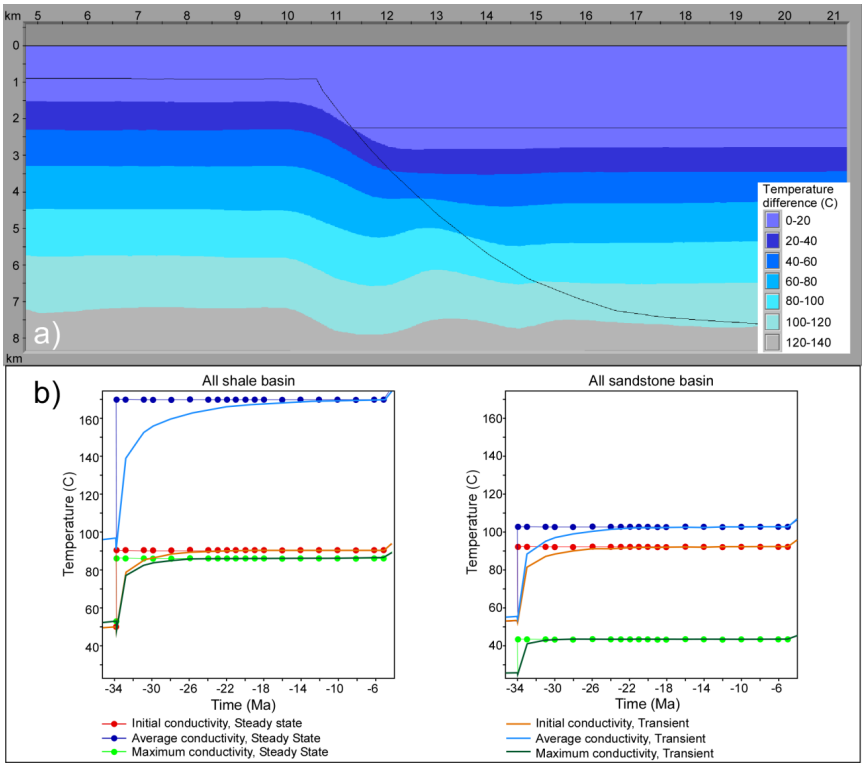

Figure 10. (**a**) Thermal difference between transient temperatures of basin (10 kyr after fault slip) modeled with average conductivity to basin modeled with default conductivity. (**b**) Point plot results from location of point given in Figure 8b, showing the steady state and transient temperatures for the three tested conductivities for shale and sandstone. Conductivity values given in Table 2.

In the case where the thermal conductivity is fixed and the specific heat capacities are changed in the different modeling scenarios (Table 2, lower part), the steady state temperatures for all the scenarios are, as expected, the same (Figure 11). However, with increasing specific heat, the time needed for the basin to obtain steady state increases (Figure 11). This is especially visible in the point plot for sandstone basin in Figure 11, because of large difference in the published heat capacity values of sandstone, but the effect is also visible for the shale basin. For all tested scenarios steady state is obtained between 8–18 Myr after fault slip.

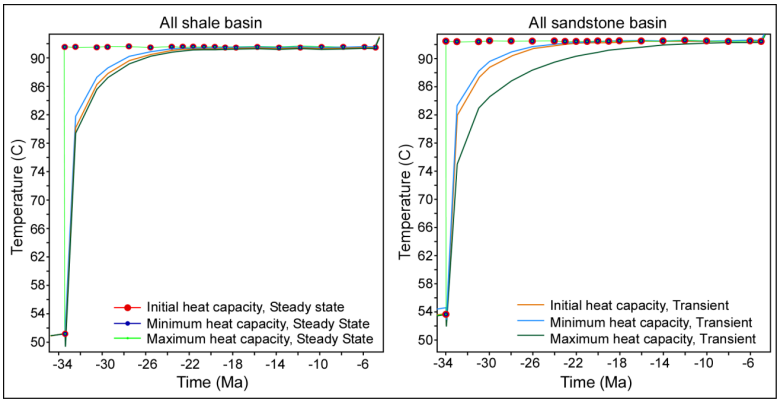

Figure 11. Resulting temperatures for the three tested specific heat capacities for shale and sandstone. Location of studied point indicated in Figure 8b. Heat capacity values given in Table 2.

To accommodate the fact that basins commonly consists of different lithologies, the polygon with syn- and post-rift deposits have been changed in the following simulation (Figure 12a). The thermal conductivity is fixed with values as for the default shale or sandstone (Table 2). However, the specific heat capacity is changed using default, minimum, and maximum values for the sandstone and shale (Table 2). With the presence of a sandstone layer in an otherwise shale basin, the results show that the temperatures in the basin increases. For the opposite case, a layer of shale in an otherwise sandstone basin, the temperatures in the basin decreases (Figure 12b).

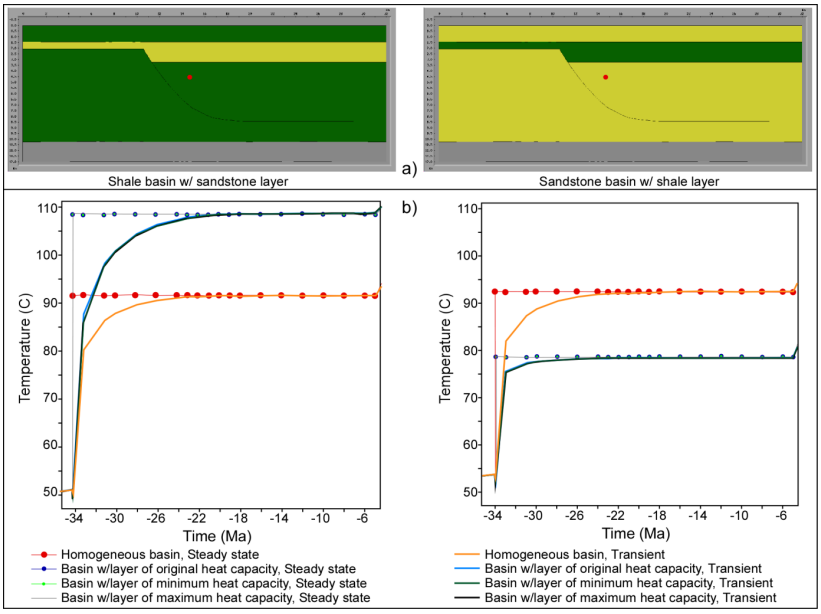

Figure 12. (**a**) Shale and sandstone basins with sandstone layer and shale layer respectively. The red point indicates location for point plot in (**b**). (**b**) Results show the temperatures for the three tested heat capacities for shale basin with one sandstone layer and sandstone basin with one shale layer. For comparison, temperatures for homogeneous basin are also plotted. For heat capacity values see Table 2.

The variation of specific heat capacity in a homogeneous basin resulted in quite a time gap (8–18 Myr) for the sandstone basin to regain steady state (Figure 11). However, the shale basin required less time to arrive at steady state for the tested specific heat capacities (8–10 Myr). For homogeneous basins, shale or sandstone, steady state was regained around 10 Myr after fault slip (Figure 12b). The presence of another lithology influences the basin temperatures and thus the time needed for the basins to regain steady state. For a shale basin with a sandstone layer, steady state was obtained around 13 Myr after fault slip for all the specific heat capacities. Sandstone basin with a shale layer regains steady state around 6 Myr after fault slip regardless of the specific heat capacities (Figure 12b). These results are related to the porosities at the depth at which the different lithology layers are modeled and the contrasting thermal conductivity for shale and sandstone.

3.1.5. Basal Heat Flow

The basal heat flow, which is the heat sourced from the mantle, transferred through the basin and constitutes the lower boundary condition in the models, is so far kept constant at 47 mW·m^{-2}. This basal heat flow value is slightly above one heat flow unit and is typical for some continental shelves, e.g., parts of the Norwegian Continental Shelf. However, to study the influence of the basal heat flow on the temperature development in the basin, three additional values were tested: 40 mW·m^{-2}, 60 mW·m^{-2}, and 80 mW·m^{-2} (Table 1). Figure 13b shows the results for 40 and 80 mW·m^{-2} together with the default heat flow (47 mW·m^{-2}). Increased heat flow leads to higher steady-state temperatures and longer time is therefore needed for the basin to regain steady state (Figure 13b). The resulting transient temperatures of basins modeled with 80 mW·m^{-2} and 40 mW·m^{-2} show thermal differences up to 140 °C (Figure 13a). For the tested values, the models regain steady state approximately between 9 and 12 Myr after the fault slip. Increasing basal heat flow gives higher temperatures in the basin, and as a consequence, a longer time is needed for the basin to arrive at steady state after fault slip.

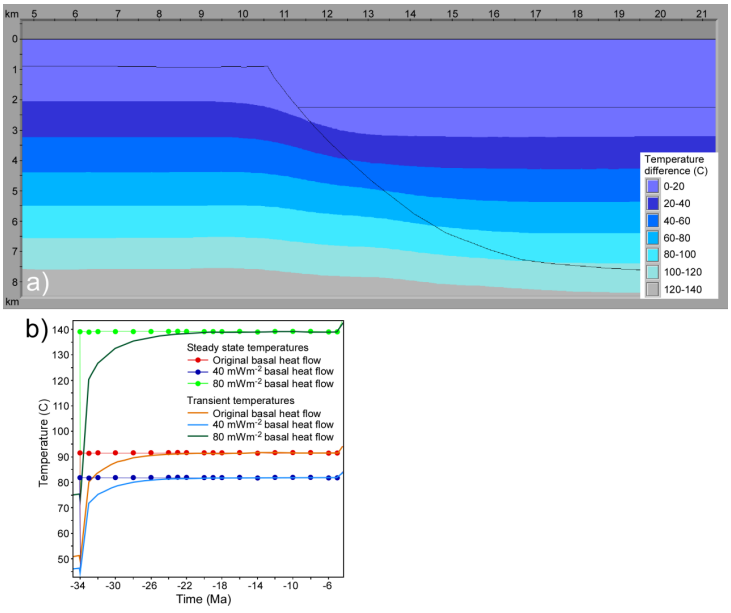

Figure 13. (**a**) Thermal difference between transient temperatures in basin with basal heat flow of 80 mW·m^{-2}, to basin with basal heat flow of 40 mW·m^{-2} at 10 kyr after fault slip. (**b**) Results show the temperatures for the default and the two extreme values for heat flow: 47 mW·m^{-2}, 40 mW·m^{-2}, and 80 mW·m^{-2}. Location of studied point is indicated in Figure 8b.

3.2. Restoration Methods

Different fault restoration methods cause different basin geometries. It is of interest to explore what effect these different geometries have on the resulting basin temperatures. In addition to vertical shear, we have therefore tested the basin reconstruction for 10° antithetic and synthetic shear, 20° and 30° antithetic shear and a case without fault reconstruction (Table 1). Basin reconstruction without fault restoration was done by moving the hanging wall section vertically up such that the timeline split by the fault zone is horizontally connected. This process gives no lateral mass movements of the basin. Vertical simple shear modeling was, as mentioned in the method section, done by BMT, while the alternative fault reconstructions were performed with Move. Antithetic simple shear results in a wider basin (Figure 2) and the larger the angle, the wider the basin. Synthetic simple shear results in a narrower basin (Figures 2 and 14) relative to the other methods. Vertical simple shear falls in between these two, while basin reconstruction without fault restoration results in a geometry which is quite different from the other restored scenarios. Figure 14 shows the resulting geometries of the fault plane and top and bottom basement after fault slip of the six tested reconstruction methods. The basins with non-restored fault and restored by 10° synthetic inclined shear (purple and green line respectively, Figure 14) result in the shallowest hanging wall and top basement.

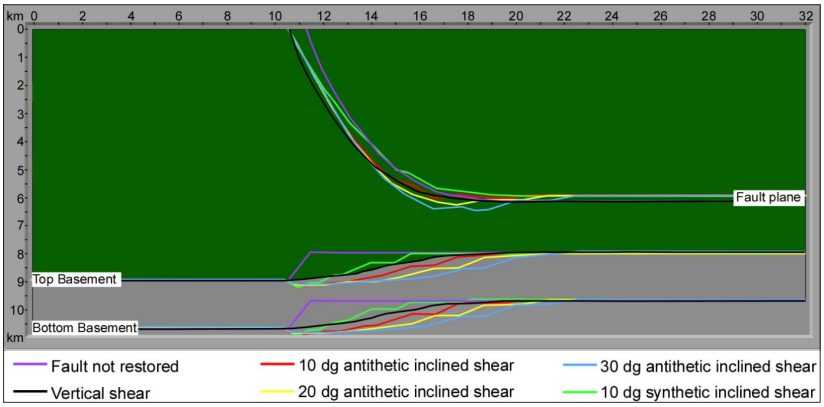

Figure 14. Resulting basin geometries after fault slip with the tested fault restoration methods. The different colored lines represent the resulting geometry of fault plane and Top and Bottom Basement after fault is restored by the six tested restoration methods. dg = degrees.

The geometry variations resulting from the tested restoration methods involve varying footwall and hanging wall area and burial depth, which result in differences in the thermal calculations, especially in the footwall section. Therefore, the thermal differences between them are concentrated in the footwall part of the basin at the time of fault slip (Figure 15). Figure 15c shows that the temperatures prior to fault slip show a larger difference on the footwall side compared to the hanging wall side. The comparison between the non-restored basin to basin restored by 30° antithetic shear, shows the largest area with thermal differences (Figure 15a), while the thermal differences between vertically- and non-restored basins are the most pronounced (Figure 15b). Although the thermal differences do not last long, ~1 Myr, such temperature differences might play a role concerning timing of generation and ultimately migration of hydrocarbons. For this particular case, the modeled thermal differences result in up to 40% maturation difference of the potential organic matter in a limited time and area of the footwall section (not shown here). All the tested restoration methods require approximately 10 Myr to achieve a steady state after fault slip. We therefore conclude that the tested restoration methods do not lead to large differences in time needed for the basins to achieve steady state. However,

temperature differences due to different restoration methods may lead to temperature variations that might influence the maturation calculations.

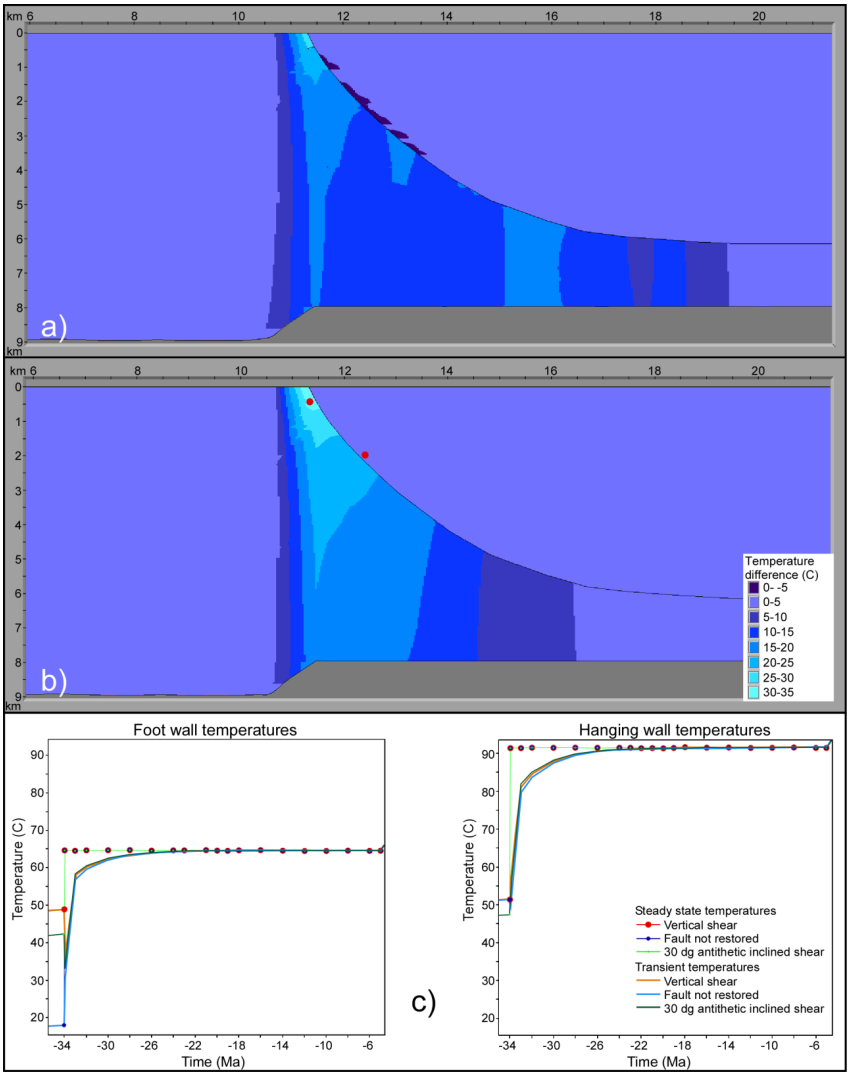

Figure 15. (**a**) Temperature difference between a scenario restored with 30 degrees antithetic inclined shear, compared to a scenario with non-restored fault. (**b**) Temperature difference for a scenario restored with vertical shear compared to a scenario with non-restored fault. (**c**) Temperature point plot from foot wall (left) and hanging wall (right) in the two points indicated in (**b**).

3.3. Sill Intrusions in the Basin

As mentioned above, earlier studies have pointed out the importance of host-rock temperatures at time of emplacement for the resulting thermal effects of intrusions [8,13,16–18]. In our study two sills, ~50 m thick, one in the hanging wall and one in the footwall, have been modeled to intrude the basin with increasing time lapse after fault slip. Figure 16 shows the results for sills intruding at time

of fault slip, 1 Myr and 10 Myr after fault slip. There is a clear thermal instability on both sides of the fault zone. However, due to the masses of faulted rock and larger deposits of sediments in the hanging wall section, the thermal effects of the fault displacement are more pronounced here. Therefore, the largest differences in the thermal effects of the sills as time passes are expected to be found here.

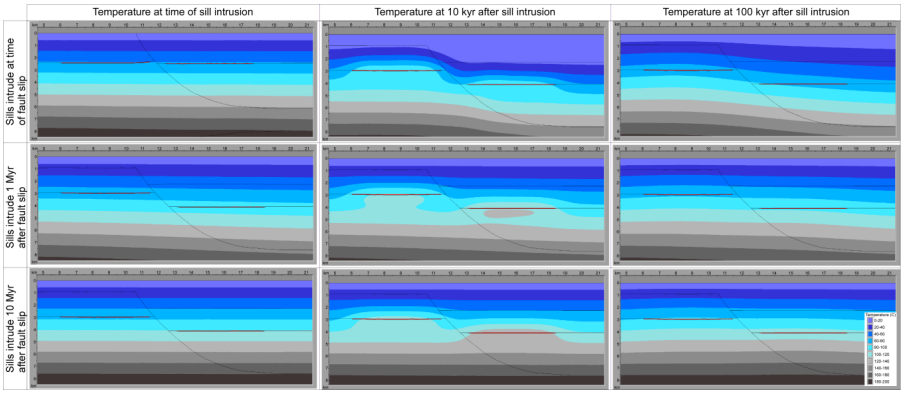

Figure 16. Temperature results for sills intruding with different timing in relation to fault slip. Temperatures to the left are at time of intrusion, in the middle, 10 kyr after intrusion, to the right, 100 kyr after intrusion.

At the time of intrusion, the temperatures in the close proximity of the sills increases dramatically (cf., [25]). As time passes the area with increased temperatures grow and consequently the temperatures starts to fall. The thermal effect of sills has a quick rise and fall within the first 1 Myr after intrusion.

Modeling results at 1000 years after fault slip show that there is a temperature difference up to 40 °C on either side of the fault zone (Figure 4). Results also show that as time passes the basin regains steady state (Figure 6a–c), which for most scenarios in this study occur somewhere between 3 and 22 Myr after fault slip. For sills intruding at time of fault slip the host-rock temperature effects are lower compared to sills intruding into a basin with a time lapse after fault slip, which have temperatures closer to that of a basin in steady state. A consequence is that sills intruding with a time lapse in relation to fault slip have higher background temperatures and the thermal effects will be more prominent (Figure 16). These thermal differences are still present 100 kyr after sill intrusion. In the hanging wall there is a temperature difference around 40 °C between the cases where the sills intrude at time of fault slip and 10 Myr after fault slip (Figure 16). The highest potential host-rock temperature effect of intruding sills will be in a steady state basin.

The largest thermal differences between basins with faults restored in different ways, was found between basin with fault restored by vertical shear to basin with non-restored fault (Figure 15b). Therefore, we have tested the possible influence of a non-restored fault basin with sills on the calculated thermal effects. As the thermal differences between a basin restored by vertical shear to a basin with a non-restored fault was found in the footwall part of the fault zone (Figure 15b), this is also the area where it is expected that possible differences in thermal effects of sills will be found (Figure 17a). However, the thermal results of the basin with sills and non-restored fault show very small thermal differences from basin with sills and fault restored by vertical shear (Figures 16 and 17a). The most pronounced thermal difference is found between the scenarios where sills intrude 1 Myr after fault slip. These small temperature differences will not significantly influence the maturation calculations for the two scenarios.

Sedimentary basins worldwide normally consist of changing layers of different lithologies with contrasting properties. A homogeneous shale basin with a lower thermal conductivity, such as the average conductivity used in this study (Table 2), result in a warmer basin (Figure 10a,b) and

consequently gives a higher host-rock temperature effect for intruding sills. This emphasizes that the basin lithologies and their thermal conductivities have large influence on the temperatures in the basin. We have here tested a case where the sills intrude into a shale basin with a sandstone layer (Figure 12a). The results show no differences for the sills intruding into the basin at time of fault slip (Figure 17b). However, as time passes (1 Myr and 10 Myr after fault slip) the presence of the sandstone layer makes a difference in the resulting thermal effects of the sill intrusions. Sills intruding 10 Myr after fault slip cause thermal differences in some areas up to 20 °C in both the footwall and hanging wall 10 kyr after sill intrusion (Figures 16 and 17b).

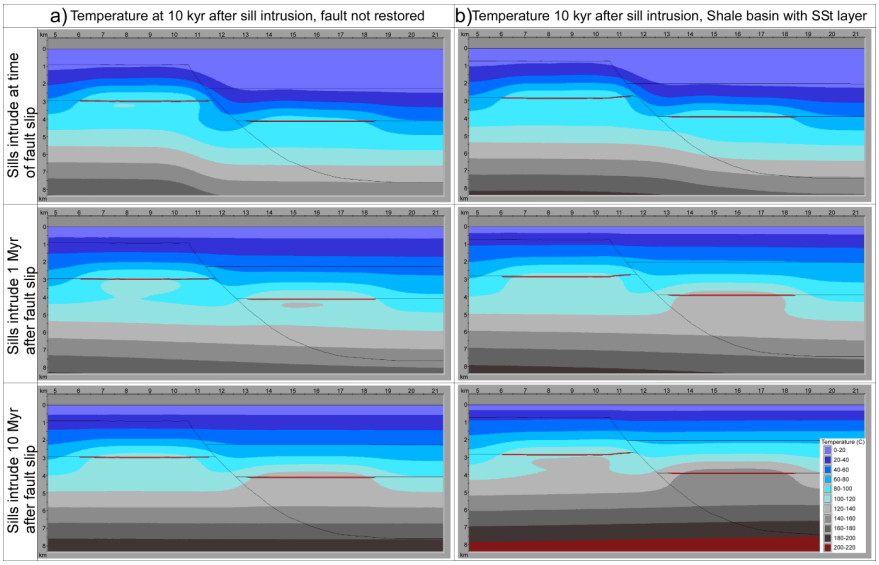

Figure 17. (**a**) Calculated temperatures 10 kyr after sills intrude into a basin with non-restored faults. (**b**) Calculated temperatures 10 kyr after sills intrude into a shale basin with a sandstone layer as shown in Figure 12a left.

As the results in Figures 16 and 17 show, the thermal impact of sill intrusions are more pronounced when emplaced into a basin closer to thermal steady state. This more pronounced thermal impact also influences to a small degree the maturation levels around the sills, especially the area above the sills in the hanging wall (Figure 18a). Reports from onshore and offshore sedimentary basins with magmatic intrusions show that sills often occur in clusters (e.g., [6,9,52,67]). It is considered that multiple sills intruding at different levels within a certain time frame thermally impacts a larger rock volume of the basin compared to one single intrusion (e.g., [8,21,68]). To replicate a basin with clusters of sills, two more sills have been added to the model, one on either side of the fault zone. The thermal effect of sill swarms intruding with different timing relative to fault slip have a large impact on the matured organic material, particularly in the area between the sills on both sides of the fault zone (Figure 18b). In the heterogeneous basin, the warmer host-rock temperatures compared to the homogeneous basin, result in more transformed organic material on both sides of the fault zone for sills intruding at time of fault slip, as well as for sills intruding 10 Myr after fault slip. However, the maturation differences between the homogeneous and heterogeneous basins are more prominent when the sills intrude 10 Myr after fault slip (Figure 18b).

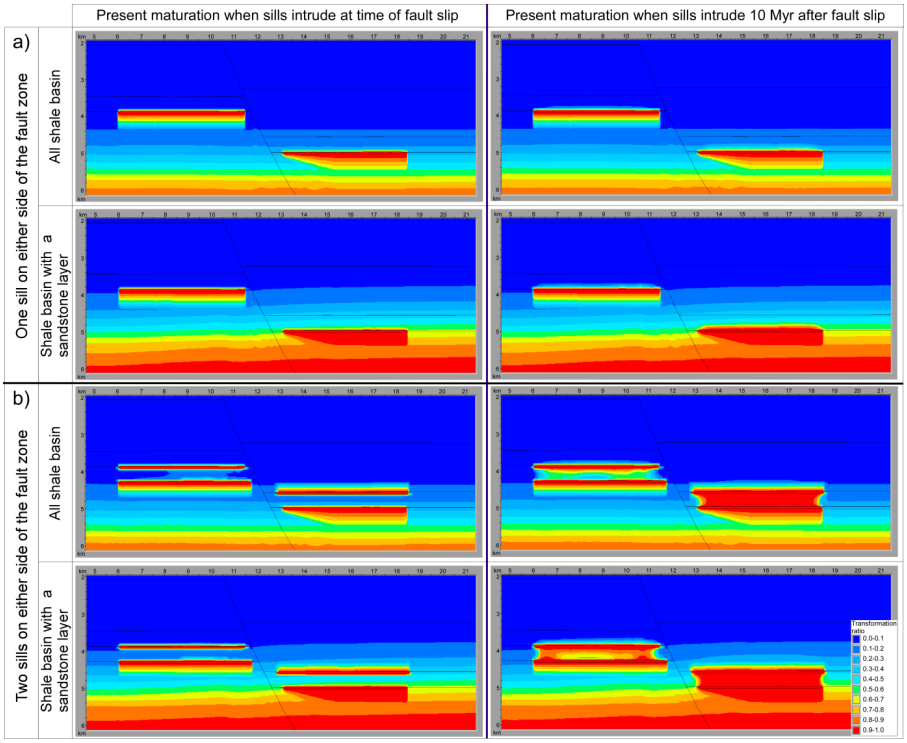

Figure 18. (**a**) Calculated maturation for one sill intruding on either side of the fault zone. (**b**) Calculated maturation for two sills intruding on both sides of the fault zone. Left side show results for sills intruding at time of fault slip. Right side show results for sills intruding 10 Myr after fault slip.

4. Discussion

The purpose of this work was to study the transient thermal effects in structurally complex basins with normal faults and sill intrusions. To uncover trends of several parameters transient thermal effects in sedimentary basins, both extreme and realistic values were tested. Three specific cases were addressed: the transient thermal effects of normal faulting, the ultimate effect of fault restoration method on thermal modeling, and the impact of sill intrusions in structurally complex basins. Interesting effects were discovered and are discussed separately in the following.

4.1. Transient Thermal Effects in Relation to Normal Fault Slip

Figure 4 shows that the geothermal gradient, especially in the hanging wall, changes abruptly after fault displacement and with time the basin arrives at a thermal steady state (Figure 6). The isotherms in the footwall are somewhat affected by down-faulted colder rocks and deposition of colder sediments in the hanging wall, which is in accordance with the work by ter Voorde and Bertotti [29]. By preserving a constant heat flow from the basement the model has been simplified which is acceptable as it does not change the relative differences between compared scenarios. A constructed synthetic profile has been used to uncover the thermal effects of normal faulting in structurally complex basins. Steady state is regained 3–22 Myr after the fault slip, but the time elapsed for the tested parameters and model runs to achieve this varies considerably: for fault displacement 9–11 Myr, thermal conductivity 3–22 Myr, specific heat capacity 8–18 Myr and basal heat flow 9–12 Myr. For the remaining tested

parameters (Table 1) the variation of time needed to restore steady state is much smaller between the tested values, only some 100 kyr.

The syn- and post-rift deposits (Figure 1) in the studied section are 1800 m thick. These sediments are modeled to be deposited over five different time spans (Table 1); 20, 10, 5, and 1 Myr and 10 kyr, which correspond to a sedimentation rate of 0.09–180 mm·year^{-1}. The sedimentation rate roughly overlaps the reported sedimentation rates (0.4–100 mm·year^{-1} for the referenced papers) (e.g., [69–75]). ter Voorde and Bertotti [29] suggest that the extension rate somewhat controls the thermal effect of sediment deposition. They argue that high sedimentation rates will temporarily cool the basin while low sedimentation rates lead to heating. According to their study the "turning points" are at sedimentation rates of 2.0, 2.2, and 1.4 mm·year^{-1} for shale, siltstone, and sandstone, respectively. Our results show that sedimentation rates > 0.18 mm·year^{-1} for shale result in basins with transient thermal effects, in agreement with results reported by Ehlers et al. [34]. The numerical temperature model is different in the two studies. Additionally, the resolution of the finite difference grid is much finer in our study as the focus is on a smaller part of the basin compared to the work by ter Voorde and Bertotti [29]. These elements may possibly be the reason for the different results.

All the tested deposition time spans ≤10 Myr for the syn- and post-rift sediments regain steady state approximately 10 Myr after fault slip. However, there is a difference of 600 kyr for regaining steady state between the modeled scenarios. When faulting and deposition occur over a time span of 10 Myr, steady state is restored 200 kyr after the fault slip ceased. Basins with faulting and deposition over a time span of 10 kyr and 1 Myr, regains steady state after 9.6 and 9.7 Myr, respectively. Although the compared models keep the basin in an unstable thermal condition over approximately the same time span, the slow rate of faulting and deposition makes the thermal instability less prominent as opposed to basins with a high rate of faulting and deposition (Figure 8). This coincides with the result for the models were the fault displacements are varied. The larger the fault slip, the larger the thermal differences on either side of the fault zone (Figure 7), which results in longer time required for the basin to regain steady state. For basins with faulting and deposition occurring over >10 Myr, the basin is close to, or in, steady state throughout the whole deposition process; this is in accordance with Bertotti and ter Voorde [30] and ter Voorde and Bertotti [29].

In addition, our calculations show that there is a 40 ºC difference after fault slip from one side of the fault zone to the other. Larger temperature differences have been reported in the literature, e.g., by Graseman and Mancktelow [76] (and references therein) who observed differences above 100 °C on either side of the Simplon Fault Zone in Switzerland. Although such a high difference may not be enough to cause regional disturbances in the geothermal field [30], it can lead to significant local maturation differences of deposited organic material if such thermal differences occurred in basins of sedimentary rocks. Since the oil window typically lies between 80 and 150 °C [77], some tens of degrees difference in temperature may thus lead to different stages of organic maturation on either side of a fault zone. The maturation calculations in BMT follow the Arrhenius equation, which ties the reaction rates of kerogen to the temperature differences and the activation energies of the kerogen type. For given activations energies and temperatures, the reaction rates of kerogen are roughly doubled for every 10 °C rise (e.g., [39]). This indicates that a 10 °C difference will have implications for the estimated maturation in the basin.

Figure 10 demonstrates the importance of the thermal conductivity for the obtained temperature levels in the basin. Worldwide basins show a variety of alternating lithologies, and consequently differences in thermal conductivities [38,63]). Our modeling shows that thermal conductivity, as well as the fault movement, influence both the steady state and the transient temperatures in the basin (Figure 12), and therefore the time needed to regain steady state. This is in keeping with results reported by Fjeldskaar et al. [78] who demonstrated the need for an accurate description of the thermal-conductivity variation to obtain a correct thermal history, on which the prediction of maturation is based.

The thermal conductivity of lithologies, amount of fault slip, time span of faulting and deposition, angle of fault zone, and basal heat flow will influence both the size of the affected area and level of the thermal imbalance. Specific heat capacity will determine the time needed for a basin to regain steady state (Figure 11) [26,35].

4.2. Fault Restoration and Its Effect on Thermal Modeling

Hydrocarbons are often trapped in structurally complex basins, yet structural reconstruction is often over-simplified in traditional basin modeling [26]. We have shown that the tested restoration methods do not lead to substantial differences in the thermal estimates. Dula [40] concludes that 20 degrees antithetic simple shear result in a geometry resembling the natural basin the most. However, resulting thermal calculations for vertical shear and 20 degrees antithetic shear show negligible differences. We therefore conclude that thermal estimates of transects restored by vertical shear give reasonable results.

The largest thermal differences are found between basins with the greatest deviation in restored geometry and, consequently, deviation in burial depth. Thermal differences up to 35 °C are found when the temperatures obtained for basin restored by vertical shear are compared to basin with non-restored fault. Fjeldskaar et al. [26] demonstrated the importance of fault reconstruction for the temperature modeling on a 2D section from the Gulf of Mexico. Up to 70 °C in temperature differences were observed in the footwall part of the basin between model with reconstructed faults versus model with no fault reconstruction. This strongly suggests that accounting for the structural evolution in sedimentary basins is essential for a reliable thermal and maturation modeling. The results from this study along with those of Fjeldskaar et al. [26] emphasize the importance of proper structural reconstruction of sedimentary basins and highlights the need to study the transient thermal effects that occur in a basin proceeding a fault slip in order to make good thermal and maturation estimates.

4.3. Fault Slip and Magmatic Intrusions

As mentioned above, the pre-intrusion host-rock temperatures are acknowledged to be important for the thermal effect of magmatic intrusions and the size of the thermal aureole (e.g., [8]). Fault slip and magmatic intrusions may occur within the same timeframe (e.g., [30,64,65]). Results in this study show that the thermal effects of magmatic intrusions are sensitive to the timing of the fault slip relative to the timing of the sill emplacement (Figures 16–18). The basin with no sills shows that millions of years are required to restore steady state after fault movement (Figures 5 and 6). Before fault slip, sediments in the hanging wall are buried at shallower depths in the basin compared to after fault slip. The cold sediments in the hanging wall will gradually experience a temperature increase up to 40 °C over a time span of ~10 Myr. With warmer host-rock temperatures the thermal effect of intrusions is higher. Figures 8 and 10–12 show temperature histories as a function of various parameters with time to equilibrium of several Myr. However, temperatures rebound within 1 Myr or less to only a few degrees from steady state temperatures. Sedimentary basins in general would possibly not show variation in maturation due to transient thermal effects over ~1 Myr. Unless, the thermal differences were of a certain magnitude, as the reaction rates of kerogen is doubled for every 10 °C rise (e.g., [39]) as mentioned above. Sydnes et al. [25] show that the main thermal effect of magmatic sill intrusions occurs within the first 1 Myr after intrusion. This indicates that if faulting and sill intrusion occurs within the same timeframe, two transient thermal effects operate simultaneously in the basin. Disregarding these transient thermal effects could possibly lead to over- or underestimation of the basin maturation.

Sills intruding around the time of fault slip are emplaced into a basin with lower background temperatures than sills intruding 10 Myr after fault displacement. However, these differences in host-rock temperatures lead to larger thermal effects (Figure 16), as mentioned above, but do not result in large differences in maturation of organic material when one sill intrudes on both sides of the fault zone (Figure 18a). This is in contrast to the results of Aarnes et al. [8] who concluded that the host-rock temperature is an important parameter in relation to aureole thickness and thus the amount

of generated gas after intrusion of one sill. They found that increasing the host-rock temperature by 50 °C has a larger impact on the aureole thickness than both the option of increasing the temperature of the intruding magma by 50 °C or by increasing the sill thickness by 50 m. They also found that thinner sills have smaller thermal aureoles than thicker sills [8]. In this study ~50 m thick sills have been used as opposed to the work by Aarnes et al. [8], who studied a 100 m thick sill. This difference in sill thickness might possibly be the reason for the different conclusions in these two studies.

As for sill clusters, a 40 °C difference in background temperature results in a larger area with matured organic material around the intruded sills (Figure 18b). This is in agreement with Aarnes et al. [21] and Sydnes et al. [25] who showed that the thermal aureole of sill clusters at multiple levels thermally impacts a larger volume of surrounding rocks than single sills. Both these studies also show that sill thickness plays a role in the thermal and maturation effects. A 100 m thick sill will mature organic material in a larger rock volume than a thinner sill [21,25].

Figure 10 shows clearly that the thermal conductivity plays a significant role for the obtained basin temperatures. The results of sills intruding into a heterogeneous shale basin with a sandstone layer has a greater thermal effect on the surrounding host rocks, and is especially visible for sills intruding 10 Myr after fault slip (Figure 17). With the presence of higher thermal conductivity lithologies the host-rock temperatures increases and the thermal and maturation effect of magmatic intrusions are enhanced (Figure 18a,b), a conclusion supported by others (e.g., [8,16,21]).

4.4. Limitations of the Study

4.4.1. Assumptions

A simple model with one listric fault and one faulting event has been used in this study. The layers end horizontally in the fault zone and most of the tested scenarios assume a homogeneous lithology. Deposited sediments are modeled to reach the surface in every timestep, meaning that there are no constraints on the sediment supply and sea level is not accounted for. The magmatic sill intrusions are modeled to be horizontal and concordant to the layering with a constant sill thickness. Natural basins commonly consist of several faults, several faulting events, and different fault dips possibly dipping in various directions. Furthermore, layers often show a bending downwards towards the fault zone of a listric fault and they commonly show a large lithological heterogeneity, which might lead to a variation in physical properties. All these factors may result in variations in the estimated transient thermal effects and the time needed for the basin to regain steady state after fault slip, and contribute to contrasting host-rock temperatures. The occurrence of salt in the vicinity of sills will in particular influence the thermal situation in basins. Including all the above mentioned factors is possible and will turn the model into a more realistic example. However, doing so will limit the general conclusions that can be drawn from our study. By keeping the model simple the study is focused on fundamental questions related to transient thermal effects in basins with normal faults and magmatic sills. Revealed trends in this study are therefore applicable for basins in general with such features, as the relative differences between the tested parameters will remain more or less the same.

Sills vary normally in thickness and shape, e.g., saucer-shaped, v-shaped, and transgressive sills (cf., [67,79,80]). Sill thickness influences the temperature effects in the surrounding area; a thick magmatic sill has a wider thermal influence on the surroundings than a thin sill. It influences the size of the thermal aureole surrounding it (e.g., [8,25]) and an uneven sill thickness could possibly lead to an uneven thermal aureole. In a 2D model, the intrusion is extended infinitely in the 3rd direction. This is a good approximation as sills commonly have much larger horizontal dimensions compared to the vertical dimension. The sills are often several km in lengths and widths, while possibly only 50–100 m thick. For typical sill dimensions, the 2D modeling is sufficient for realistic temperature calculations. Fjeldskaar et al. [7] studied the 3D effect of magmatic sill intrusions and investigated what length/width ratio of the sill that requires a 3D calculation to give realistic temperature results.

In the temperature modeling the initial temperature of the intruding magma is set to 1000 °C and latent crystallization heat is not accounted for. Most magmas have temperatures ranging from 700 to 1300 °C (cf., [81] and references therein) making the chosen temperature in this study a mean value. Higher magma temperatures will increase the thermal effects of the sills, whilst a lower magma temperature will have the opposite effect. However, the relative differences between the compared models in this study will stay the same, as the intruding magma initial temperature is constant in all models.

Magmatic sills are often fed by dykes in magmatic upwelling zones. These near vertical features will contribute with additional heat to the thermal history of basins with sills. However, magmatic sills can also be fed by other sills over relatively large distances which has been observed in the field (e.g., [52]).

Latent heat of crystallization is thermal energy released when the sill undergoes a phase transition from liquid to solid. The composition of the magma may differ, which may lead to different timing of the emissions of latent heat as components have different crystallization temperatures. Peace et al. [62] have estimated the additional latent heat to be 488 °C, which is a substantial thermal contribution. Heat due to solidification of the magma will be released as long as the sill contains liquids and until the sill has solidified completely. However, introducing this additional heat as one pulse, either by increasing the starting temperature of the magma or introducing it as an additional heat when the sills start to cool, may result in an overestimation of the effect of sills [20].

4.4.2. Temperature Model

The temperature calculations are done by a finite difference scheme. The grid resolution is very high around magmatic sills and in areas of irregular structures. Fjeldskaar et al. [7] showed that the numerical temperature results for magmatic sills match the analytical solutions quite well, both spatially and temporally. On this basis, we argue that the uncertainty of the conduction-temperature calculations is of minor importance.

In our model we assume that the sills cool by conduction, but it is possible that the process could be accelerated by convection. Water convecting in the vicinity of sill intrusions could significantly modify the temperature and maturity effect of intrusions. Convection of hot fluids from the magma, the host-rock water, and decomposition products of kerogen is dependent on the permeability of porous host rocks or hydrofracturing in less porous host rocks (cf., [60,61,82–84]. How the fluids from magma and host rock affect the fluid pressure and flow is determined by the host-rock porosity, permeability, and amount of fluids present [85]. Wang and Manga [83] showed that for rocks with low permeability (<10 mD) symmetrical contact aureoles are produced, implying that conduction is the favorable cooling method for sills and host rocks after emplacement. On the other hand, rocks of high permeability (>50 mD) show maturation asymmetry above the sill, implying occurrence of convection-influenced maturation [83]. Annen [84] studied the maximum temperatures of three rocks of different water saturations: dry, hydrated and total water saturated, and found that in close proximity to an intrusion (~10 m) there were no differences in the temperatures, whereas at a distance of 50 m there was a ~50 °C maximum temperature difference. Dry rock has the highest temperature and water saturated rock the lowest. This means that convection of water lowered the temperature by ~50 °C. It was concluded that diffusivity contrasts between magma and host rock and incremental sill emplacement had more effect on the aureole thickness than host-rock water content [84]. For the present study this implies that for highly porous and permeable lithologies (e.g., sandstone) the predicted time for cooling might be overestimated. However, for less porous and permeable lithologies (e.g., shale) the estimated cooling rates would be adequate. This was also shown by temperature and maturity modeling on data from offshore Norway [7].

Another aspect of convection, is the possible increased permeability that occurs when sills are emplaced. Sill emplacement may potentially induce stresses high enough on the surrounding host rocks to reactivate or produce new shear fractures or open up tensile fractures (e.g., [86,87]), allowing

for increased permeability and possibly increased convection. However, accumulation of stresses and reactivation and/or production of faults and fractures are highly area specific and dependent on, e.g., the lithology, deformation features and existing weakness zones. Although increased convection due to emplacement of sills have been identified on seismic images (e.g., [67]) it is too area specific to be included in a study aiming for some general conclusions.

Radioactive decay within the sedimentary section itself can generate heat, but is not accounted for in this study. Rybach [88] found, however, that the contribution of radioactivity in the sedimentary section was generally no more than a few percent of the overall heat budget, which support that the errors by not accounting for radioactive heat, is insignificant. Others have concluded for the opposite and advocate for including radiogenic heat production in the thermal history modeling (e.g., [89,90]), but also emphasize the large area-variations in radiogenic heat production for the same lithologies [90].

Frictional heating from fault displacement may potentially have implications for the thermal history in a basin. ter Voorde and Bertotti [29] calculated for shear stress of 100 MPa and an extension rate of 2 mm·year^{-1} that the thermal contribution from frictional heat would be 2.5 °C. They concluded that this could not influence the thermal situation in the basin to a significant degree. However, with higher extensional rates and larger shear stress the frictional heating may become important.

4.4.3. Kerogen Type

Simulations of kerogen maturation can only be as good as the kinetic parameters used in the model. The parameters are derived from laboratory experiments, and are assumed to be applicable to geological processes although the scales are different by orders of magnitude. Thus the uncertainty in the calculated maturity can be significant.

As mentioned above, the maturation modeling in our study assumes kerogen type II, which is considered to be the most abundant among marine shales [39]. Kerogen degradation is temperature dependent following the Arrhenius law (e.g., [39,63]). Due to kerogen types having different activation energies, reaction rates of other kerogen types in the models presented here, could result in different maturity effects in the modeled scenarios.

5. Concluding Remarks

We have studied the transient thermal effects in a constructed basin with magmatic sill intrusions and one normal faulting event. Several factors related to faulting, physical properties, and fault restoration methods have been tested to study possible differences in resulting calculated temperature regimes over time. Sills of modest sill thickness (50 m) have been modeled to intrude before the basin has regained steady state after fault slip, enabling the study of two transient thermal effects acting simultaneously in the basin.

From the results in this study, the following conclusions can be drawn:

- After fault slip, the basin is thermally unstable and is influenced by transient thermal effects that may last up to several million years. This implies that transient thermal effects should be accounted for if sills are emplaced after the structural events, as they might affect the pre-intrusion host-rock temperatures.
- With increasing fault displacement, the temperature effects of fault slip on either side of the fault zone increases, as does the time the basin is thermally unstable.
- For faulting and deposition occurring over a time span of more than 10 Myr, the basin is in, or close to, a steady state throughout the entire period. However, for the same basin, but with faulting and deposition occurring over less than 10 Myr, the basin is thermally unstable for ~10 Myr. This means that the shorter the time used on faulting and deposition, the longer is the time the basin is thermally unstable.
- Different fault angles barely influence the time the basin is in a transient state. All tested angles lead to steady state ~10 Myr after fault slip. However, different fault angles cause changes in

the foot wall and hanging wall areas and thus affect the host-rock temperature and therefore the temperature effect of potential sills.

- Thermal conductivity is the parameter influencing pre-intrusion host-rock temperatures in the basin the most. As temperatures increase, so does the time needed for the basin to regain steady state after fault slip. For basins with identical temperature regimes, the specific heat capacity is the important property determining the time needed for the basin to regain steady state.
- The obtained temperatures in the basin increase with increasing basal heat flow, thereby increasing the time needed to arrive at a steady state after fault slip.
- Different restoration methods result in basins of different geometries, leading to temporary thermal differences mainly in the footwall part of the basin. The largest thermal differences are found between basins with fault restored to basin with non-restored fault.
- Disregarding transient thermal effects proceeding normal fault slip may lead to both under- or overestimation of pre-intrusion host-rock temperature. This will influence the calculated effects of intruded sills and has implications for the estimate of how magmatic intrusions influence hydrocarbon maturation and is particularly the case for sills intruding as clusters at multiple levels.
- A basin that has regained steady state after normal faulting has the highest potential host-rock temperature.

Emplacement of magmatic intrusions may possibly affect the reservoir quality and the fault and fracture permeability in their vicinity. Future work should evolve around the effects magmatic intrusions have on the diagenetic processes in its surroundings.

Author Contributions: Conceptualization, M.S., W.F., I.G. and I.F.L.; methodology, M.S., W.F. and I.G.; validation, W.F.; investigation, M.S..; writing—original draft preparation, M.S..; writing—review and editing, W.F., R.M., I.G. and I.F.L.; visualization, M.S. and I.G..; supervision, W.F. and R.M..; project administration, I.F.L..; funding acquisition, I.F.L.

Funding: This research was partly funded by The Research Council of Norway and Tectonor AS as a part of the PhD project 'Effects of magmatic intrusions on temperature history and diagenesis in sedimentary basins—and the impact on petroleum systems', RCN project number 257492.

Acknowledgments: We want to express gratitude for the support. The authors acknowledge the use of the Move Software Suite granted by Petroleum Experts Limited. Nestor Cardozo is thanked for fruitful discussions throughout the course of designing the study. Craig Magee is thanked for providing helpful comments and three anonymous referees are thanked for constructive reviews.

Conflicts of Interest: The authors declare no conflict of interest.

Appendix A

Numerical temperature model,
The following equation is discretizised,

$$\frac{\partial}{\partial x}Kh\frac{\partial T}{\partial x}+\frac{\partial}{\partial z}Kv\frac{\partial T}{\partial z}=\frac{\partial}{\partial t}(cT) \tag{A1}$$

where T is the temperature, Kh is the horizontal conductivity, and Kv is the vertical conductivity. Finite differences and a cell-centered grid are used. In the block with indices (ij) the expression

$$\frac{\partial}{\partial z}Kh\frac{\partial T}{\partial z} \tag{A2}$$

is evaluated by the following formula [91]:

$$\left[\frac{\partial}{\partial x}Kh\frac{\partial T}{\partial x}\right]ij=\frac{1}{\delta x_i}\left[Kh_{i+\frac{1}{2},j}\left(\frac{2\left(T_{i+1,\,j}-T_{i,j}\right)}{\delta x_i+\delta x_{i+1}}\right)-Kh_{i-\frac{1}{2},j}\left(\frac{2\left(T_{i,j}-T_{i-1,j}\right)}{\delta x_{i-1}+\delta x_i}\right)\right] \tag{A3}$$

$Kh_{i+\frac{1}{2},j}$ is the value of Kh at the boundary between the blocks (i,j) and $(i + 1,j)$. It is computed as the harmonic mean of $Kh_{i,j}$ and $Kh_{i+1,j}$.

The expression $\frac{\partial}{\partial z} Kv \frac{\partial T}{\partial z}$ is treated analogously.

This gives M · N equations to find the $T_{i,j}$, unknowns, where i = 1,2, … ,M, j =1,2, … ,N. Here, M and N are the number of blocks in x-direction and z-direction, respectively.

We use both Dirichlet and Neumann boundary conditions for the temperature model. For Dirichlet boundary conditions the temperature, T, at the boundary is given whereas for Neumann conditions the heat flux, $Kh\frac{\partial T}{\partial x}$ and $Kv\frac{\partial T}{\partial z}$, is given. A Neumann boundary condition with a heat flux of zero is used for the basin edges.

An iterative method is used to solve the linear system. Conjugate gradients are used as an acceleration method [92,93]. The conjugate gradient method is preconditioned by nested factorization [94].

References

1. Schutter, S.R. Occurrences of hydrocarbons in and around igneous rocks. In *Hydrocarbons in Crystalline Rocks*; Petford, N., McCaffrey, K.J.W., Eds.; Geological Society, Special Publications: London, UK, 2003; Volume 214, pp. 35–68.
2. Zou, C.; Zhang, G.; Zhu, R.; Yuan, X.; Zhao, X.; Hou, L.; Wen, B.; Wu, X. *Volcanic Reservoirs in Petroleum Exploration: Petroleum Industry Press*; Elsevier Inc.: Amsterdam, The Netherlands, 2013.
3. Senger, K.; Planke, S.; Polteau, S.; Ogata, K.; Svensen, H. Sill emplacement and contact metamorphism in a siliciclastic reservoir on Svalbard, Arctic Norway. *Nor. J. Geol.* **2014**, *94*, 155–169.
4. Schutter, S.R. Hydrocarbon occurrence and exploration in and around igneous rocks. In *Hydrocarbons in Crystalline Rocks*; Petford, N., McCaffrey, K.J.W., Eds.; Geological Society, Special Publications: London, UK, 2003; Volume 214, pp. 7–33.
5. Svensen, H.; Planke, S.; Malthe-Sørenssen, A.; Jamtveit, B.; Myklebust, R.; Eidem, T.R.; Rey, S.S. Release of methane from a volcanic basin as a mechanism for initial Eocene global warming. *Nature* **2004**, *429*, 542–545. [CrossRef] [PubMed]
6. Svensen, H.; Planke, S.; Corfu, F. Zircon dating ties NE Atlantic sill emplacement to initial Eocene global warming. *J. Geol. Soc.* **2010**, *167*, 433–436. [CrossRef]
7. Fjeldskaar, W.; Helset, H.M.; Johansen, H.; Grunnaleite, I.; Horstad, I. Thermal modelling of magmatic intrusions in the Gjallar Ridge, Norwegian Sea: Implications for vitrinite reflectance and hydrocarbon maturation. *Basin Res.* **2008**, *20*, 143–159. [CrossRef]
8. Aarnes, I.; Svensen, H.; Connolly, J.A.D.; Podladchikov, Y.Y. How contact metamorphism can trigger global climate changes: Modeling gas generation around igneous sills in sedimentary basins. *Geochim. Et Cosmochim. Acta* **2010**, *74*, 7179–7195. [CrossRef]
9. Svensen, H.; Corfu, F.; Polteau, S.; Hammer, Ø.; Planke, S. Rapid magma emplacement in the Karoo Large Igneous Province. *Earth Planet. Sci. Lett.* **2012**, *325–326*, 1–9. [CrossRef]
10. Moorcroft, D.; Tonnelier, N. Contact Metamorphism of Black shales in the Thermal Aureole of a dolerite sill within the Karoo Basin. In *Origin and Evolution of the Cape Mountains and Karoo Basin, Regional Geology Reviews*; Linol, B., de Wit, M.J., Eds.; Springer International Publishing: Cham, Switzerland, 2016; pp. 75–84.
11. Othman, R.; Arouri, K.R.; Ward, C.R.; McKirdy, D.M. Oil generation by igneous intrusions in the northern Gunnedah Basin, Australia. *Org. Geochem.* **2001**, *32*, 1219–1232. [CrossRef]
12. Monreal, F.R.; Villar, H.; Baudino, R.; Delpino, D.; Zencich, S. Modeling an atypical petroleum system: A case study of hydrocarbon generation, migration and accumulation related to igneous intrusions in the Neuquen Basin, Argentina. *Mar. Pet. Geol.* **2009**, *26*, 590–605. [CrossRef]
13. Spacapan, J.B.; Palma, J.O.; Galland, O.; Manceda, R.; Rocha, E.; D'Odorico, A.; Leanza, H.A. Thermal impact of igneous sill-complexes on organic-rich formations and implications for petroleum systems: A case study in the northern Neuquén Basin, Argentina. *Mar. Pet. Geol.* **2018**, *91*, 519–531. [CrossRef]
14. Wang, D.; Song, Y. Influence of different boiling points of pore water around an igneous sill on the thermal evolution of the contact aureole. *Int. J. Coal Geol.* **2012**, *104*, 1–8. [CrossRef]

15. Wang, D.; Zhao, M.; Qi, T. Heat-transfer-model analysis of the thermal effect of intrusive sills on organic-rich host rocks in sedimentary basins. In *Earth Sciences*; Dar, I.A., Ed.; InTech: London, UK, 2012.
16. Dow, W.G. Kerogen studies and geological interpretations. *J. Geochem. Explor.* **1977**, *7*, 79–99. [CrossRef]
17. Bostick, N.H.; Pawlewicz, M.J. Paleotemperatures based on vitrinite reflectance of shales and limestones in igneous dike aureoles in the Upper Cretaceous Pierre Shale, Walsenburg, Colorado. In *Hydrocarbon Source Rocks of the Greater Rocky Mountain Region*; Woodward, J.G., Meissner, F.F., Clayton, C.J., Eds.; Rocky Mountain Association of Geologists Symposium: Denver, CO, USA, 1984; pp. 387–392.
18. Raymond, A.C.; Murchison, D.G. Development of organic maturation in the thermal aureoles of sills and its relation to sediment compaction. *FUEL* **1988**, *67*, 1599–1608. [CrossRef]
19. Aarnes, I.; Planke, S.; Trulsvik, M.; Svensen, H. Contact metamorphism and thermogenic gas generation in the Vøring and Møre basins, offshore Norway, during the Paleocene-Eocene thermal maximum. *J. Geol. Soc.* **2015**, *172*, 588–598. [CrossRef]
20. Galushkin, Y.I. Thermal effects of igneous intrusions on maturity of organic matter: A possible mechanism of intrusion. *Org. Geochem.* **1997**, *26*, 645–658. [CrossRef]
21. Aarnes, I.; Svensen, H.; Polteau, S.; Planke, S. Contact metamorphic devolatilization of shales in the Karoo Basin, South Africa, and the effects of multiple sill intrusions. *Chem. Geol.* **2011**, *281*, 181–194. [CrossRef]
22. Wang, D. Comparable study on the effect of errors and uncertainties of heat transfer models on quantitative evaluation of thermal alteration in contact metamorphic aureoles: Thermophysical parameters, intrusion mechanism, pore-water volatilization and mathematical equations. *Int. J. Coal Geol.* **2012**, *95*, 12–19.
23. Wang, D.; Song, Y.; Xu, H.; Ma, X.; Zhao, M. Numerical modeling of thermal evolution in the contact aureole of a 0.9 m thick dolerite dike in the Jurassic siltstone section from Isle of Skye, Scotland. *J. Appl. Geophys.* **2013**, *89*, 134–140. [CrossRef]
24. Liu, E.; Wang, H.; Uysal, I.T.; Zhao, J.-X.; Wang, X.-C.; Feng, Y.; Pan, S. Paleogene igneous intrusion and its effect on thermal maturity of organic-rich mudstones in the Beibuwan Basin, South China Sea. *Mar. Pet. Geol.* **2017**, *86*, 733–750. [CrossRef]
25. Sydnes, M.; Fjeldskaar, W.; Løtveit, I.F.; Grunnaleite, I.; Cardozo, N. The importance of sill thickness and timing of sill emplacement on hydrocarbon maturation. *Mar. Pet. Geol.* **2018**, *89*, 500–514. [CrossRef]
26. Fjeldskaar, W.; Andersen, Å.; Johansen, H.; Lander, R.; Blomvik, V.; Skurve, O.; Michelsen, J.K.; Grunnaleite, I.; Mykkeltveit, J. Bridging the gap between basin modelling and structural geology. *Reg. Geol. Metallog.* **2017**, *72*, 65–77.
27. Benfield, A.E. The effect of uplift and denudation on underground temperatures. *J. Appl. Phys.* **1949**, *20*, 66–70. [CrossRef]
28. Birch, F. Flow of heat in the Front Range, Colorado. *Geol. Soc. Am. Bull.* **1950**, *61*, 567–630. [CrossRef]
29. ter Voorde, M.; Bertotti, G. Thermal effects of normal faulting during rifted basin formation, 1. A finite difference model. *Tectonophysics* **1994**, *240*, 133–144. [CrossRef]
30. Bertotti, G.; ter Voorde, M. Thermal effects of normal faulting during rifted basin formation, 2. The Lugano-Val Grande normal fault and the role of pre-existing thermal anomalies. *Tectonophysics* **1994**, *240*, 145–157. [CrossRef]
31. Johnson, C.; Harbury, N.; Hurford, A.J. The role of extension in the Miocene denudation of the Nevado-Filábride Complex, Betic Cordillera (SE spain). *Tectonics* **1997**, *16*, 189–204. [CrossRef]
32. Bertotti, G.; Seward, D.; Wijbrans, J.; ter Voorde, M.; Hurford, A.J. Crustal thermal regime prior to, during, and after rifting: A geochronological and modeling study of the Mesozoic South Alpine rifted margin. *Tectonics* **1999**, *18*, 185–200. [CrossRef]
33. Ehlers, T.A.; Chapman, D.S. Normal fault thermal regimes: Conductive and hydrothermal heat transfer surrounding the Wasatch fault, Utah. *Tectonophysics* **1999**, *312*, 217–234. [CrossRef]
34. Ehlers, T.A.; Armstrong, P.A.; Chapman, D.S. Normal fault thermal regimes and the interpretation of low-temperature thermochronometers. *Phys. Earth Planet. Inter.* **2001**, *126*, 179–194. [CrossRef]
35. Lander, R.H.; Langfeldt, M.; Bonnell, L.; Fjeldskaar, W. *BMT User's Guide*; Tectonor AS Proprietary Publication: Stavanger, Norway, 1994.
36. Fjeldskaar, W. BMT^{TM}—Exploration tool combining tectonic and temperature modeling: Business Briefing: Exploration & Production. *Oil Gas Rev.* **2003**, 1–4.
37. Sclater, J.G.; Christie, P.A.F. Continental stretching: An explanation of the post-mid-cretaceous subsidence of the central North Sea basin. *J. Geophys. Res.* **1980**, *85*, 3711–3739. [CrossRef]

38. Čermák, V.; Rybach, L. Thermal properties: Thermal conductivity and specific heat of minerals and rocks. In *Landolt-Börnstein Zahlenwerte und Functionen aus Naturwissenschaften und Technik, Neue Serie, Physikalische Eigenschaften der Gesteine*; Angeneister, G., Ed.; Springer Verlag: Berlin/Heidelberg, Germany; New York, NY, USA, 1982; pp. 305–343.
39. Tissot, B.P.; Welte, D.H. *Petroleum Formation and Occurrence*, 2nd ed.; Springer-Verlag: Berlin/Heidelberg, Germany, 1984.
40. Dula, W.F. Geometric Models of Listric normal Faults and Rollover Folds. *Am. Assoc. Pet. Geol. Bull.* **1991**, *75*, 1609–1625.
41. Fossen, H. *Structural Geology*; Cambridge University Press: Cambridge, UK, 2010.
42. Osagiede, E.E.; Duffy, O.B.; Jackson, C.A.-L.; Wrona, T. Quantifying the growth history of seismically imaged normal faults. *J. Struct. Geol.* **2014**, *66*, 382–399. [CrossRef]
43. Magee, C.; Maharaj, S.M.; Wrona, T.; Jackson, C.A.-L. Controls on the expression of igneous intrusions in seismic reflection data. *Geosphere* **2015**, *11*, 1024–1041. [CrossRef]
44. Schofield, N.; Holford, S.; Millett, J.; Brown, D.; Jolley, D.; Passey, S.R.; Muirhead, D.; Grove, C.; Magee, C.; Murray, J.; et al. Regional Magma Plumbing and emplacement mechanisms of the Faroe-Shetland sill Complex: Implications for magma transport and petroleum systems within sedimentary basins. *Basin Res.* **2017**, *29*, 41–63. [CrossRef]
45. Eide, C.H.; Schofield, N.; Lecomte, I.; Buckley, S.J.; Howell, J.A. Seismic interpretation of sill complexes in sedimentary basins: Implications for the sub-sill imaging problem. *J. Geol. Soc.* **2017**, *175*, 193–209. [CrossRef]
46. Francis, E.A. Magma and sediment-I: Emplacement mechanism of late Carboniferous tholeiite sills in northern Britain. *J. Geol. Soc.* **1982**, *139*, 1–20. [CrossRef]
47. Chevallier, L.; Woodford, A. Morpho-tectonics and mechanism of emplacement of the dolerite rings and sills of the western Karoo, South Africa. *S. Afr. J. Geol.* **1999**, *102*, 43–54.
48. Galerne, C.Y.; Neumann, E.-R.; Planke, S. Emplacement mechanisms of sill complexes: Information from the geochemical architecture of the Golden Valley Sill Complex, South Africa. *J. Volcanol. Geotherm. Res.* **2008**, *177*, 425–440. [CrossRef]
49. Galerne, C.Y.; Galland, O.; Neumann, E.-R.; Planke, S. 3D relationships between sills and their feeders: Evidence from the Golden Valley Sill Complex (Karoo Basin) and experimental modelling. *J. Volcanol. Geotherm. Res.* **2011**, *202*, 189–199. [CrossRef]
50. Hansen, J.; Jerram, D.A.; McCaffrey, K.; Passey, S.R. Early Cenozoic saucer-shaped sills of the Faroe Islands: An example of intrusive styles in basaltic lava piles. *J. Geol. Soc.* **2011**, *168*, 159–178. [CrossRef]
51. Richardson, J.A.; Connor, C.B.; Wetmore, P.H.; Connor, L.J.; Gallant, E.A. Role of sills in the development of volcanic fields: Insights from lidar mapping surveys of the San Rafael Swell, Utah. *Geology* **2015**, *43*, 1023–1026. [CrossRef]
52. Eide, C.H.; Schofield, N.; Jerram, D.A.; Howell, J.A. Basin-scale architecture of deeply emplaced sill complexes: Jameson Land, East Greenland. *J. Geol. Soc.* **2016**, *174*, 23–40. [CrossRef]
53. Walker, R.J.; Healy, D.; Kawanzaruwa, T.M.; Wright, K.A.; England, R.W.; McCaffrey, K.J.W.; Bubeck, A.A.; Stephens, T.L.; Farrell, N.J.C.; Blenkinsop, T.G. Igneous sills as a record of horizontal shortening: The San Rafael sub-volcanic field, Utah. *Geol. Soc. Am. Bull.* **2017**, *129*, 1052–1070. [CrossRef]
54. Svensen, H.H.; Frolov, S.; Akhmanov, G.G.; Polozov, A.G.; Jerram, D.A.; Shiganova, O.V.; Melnikov, N.V.; Iyer, K.; Planke, S. Sills and gas generation in the Siberian Traps. *Philos. Trans. R. Soc. A Math. Phys. Eng. Sci.* **2018**, *376*, 1–18. [CrossRef]
55. Svensen, H.H.; Polteu, S.; Cawthron, G.; Planke, S. Sub-volcanic Intrusions in the Karoo Basin, South Africa. In *Physical Geology of Shallow Magmatic Systems: Dykes, Sills and Laccoliths (Advances in Volcanology)*; Breitkreuz, C., Rocchi, S., Eds.; Springer International Publishing AG: Cham, Switzerland, 2018; pp. 349–362.
56. Lange, R.A.; Cashman, K.V.; Natrosky, A. Direct measurements of latent heat during crystallization and melting of a ugandite and an olivine basalt. *Contrib. Mineral. Petrol.* **1994**, *118*, 169–181. [CrossRef]
57. Atkins, P.; de Paula, J.; Keller, J. *Atkins' Physical Chemistry*; Oxford University Press: Oxford, UK, 2017.
58. Svensen, H.; Planke, S.; Jamtveit, B.; Pedersen, T. Seep carbonate formation controlled by hydrothermal vent complexes: A case study from the Vøring Basin, the Norwegian Sea. *Geo-Mar. Lett.* **2003**, *23*, 351–358. [CrossRef]
59. Svensen, H.; Planke, S.; Polozov, A.G.; Schmidbauer, N.; Corfu, F.; Podladchikov, Y.Y.; Jamtveit, B. Siberian gas venting and the end-Permian environmental crisis. *Earth Planet. Sci. Lett.* **2009**, *277*, 490–500. [CrossRef]

60. Iyer, K.; Rüpke, L.; Galerne, C.Y. Modeling fluid flow in sedimentary basins with sill intrusions: Implications for hydrothermal venting and climate change. *Geochem. Geophys. Geosyst.* **2013**, *14*, 5244–5262. [CrossRef]
61. Iyer, K.; Schmid, D.W.; Planke, S.; Millett, J. Modelling hydrothermal venting in volcanic sedimentary basins: Impact on hydrocarbon maturation and paleoclimate. *Earth Planet. Sci. Lett.* **2017**, *467*, 30–42. [CrossRef]
62. Peace, A.; McCaffrey, K.; Imber, J.; Hobbs, R.; van Hunen, J.; Gerdes, K. Quantifying the influence of sill intrusion on the thermal evolution of organic-rich sedimentary rocks in nonvolcanic passive margins: An example from ODP 210–1276, offshore Newfoundland, Canada. *Basin Res.* **2017**, *29*, 249–265. [CrossRef]
63. Allen, P.A.; Allen, J.R. *Basin Analysis: Principles and Application to Petroleum Play Assessment*, 3rd ed.; Wiley-Blackwell: Chichester, West Sussex, UK, 2014.
64. Hendrie, D.B.; Kusznir, N.J.; Hunter, R.H. Jurassic extension estimates for the North Sea 'triple junction' from flexural backstripping: Implications for decompression melting models. *Earth Planet. Sci. Lett.* **1993**, *116*, 113–127. [CrossRef]
65. Trommsdorf, V.; Piccardo, G.B.; Montrasio, A. From magmatism through metamorphism to sea floor emplacement of subcontinental Adria lithosphere during pre-Alpine rifting (Malenco, Italy). *Schweiz. Mineral. Und Petrogr. Mitt.* **1993**, *73*, 191–203.
66. Somerton, W.H. Thermal properties and temperature-related behavior of rock/fluid systems. In *Developments in Petroleum Sciences*; Elsevier: Amsterdam, The Netherlands, 1992.
67. Planke, S.; Rasmussen, T.; Rey, S.; Myklebust, R. Seismic characteristics and distribution of volcanic intrusions and hydrothermal vent complexes in the Vøring and Møre basins. In *Petroleum Geology: North-West Europe and Global Perspectives—Proceedings of the 6th Petroleum Geology Conference*; Dorè, A.G., Vining, B.A., Eds.; Geological Society: London, UK, 2005; pp. 833–844.
68. Hanson, R.B.; Barton, M.D. Thermal development of Low-Pressure Metamorphic Belts: Results from two-dimensional numerical models. *J. Geophys. Res.* **1989**, *94*, 10363–10377. [CrossRef]
69. Kennett, J.P.; Watkins, N.D.; Vella, P. Paleomagnetic Chronology of Pliocene-Early Pleistocene Climates and the Plio-Pleistocene Boundary in New Zealand. *Science* **1971**, *171*, 276–279. [CrossRef] [PubMed]
70. Kennet, J.P.; Watkins, N.D. Late Miocene-Early Pliocene Paleomagnetic Stratigraphy, Paleoclimatology, and Biostratigraphy in New Zealand. *Geol. Soc. Am. Bull.* **1974**, *85*, 1385–1398. [CrossRef]
71. Karlin, R.; Levi, S. Geochemical and sedimentological control of the magnetic properties of hemipelagic sediments. *J. Geophys. Res.* **1985**, *90*, 10373–10392. [CrossRef]
72. Turner, G.M.; Roberts, A.P.; Laj, C.; Kissel, C.; Mazaud, A.; Guitton, S.; Christoffel, D.A. New paleomagnetic results from Blind River: Revised magnetostratigraphy and tectonic rotation of the Marlborough region, South Island, New Zealand. *N. Z. J. Geol. Geophys.* **1989**, *32*, 191–196. [CrossRef]
73. Tric, E.; Laj, C.; Jéhanno, C.; Valet, J.-P.; Kissel, C.; Mazaud, A.; Iaccarino, S. High-resolution record of the Upper Olduvai transition from Po Valley (Italy) sediments: Support for dipolar transition geometry? *Phys. Earth Planet. Inter.* **1991**, *65*, 319–336. [CrossRef]
74. Szmytkiewicz, A.; Zalewska, T. Sediment deposition and accumulation rates determined by sediment trap and ^{210}Pb isotope methods in the Outer Puck Bay (Baltic Sea). *Oceanologia* **2014**, *56*, 85–106. [CrossRef]
75. Peketi, A.; Mazumdar, A.; Joao, H.M.; Patil, D.J.; Usapkar, A.; Dewangan, P. Coupled C-S-Fe geochemistry in a rapidly accumulating marine sedimentary system: Diagenetic and depositional implications. *Geochem. Geophys. Geosyst.* **2015**, *16*, 2865–2883. [CrossRef]
76. Graseman, B.; Mancktelow, N.S. Two-dimensional thermal modelling of normal faulting: The Simplon Fault zone, Central Alps, Switzerland. *Tectonophysics* **1993**, *225*, 155–165. [CrossRef]
77. Gluyas, J.; Swarbrick, R. *Petroleum Geosciences*; Blackwell Publishing: Oxford, UK, 2015.
78. Fjeldskaar, W.; Christie, O.H.J.; Midttømme, K.; Virnovsky, G.; Jensen, N.B.; Lohne, A.; Eide, G.I.; Balling, N. On the determination of thermal conductivity of sedimentary rocks and the significance for basin temperature history. *Pet. Geosci.* **2009**, *15*, 367–380. [CrossRef]
79. Jackson, C.A.-L.; Schofield, N.; Golenkov, B. Geometry and controls on the development of igneous sill-related forced folds: A 2-D seismic reflection case study from offshore southern Australia. *Geol. Soc. Am. Bull.* **2013**, *125*, 1874–1890. [CrossRef]
80. Galland, O.; Bertelsen, H.S.; Eide, C.H.; Guldstrand, F.; Haug, Ø.T.; Leanza, H.A.; Mair, K.; Palma, O.; Planke, S.; Rabbel, O.; et al. Storage and transport of magma in the layered crust—Formation of sills and related flat-lying intrusions. In *Volcanic and Igneous Plumbing Systems, Understanding Magma Transport, Storage and Evolution in the Earth's Crust*; Burchardt, S., Ed.; Elsevier: Amsterdam, The Netherlands, 2018; pp. 113–138.

81. Jain, S. *Fundamentals of Physical Geology*; Springer Geology: New Dehli, India, 2014.
82. Podladchikov, Y.Y.; Wickham, S.M. Crystallization of Hydrous Magmas: Calculation of Associated Thermal Effects, Volatile Fluxes, and Isotopic Alteration. *J. Geol.* **1994**, *102*, 25–45. [CrossRef]
83. Wang, D.; Manga, M. Organic matter maturation in the contact aureole of an igneous sill as a tracer of hydrothermal convection. *J. Geophys. Res. Solid Earth* **2015**, *120*, 4102–4112. [CrossRef]
84. Annen, C. Factors affecting the thickness of thermal aureoles. *Front. Earth Sci.* **2017**, *5*, 1–13. [CrossRef]
85. Hanson, R.B. The hydrodynamics of contact metamorphism. *Geol. Soc. Am. Bull.* **1995**, *107*, 595–611. [CrossRef]
86. Gudmundsson, A.; Løtveit, I.F. *Sills as Fractured Hydrocarbon Reservoir: Examples and Models*; Geological Society London Special Publications: London, UK, 2012; Volume 374, pp. 252–271.
87. Montanari, D.; Bonini, M.; Cori, G.; Agostini, A.; Ventisette, C.D. Forced folding above shallow magma intrusions: Insights on supercritical fluid flow from analogue modelling. *J. Volcanol. Geotherm. Res.* **2017**, *345*, 67–80. [CrossRef]
88. Rybach, L. Amount and significance of radioactive heat sources in sediments. In *Thermal Modelling in Sedimentary Basins*; Burrus, J., Ed.; Technip: Paris, France, 1986; pp. 311–323.
89. Keen, C.E.; Lewis, T. Measured radiogenic heat production in sediments from continental margin of eastern North America: Implications for petroleum generation. *AAPG Bull.* **1982**, *66*, 1402–1407.
90. McKenna, T.E.; Sharp, J.M. Radiogenic heat production in sedimentary rocks of the Gulf of Mexico Basin, South Texas. *AAPG Bull.* **1998**, *82*, 484–496.
91. Thomas, G.W. *Principles of Hydrocarbon Reservoir Simulation*, 2nd ed.; International Human Resources Development Corporation: Boston, MA, USA, 1982.
92. Hageman, L.A.; Young, D.M. *Applied Iterative Methods*; New York Academic Press: New York, NY, USA, 1981.
93. Young, D.M.; Jea, K.C. *Generalized Conjugate Acceleration of Iterative Methods, Part 2: The Nonsymmetrizable Case*; Report CNA-163; Center for Numerical Analyses, University of Texas at Austin: Austin, TX, USA, 1981.
94. Appleyard, J.R.; Chesire, I.M. *Nested factorization: Proceedings of the Seventh Symposium on Reservoir Simulation*; SPE Paper 12264; Society of Petroleum Engineers of AIME: San Francisco, CA, USA, 1983.

Paper 3: The influence of magmatic intrusions on diagenetic processes and stress accumulation

Magnhild Sydnes, Willy Fjeldskaar, Ivar Grunnaleite, Ingrid Fjeldskaar Løtveit, Rolf Mjelde

Published in Geosciences, 9, 477, Special Issue "Future Advances in Basin Modeling: Suggestions from Current Observations, Analyses and Simulations"

geosciences

MDPI

Article

The Influence of Magmatic Intrusions on Diagenetic Processes and Stress Accumulation

Magnhild Sydnes [1,2,*], Willy Fjeldskaar [1], Ivar Grunnaleite [1], Ingrid Fjeldskaar Løtveit [1] and Rolf Mjelde [2]

[1] Tectonor AS, P.O. Box 8034, NO-4068 Stavanger, Norway; wf@tectonor.com (W.F.); ig@tectonor.com (I.G.); ifl@tectonor.com (I.F.L.)
[2] Department of Earth Science, University of Bergen, Box 7803, 5020 Bergen, Norway; Rolf.Mjelde@uib.no
* Correspondence: ms@tectonor.com

Received: 27 September 2019; Accepted: 11 November 2019; Published: 13 November 2019

Abstract: Diagenetic changes in sedimentary basins may alter hydrocarbon reservoir quality with respect to porosity and permeability. Basins with magmatic intrusions have specific thermal histories that at time of emplacement and in the aftermath have the ability to enhance diagenetic processes. Through diagenesis the thermal conductivity of rocks may change significantly, and the transformations are able to create hydrocarbon traps. The present numerical study quantified the effect of magmatic intrusions on the transitions of opal A to opal CT to quartz, smectite to illite and quartz diagenesis. We also studied how these chemical alterations and the sills themselves have affected the way the subsurface responds to stresses. The modeling shows that the area in the vicinity of magmatic sills has enhanced porosity loss caused by diagenesis compared to remote areas not intruded. Particularly areas located between clusters of sills are prone to increased diagenetic changes. Furthermore, areas influenced by diagenesis have, due to altered physical properties, increased stress accumulations, which might lead to opening of fractures and activation/reactivation of faults, thus influencing the permeability and possible hydrocarbon migration in the subsurface. This study emphasizes the influence magmatic intrusions may have on the reservoir quality and illustrates how magmatic intrusions and diagenetic changes and their thermal and stress consequences can be included in basin models.

Keywords: magmatic intrusions; diagenesis; stress; porosity; permeability; basin modeling; stress modeling

1. Introduction

Magmatic intrusions are commonly emplaced with much higher temperatures compared to their host rocks. Therefore, when emplaced into sedimentary basins, they may influence all parts of the petroleum system [1]. Several studies have shown how such intrusions influence the temperatures and hydrocarbon maturation in sedimentary basins (e.g., [2–11]). Other studies focus on the stress induced by the sills on the host rocks as they intrude (e.g., [12,13]). However, only a few studies have reported on the effect magmatic sill intrusions have on the diagenetic processes in sedimentary basins. Haile et al. [14] concluded in their work at Edgeøya (Svalbard) that conductive heat from intrusions did not seem to have affected the diagenetic products in the area. However, at Wilhelmøya (Svalbard) there is evidence suggesting that hydrothermal fluid flow originating from sills has affected the chemical transformations [15]. In a study of sandstones at Traill Ø (East Greenland) it was concluded that a combination of conductive and convective heat from magmatism enhanced the diagenetic process [16].

In essence, porosity and permeability determine the quality of petroleum reservoirs [17,18]. At the time of sediment deposition, the process of sediment lithification starts [19], driven by mechanical

and chemical diagenesis. Mechanical alterations are related to compaction of the sediments by burial, while chemical alteration is the compaction occurring when chemical compounds are dissolved and re-deposited or new components are precipitated. While the mechanical changes are strictly a result of increasing burial depth and vertical loading, chemical changes are less predictable and highly dependent on the chemical compounds and the temperature (e.g., [20]). Diagenesis results in porosity loss, increased rock densities and seismic velocities (e.g., [21–25]). Due to the sensitivity of chemical diagenesis to temperature, basins subjected to magmatic intrusions are particularly prone to abrupt and sudden changes of physical properties. Laboratory measurements show an increase of physical rock strength (>100%) on the transition of opal A to opal CT [23], which imply that diagenetic processes may also affect the way the rocks respond to subsurface stresses.

Diagenetic transformations are reported from sedimentary basins worldwide (e.g., [26–34]). The Monterey Formation in California, USA, has been extensively studied with regard to the transformation of opal A to opal CT (e.g., [35–39]), but diagenetic alterations have also been observed several places in wells and on seismic data from the Norwegian Continental Shelf (e.g., [24,40–47]). All of the latter studies report observed transitions of either opal A to opal CT or smectite to illite in the Vøring Basin, offshore mid-Norway. We used a 2D section from the Vøring Basin with numerous sills as the basis for the modeling, as it represents the structures of a magmatic basin better as opposed to a synthetic profile. Modeling of a real 2D section will thus give more realistic results, even though the parameters are of global nature. A detailed case study of the effects of magmatic intrusions on diagenesis in the Vøring Basin is beyond the scope of this work.

The main goal of the study is to quantify the effect of magmatic intrusions on transitions of opal A to opal CT to quartz, smectite to illite, and quartz diagenesis which was done with basin modeling software (BMT^{TM}, [48]). A second goal is to assess the influence of diagenetic processes and of the sills themselves on the stress field in a sedimentary basin and the potential impact on fracture and fault permeability, which is of significant importance for the petroleum systems. The results show that magmatic sills and related thermal effects might have notable implications for the porosity loss due to diagenesis in their vicinity. Diagenetic alterations and the sills themselves influence the location and magnitude of stress accumulations in the basin and thereby have implications for the fault and fracture development, and implicitly for the migration of fluids.

2. An Example of the Evolution of a Volcanic Basin—The Vøring Basin

The Vøring Basin is located offshore mid-Norway and is bounded by the Bivrost Lineament to the NE and the Vøring Transform Margin to the SW (Figure 1). The area consists of grabens, basins, and structural highs developed over three main rifting episodes from Carboniferous to Eocene times (e.g., [49] and references therein); (1) Carboniferous-Permian; coincided with the onset of rifting in the North Atlantic [40,50–55]; (2) Late-Mid Jurassic to Early Cretaceous; led to subsidence and development of accommodation space for the thick Cretaceous sedimentary sequence [56,57]; (3) Late Cretaceous to Early Eocene; coincided with the opening of the North Atlantic, development of the Vøring Marginal High, and intrusion of numerous sills in the Cretaceous basin fill [49,58]. Subsequent events were dominated by seafloor spreading and accretion of oceanic crust in the expanding Norwegian-Greenland/North Atlantic Sea [59,60]. In the post-rift phase, the Vøring area experienced localized tectonic uplift, erosion, sediment deposition, subsidence, flexure, and isostatic uplift partly due to numerous glaciations and deglaciations of the Fennoscandian landmasses [61,62].

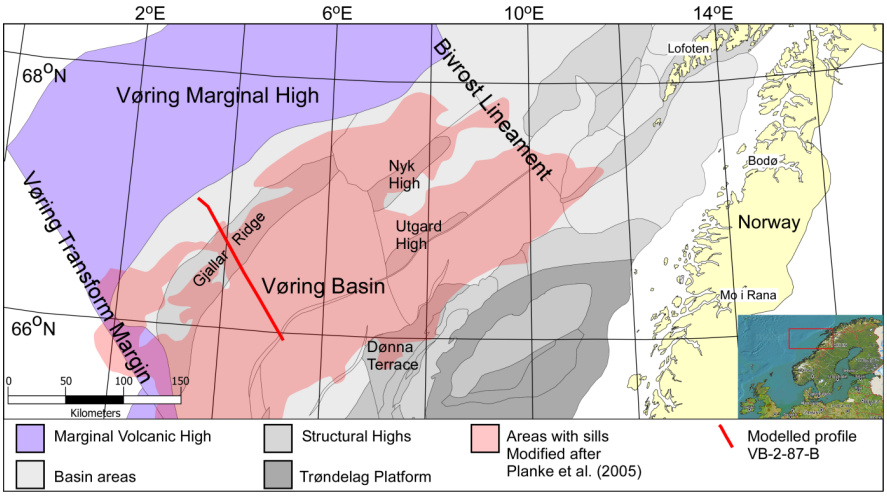

Figure 1. Location of the studied profile (VB-2-87-B) in the Vøring Basin offshore mid Norway. Modified after Sydnes et al. [10].

The sedimentary deposits of the Vøring Basin mainly consist of marine to deep marine sediments (mainly shale) with intercalated shallow marine sediments (mainly sandstone) in the Upper Jurassic and Cretaceous [49]. The Paleocene consists of shale with minor sandstone and limestone deposits [63], and the Lower Eocene consists of shales. The magmatic intrusions were emplaced in lower Eocene time within the entire sedimentary sequence. Oligocene, Neogene, and Quaternary deposits are mainly shales with some ice rafted debris in the Plio-Pleistocene. The outer Vøring Basin was in the Miocene and early Pliocene dominated by deep-water deposits consisting of biosiliceous hemipelagic sediments [46,64].

The utilized 2D transect, VB-2-87-B (Figure 1), is about 100 km long and holds some 20 interpreted sills located at ~3–5 km depth with lateral extension of the sills varying from about 3 to 30 km (Figure 2). A velocity model by Hjelstuen et al. [64] was used for depth conversion of the section. The time of intrusion activity is estimated at ~56 Ma, which is supported by ages derived from zircon dating of magmatic sills in the Vøring area (55.6 ± 0.3 Ma and 56.3 ± 0.4 Ma, 6607/5-2 and Utgard wells; [65]).

From Carboniferous and up to the beginning of Eocene, the Vøring Basin was part of an active rift phase [49]. As the active rifting ceased the Vøring area subsequently experienced thermal subsidence and ridge push due to continental break up and opening of the North Atlantic. Repeated glaciations, mainly since 2.6 Ma, have led to sediment depositions in the Vøring Basin. Currently the regional stress field of coastal and mainland Norway is somewhat affected by post-glacial uplift and erosional unloading/loading [62,66–70] in addition to compressive ridge-push. To make our results generally applicable, the section from the Vøring Basin is solely used as a basis for the modeling, and site-specific parameters such as lithology and rock properties, are substituted by global values.

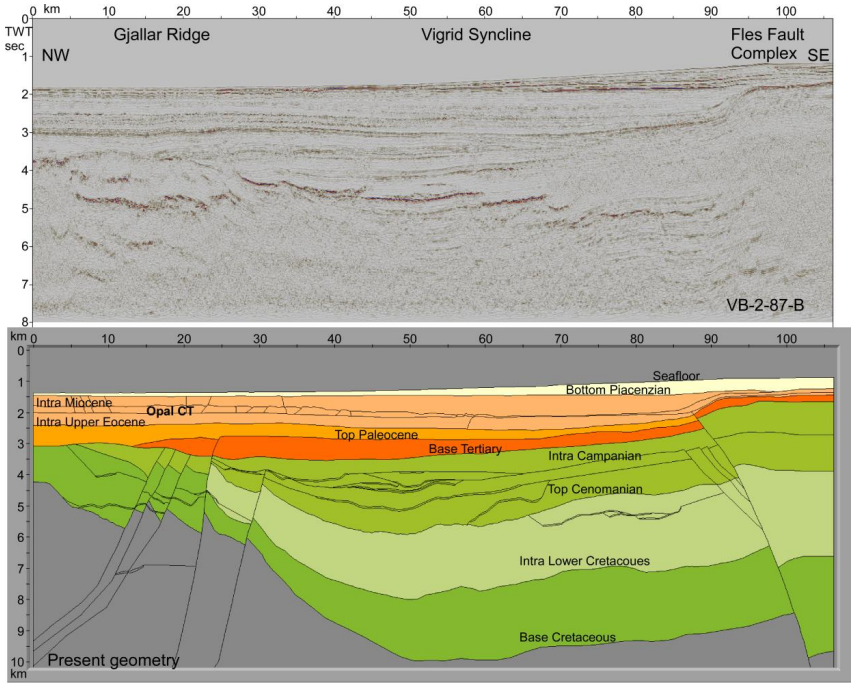

Figure 2. Seismic section and the interpreted, depth converted section of VB-2-87-B in the Vøring Basin offshore mid-Norway. Interpretation is obtained from Blystad et al., [40].

3. Methods and Results for Magmatic Intrusion's Influence on Diagenetic Processes

To perform the modeling of structural evolution, geohistory, thermal development, maturation, and diagenesis, BMT^{TM} (Tectonor AS) was used. All models are in 2D, which infer the third dimension to be infinite. This is a good approximation when sills and faults are modeled, as the third dimension commonly is much larger than the two others (e.g., [12]).

3.1. Geohistory, Temperature, Maturation, and Diagenesis

BMT is a high-resolution 2D basin modeling software utilizing a backstripping process, starting with present day geometry, in order to reconstruct the geohistory of an interpreted seismic section (Figure 2) [48,71,72]. One horizon at a time is stripped from the section and fault restoration and decompaction (based on the given porosity-depth trends assigned for the lithologies) of underlying sequences follow. This process is repeated all the way to the top basement, thus building the geohistory. The fault restoration in BMT is performed by vertical simple shear, a method that leaves no gaps in the geometry and allows for thermal and maturation calculations to be performed (cf. [48]).

BMT bases the thermal calculations on the finite difference method by conduction. The resulting temperature history depends on the thermal conductivity and specific heat capacity of the sediments as well as the basal heat flow from the mantle [48,71]. The surface temperature is the upper boundary condition in the calculations and is kept at 7 °C, whereas the lower boundary condition is the basal heat flow which is set to 47 mW·m^{-2} over the profile and over time. With these settings, the BMT calculations generate the basis for the maturation and diagenetic modeling. Kerogen type II is assumed for the maturation modeling, and maturation is calculated using classical first-order kinetics [48].

3.1.1. Silica Diagenesis—Quartz Diagenesis

Quartz diagenesis occurs over three connected steps involving dissolution of quartz grains, transport of dissolved silica over short distances, and precipitation of quartz cement on clastic quartz grains [19,73]. BMT performs quantitative estimates of quartz cementation caused by dissolution of silica as described in Walderhaug [74,75] and Lander and Walderhaug [76]. The method is based on an empirically derived quantification of quartz precipitation as a function of temperature, and the precipitation is considered rate limiting for the whole cementation process (in [75] and references therein). This is a different approach than several other quantitative models where quartz dissolution is considered the limiting factor (e.g., [77–81]). As the diagenesis is thermally dependent (e.g., [74,75]), quartz cementation is an indicator of the maximum reached temperature and the burial depth.

Diagenesis is a complex process consisting of a number of transformations occurring simultaneously. According to Walderhaug [74,75], the rate limiting step is the precipitation, which is described by first-order kinetics and is proportional to the rate constant (k) given by the Arrhenius equation (Equation (1)).

$$k = A_0 e^{\left(\frac{-E_a}{RT}\right)}, \quad (1)$$

where k is the rate constant of mineral precipitation per unit surface area (mol/cm^{2}s), A_0 is a pre-exponential constant/frequency factor (mol/cm^{2}s), E_a is the activation energy (J/mol), R is the real gas constant (8.314 J mol^{-1} K^{-1}), and T is the temperature. A_0 is the number that describes how often molecules collide within the system under consideration. E_a is the energy needed for a specific chemical reaction to occur and both parameters are unique for any reaction [17]. The kinetic equation is integrated over temperature and time for a given timestep. By multiplying this with the available grain surface area obtained from the porosity history of the reconstructed geohistory, the mineral cement precipitated is calculated. However, increasing grain coating on quartz minerals reduces the possibility for precipitation of diagenetic minerals. The porosity loss calculations in this study assume zero grain coating, the porosity loss due to cementation might therefore be overestimated.

3.1.2. Silica Diagenesis—Opal A to Quartz Via Opal CT

Diatoms and radiolarian are two examples of siliceous plankton that after death enrich deep water sediments with dissolved non-crystalline silica known as opal A [82]. Such fragments are associated with low-energy deposition environments and amorphous silica is commonly found in deep water sediments amongst clay and silt deposits. Through burial and increased temperatures opal A converts to quartz via opal CT; this is observed in several basins worldwide, as documented in the introduction. The conversion of biogenetic/amorphous silica, opal A, to diagenetic/microcrystalline silica, opal CT, and subsequently to stable/crystalline silica, quartz, occurs through several dissolutions and precipitations as the burial depth increases (e.g., [39,83,84]). This reorganization from non-crystalline to crystalline silica causes changes in rock structures, mechanical properties, porosity, and permeability and may potentially generate traps for hydrocarbons (e.g., [23,38,39,84,85]).

One approach to determine the depth of these diagenetic processes is an empirical derived schematic presentation of the relation between temperature, rock composition, and silica-phase changes [86,87], which can be used in areas of known temperatures. Another approach is to determine experimentally the reaction kinetics under given chemical conditions which can be used for basins worldwide (e.g., [22,38,88]. A third approach was discovered by Neagu et al. [25] who found a connection between rotated fault planes and amount of porosity loss due to the conversion of opal A to opal CT.

Generally, each chemical reaction has its specific pre-exponential constant and activation energy which can be derived experimentally [17]. Additionally, all chemical reaction rates are temperature dependent [89]. Therefore, the method described above for quartz diagenesis was used to predict the precipitation rate for the transition of opal A to opal CT to quartz. Laboratory studies show that the activation energy for the opal A to opal CT transition is lower than for the transition of opal CT

to quartz and this indicates that reorganization of amorphous silica to microcrystalline silica require lower temperature than the conversion of microcrystalline silica to crystalline silica [22]. This implies that the opal A/opal CT transition is expected to be located at shallower depths than the opal CT/quartz boundary.

In this study the values reported by Dralus et al. [39] for the transition of opal A→ opal CT→ quartz was used (Table 1), as their study results in improved predictions of the opal A to opal CT boundary compared to other published kinetics [38]. They also found that high content of organic matter slows the transitioning of opal A to opal CT and that different kinetic parameters are required for rocks with high and low organic content.

3.1.3. Clay Diagenesis—Smectite to Illite

During burial diagenesis, illitization of smectite is a commonly occurring mineralogical reaction of clay rich sediments and shales. The conversion is a gradual process leading to mixed layers with different illite/smectite ratios [90] and is accompanied by volume loss and reduction in permeability [91]. With increasing burial depth and temperatures, the percentage of illitic beds in the illite/smectite mixed layers increases (e.g., [24,92]). The temperature is an important factor in the smectite to illite diagenetic process (e.g., [91]), but the presence of pore water and potassium (K^+) are also essential for this transition to take place [42,93–95]. Smectite reacts with potassium, possibly sourced by K-feldspar, and the outcome is illite, silica, and water (e.g., [42]) from a complex dissolution/precipitation process where the precipitation is rate limiting (e.g., [96–99]). A common approach for modeling the conversion of smectite to illite is by using the Arrhenius equation and regarding the transformation as either a one step reaction with one reaction rate (e.g., [94,100]) or as several parallel reactions with rates spread over a defined range (e.g., [101]).

Table 1. Kinetic data used for the opal A/CT/quartz diagenesis and smectite to illite modeling. *Values obtained from Sachsenhofer et al. [103].

Diagenetic Process		E_a (kJ mol^{-1})	A_0 (mol/cm^{2}s)
Opal A—opal CT—quartz	Dralus et al. [39]	36.99 (low TOC) 33.44 (high TOC) 32.52 (Quartz)	1.04×10^{14} 3.01×10^{10} 1.96×10^{9}
Smectite to illite	Roaldset et al. [95]	33	1.02×10^{8} 2.72×10^{9}
	Huang et al. [94]	28	8.08×10^{4}
	Hillier et al. [102]*	31	1.81×10^{3}

The method described above for quartz diagenesis is also applied for the estimation of smectite to illite diagenesis. However, it is important to note that this method does not take into account the presence of chemical components that can act as catalysts or quenchers. As for quartz diagenesis, precipitation is considered rate limiting for the smectite to illite transition and it is assumed that critical chemical components, e.g., potassium, are present for the reaction to occur. Kinetic data from three different studies were tested: (1) Roaldset et al. [95], (2) Huang et al. [94], and (3) Hillier et al. [102]. Their preferred parameters are given in Table 1.

3.2. Opal A to Opal CT—Testing of the Method

To test the quantification methods described above for the diagenetic processes, 1D modeling was performed on a well in the North Sea. Roaldset and Wei [23] observed the opal A to opal CT transition to be at 1740 m depth in well 30/9-B-50H (Figure 3) in the Oseberg area (North Sea). This area has experienced several millions of years of Cenozoic tectonic quiescence [104–107] and is presently close to maximum burial depth [95], which makes this particular well excellent for testing of the

method. The stratigraphy was obtained from a well close by (well 30/6-2; Figure 3) consisting mainly of sandstones and claystones (see Table 2 for parameters).

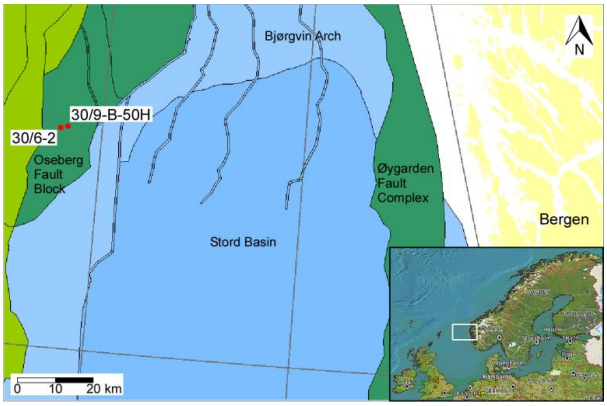

Figure 3. Location of well 30/6-2 and 30/9-B-50H on the Oseberg fault block in the North Sea. The wells are located approximately 2 km apart. Modified from map on www.npd.no.

Table 2. Lithological parameters used in the modeling, based on standard values published in the literature (e.g., [108,109]).

Lithology	Porosity—Depth Trend		Conductivity (kv) (Wm^{-1} K^{-1})		Heat Capacity ($Jkg^{-1}K^{-1}$)
	Surface Porosity	Exponential Constant (km^{-1})	Low Porosity	High Porosity	
Sandstone	0.45	0.27	3.30 (6%)	1.50 (45%)	1080
Claystone	0.63	0.51	1.70 (6%)	1.00 (60%)	940
Shale	0.63	0.51	2.00 (6%)	1.40 (60%)	1190
Basement, metamorphic			3.10	3.10	1100
Magmatic intrusions			3.10	3.10	1100
Asthenosphere			3.50	3.50	1100

Roaldset and Wei [23] showed that the opal A to opal CT transition zone coincided with a porosity reduction of around 20%. Results from the 1D model of well 30/9-B-50H shows that 20% porosity loss starts around 1740 m below seafloor (Figure 4). This coincides with the observations by Roaldset and Wei [23], which gives a strong indication that the method gives realistic results.

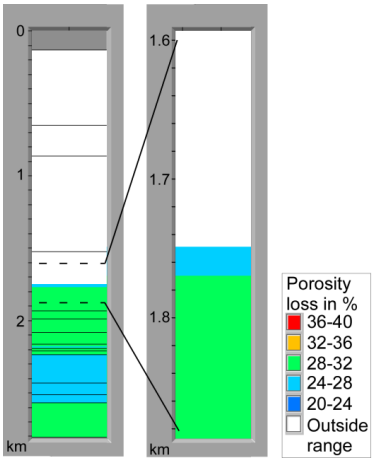

Figure 4. The modeled porosity loss in well 30/6-2 in the North Sea. The result coincides well with observations by Roaldset and Wei [23] which shows the porosity loss starting approximately around 1740 m depth.

3.3. Example from the Vøring Basin, Section VB-2-87-B

To study the effect emplaced sills have on the diagenesis in basins, the methods described in Section 3.1 were used on the seismic line VB-2-87-B (Figure 2) in the Vøring Basin (Figure 1). This transect contains approximately 20 interpreted magmatic sills, as well as a horizon denoted opal CT (Figure 2). The sills were modeled to intrude in one pulse at 56 Ma, with a magma temperature of 1000 °C which is within normal magma temperature range [12]. Table 2 summarizes the parameters used in the modeling. The thermal effect of sills and the effect on the diagenetic processes are largest the first million years after intrusion [5,10]. The figures below show results for 1 Myr after the intrusion of the sills.

3.3.1. Quartz Cement

The resulting diagenetic effects (Figure 5) show large differences between models where sills are accounted for and when they are disregarded. It is well known that sill thickness plays a role in the size of the thermal aureole, as well as the amount of matured organic matter in the vicinity of sills (e.g., [5,10]). This is also clearly illustrated in Figure 5 where results for alternatives with no sills, 50 m and 100 m thick sills are shown. The entire basin is assumed to have sandstone lithology (see Table 2 for properties). Some areas show up to 40% difference in porosity loss between the models (Figure 5). The areas where the largest differences are found are located close to the sills and in the areas between clusters of sills. With increasing sill thickness a larger area between the sill clusters have increased porosity loss (Figure 5). This is in accordance with Sydnes et al. [10] who found that the vitrinite reflectance in a well in the Barents Sea is a function of the spacing and the possible heat exchange between neighboring sills. For single, relatively shallow lying sills, the sill thickness does not impact the size of the area of porosity loss to a significant degree. However, for deeper lying single sills, the sill thickness will impact the size of the diagenetically altered area (Figure 5).

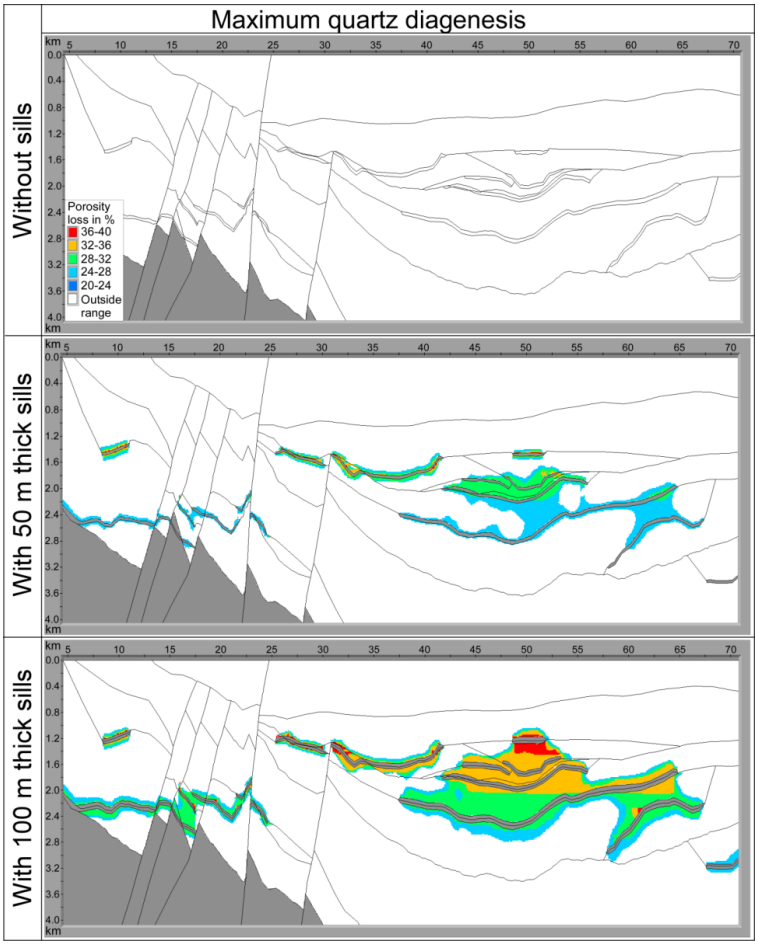

Figure 5. Results for porosity loss due to quartz diagenesis for basin holding no sills (upper), 50 m thick sills (middle), and 100 m thick sills (lower).

Quartz diagenesis due to sill emplacement will have implications for the reservoir quality in the vicinity of sills, in particular for reservoirs lying between clusters of sills. For our basin with this particular geohistory and thermal development, sills intruding at any depth in the sedimentary rocks will enhance the porosity loss due to quartz diagenesis. The generated diagenetic changes as a result of intruding sills (as shown in Figure 5) should still be visible today, as the surrounding host rocks at the same depth have not yet reached the same amount of quartz diagenesis.

3.3.2. Opal A to Opal CT to Quartz

The transition from opal A to opal CT is considered to occur over some tens of meters and up to 200 m [41]. Roaldset and Wei [23] found the transition zone of opal A to opal CT to start where the porosity reduction is around 20%. Therefore, we assume that the transition zone starts where the modeling result show 20% porosity loss and ends around 200 m deeper down. The basin is now set as all shale and assumes presence of amorphous silica. Figure 6 shows the modeled opal CT transition zone for the studied transect in the Vøring Basin with and without sills included in the calculations. The largest contrast between the two models are found in the shallower areas and for sills situated at

depths <1500 m below seafloor (Figure 6). For the scenario where sills are not included, the transition zone results in a more or less horizontal zone around 1200 m depth. When the thermal contribution of sills is included in the calculations, the opal A/CT boundary is found as shallow as approximately 700 m depth. This implies that the additional heat from the sills moved the transition zone up to 500 m shallower depths. The influence of sills on the further transition of opal CT to quartz is more or less the same as for opal A to opal CT and therefore not shown here.

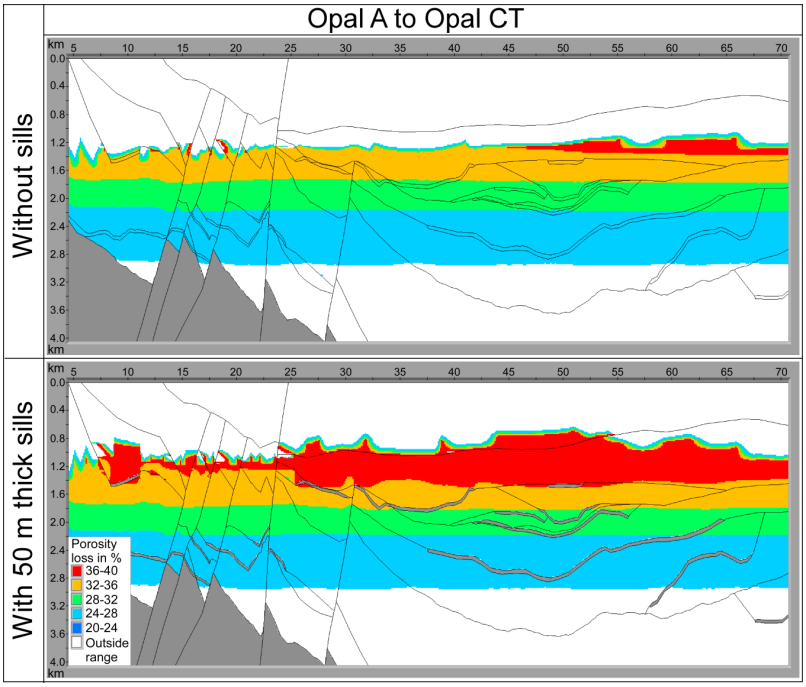

Figure 6. The results for the opal A/CT transition zone when sills are disregarded (upper) and when they are included (lower). The transition zone is assumed to start where the porosity loss exceeds 20%.

3.3.3. Smectite to Illite

Transformation of smectite to illite may occur in sediments and rocks containing clay minerals, and the basin is therefore assumed to have only shale lithology. The results for all the tested kinetic values show that magmatic intrusions and their heat contribution influence the diagenesis and result in transition of smectite to illite at shallower depths than without sills (Figure 7). However, the published and used A_0 and E_a values give significantly different results (Figure 7). The values proposed by Roaldset et al. [95] with high frequency factor (Table 1; Figure 7) give results similar to the result for the transition of opal A to opal CT (Figure 6). Without sills the transition from smectite to illite occurs around 1200 m depth and with sills this boundary lies about 500 m shallower. Results for the parameter values proposed by Hillier et al. (Table 1; [102]) show a porosity loss of 10% and increasing with depth, starting at >2000 m depths when sills are disregarded (Figure 7 pink, stippled lines lower left). For models where sills are included a porosity loss up to 40% is obtained in areas close to the sills (Figure 7). The results are quite similar to results displayed for quartz diagenesis (Figure 5). For the Vøring Basin, a transition in seismic velocity, porosity, and density, believed to resemble the smectite to illite transition, has been observed at depths corresponding to 80–90 °C [24]. The modeled isotherms of 80 and 90 °C for the model without sills are shown in Figure 7 (left). According to Peltonen et al. [24], the kinetic parameter values preferred by Roaldset et al [95] result in a transition of smectite to illite at

a shallower depth than 80–90 °C. The kinetic values of Hillier et al. [102] result in a transition zone that lies deeper than the 80–90 °C isotherm.

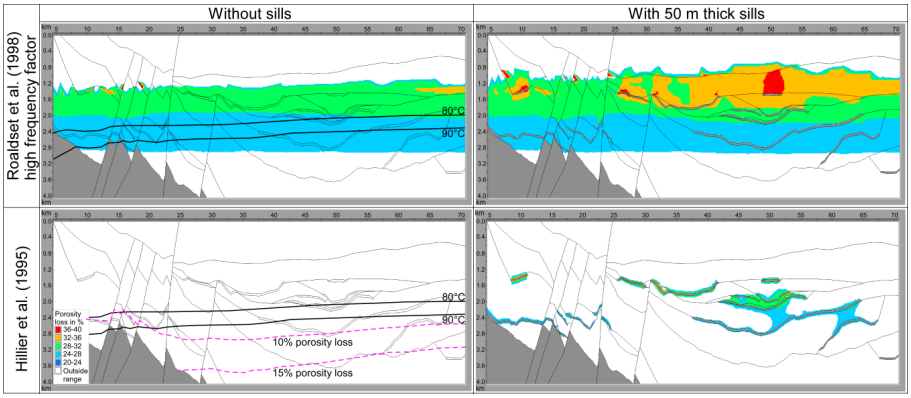

Figure 7. Modeling results of smectite to illite diagnesis when sills are disregarded (left) and when they are included (right). The kinetic parameters of Roaldset et al. [95] and Hillier et al., [102] are used (cf. Table 1). The modeled isotherm of 80–90 °C is marked for scenario without sills (left). Lower left, pink, stippled lines indicate location of 10% and 15% porosity loss.

From field observations it has been reported concurrent onset of oil generation and the conversion of smectite to illite (e.g., [110]). When comparing the resulting maturation assuming kerogen type II in the section from the Vøring Basin (Figure 8) with and without sills, there is a good correlation for both scenarios when compared to the smectite to illite conversion, when kinetic values by Hillier et al. [102] were used. Without sills the maturation starts at depths >2900 m at lateral location 50 km on the transect (Figure 8). At the same point in the transect without sills and Hillier et al. parameters ([102]; Figure 7), a porosity loss of 10% due to conversion of smectite to illite starts around 2700 m depth (Figure 7 pink, stippled lines lower left), which gives about 200 m difference in the location of the onset of hydrocarbon generation and smectite to illite conversion. For the modeled hydrocarbon maturation with sills (Figure 8) there is also a good correlation with the modeled porosity loss due to conversion to illite with the use of Hillier et al. [102] kinetic values (Figure 7).

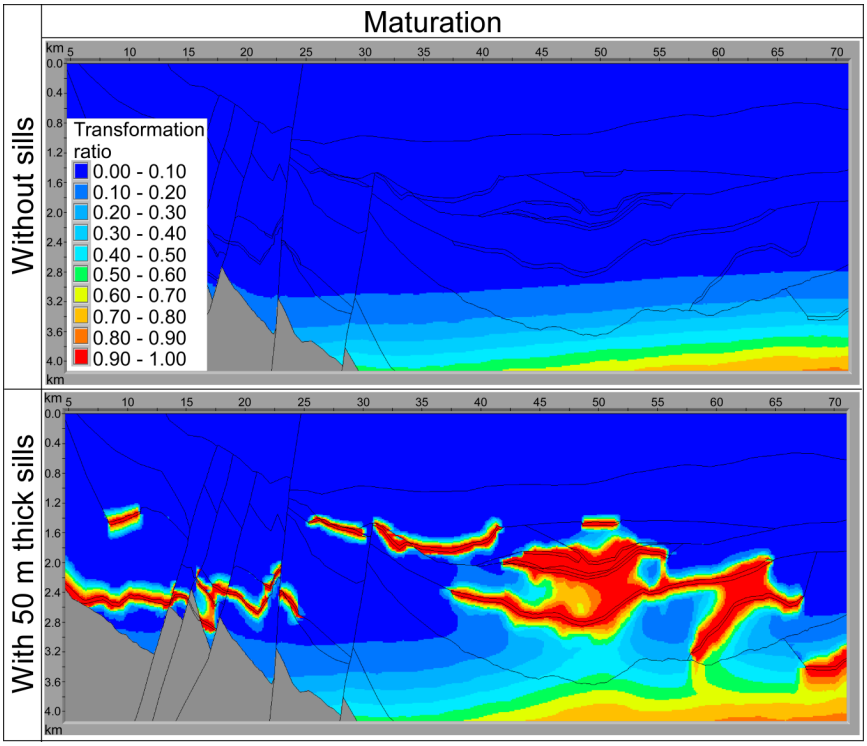

Figure 8. Hydrocarbon maturation for the studied transect without (upper) and with (lower) sills. The onset of maturation of organic material and the onset of porosity loss due to transition of smectite to illite is almost concurrent (compare to Figure 7).

4. Methods and Results for Stress Accumulation Influenced by Diagenetic Processes and Sills Themselves

As stated in the introduction, the physical properties of rocks subject to diagenesis will be altered (e.g., [22,23,95]. The increase in rock stiffness, as a consequence of diagenesis is of particular interest when studying how diagenesis may change the way the rocks respond to stresses. Additionally, the sills themselves are much stiffer than the host rocks in sedimentary basins and will accumulate stresses when subject to compressional or extensional loading [12,111].

4.1. Stress Modeling

To investigate how diagenesis and sills might affect stress accumulations in the subsurface, we used Comsol Multiphysics 5.2.a (www.comsol.com), a commercial finite element method (FEM) software that solves problems based on partial differential equations. The stress effects were studied on two synthetic cases and on the section from the Vøring Basin (Figure 2). All the models are in 2D and have fault zones divided into two separate units, consisting of a fault core which is surrounded by a damage zone with stiffnesses of 0.1 and 1 GPa, respectively (Figure 9). A typical Poisson's ratio of 0.25 [112] was used in all the models and they were all subject to either horizontal compressional or extensional stress of 5 MPa to resemble horizontal regional or local stresses. All sills were assumed to be solidified and have Young's modulus values resembling such a situation. Properties are as summarized in Table 3. The lower boundary was fastened in all models to avoid translation and rotation of the rock body.

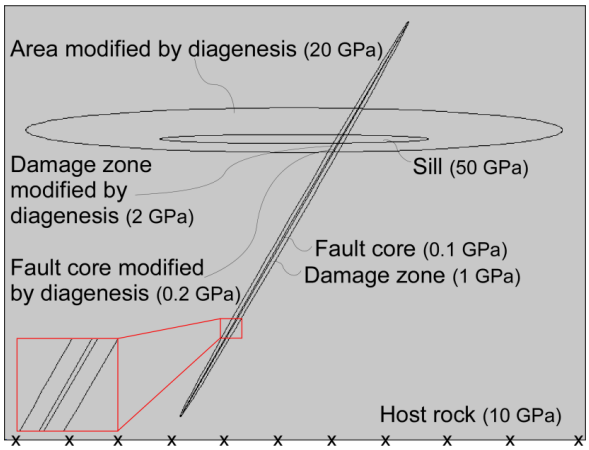

Figure 9. Schematic overview of the synthetic models with an enlargement of the fault zone and definition of the units and Young's modulus values used in the models. The X's indicate the boundary fixated to avoid translation and rotation of the rock body during loading.

Table 3. Physical properties used in the stress modeling, based on standard values for rock properties published in the literature (e.g., [111]).

Young's Modules					
Host Rock	**Area Modified by Diagenesis**	**Basement**	**Fault Core/ Damage Zone**	**Fault Core/Damage Zone Modified by Diagenesis**	**Sills**
10 GPa	20 GPa	50 GPa	0.1 GPa/1 GPa	0.2 GPa/2 GPa	50 GPa

4.2. Stress Effects of Sills and Diagenesis

In general, stress accumulations indicate areas prone to either opening of fractures or activation/reactivation of faults. Areas where tensile stresses accumulate may lead to opening of fractures or keep existing fractures open, whereas activation/reactivation of faults may occur in areas where shear stresses accumulate. Active faults and open fractures increase the permeability in the area where they are located. Typical global properties of rocks were used in the models (Table 3) and the results show the location of stress concentrations, and how sills and diagenesis affect stress accumulations. The models were based on the assumption that rocks behave as linear elastic up to 1%–3% strain at low temperature and pressure [113,114] depending on the rock strength. Strain exceeding 1%–3% commonly results in failure. Normally the shear strength of rocks lies between 1 and 12 MPa and the tensile strength is half of the shear strength, normally between 0.5 and 6 MPa [115–117]. Stresses exceeding these limits will commonly initiate fault movement and open fractures, respectively.

When comparing models where sills and sill-initiated diagenesis are accounted for versus when it is disregarded, it is possible to determine if and how these units may have influenced fracture and fault related permeability. Laboratory studies show that the physical strength of rocks increases by more than 100% on the transition of opal A to opal CT [23]. Therefore, the stiffness of the diagenetically altered area is doubled compared to the Young's modulus value of the rocks not altered by diagenesis.

Synthetic Case

A synthetic case of arbitrary dimensions shows that in a homogeneous basin, stresses build up at and around the fault tips when subject to compression and extension (Figure 10). Red and yellow colors in the models represent areas where stresses concentrate, while blue colors are areas of small to no stress accumulations. Fractures may open and increase the permeability close to the sides of the

fault tips where the tensile stresses concentrate (Figure 10). The direction of the fractures will follow the direction of σ_1 (maximum principal compressive stress) and open in the direction of σ_3 (minimum principal compressive stress or maximum principal tensile stress) [111]. Initiation of fault movement may occur at the fault tips where shear stresses accumulate, and as the shear stresses are larger at the upper tip, this is the area most likely for fault slip initiation (Figure 10).

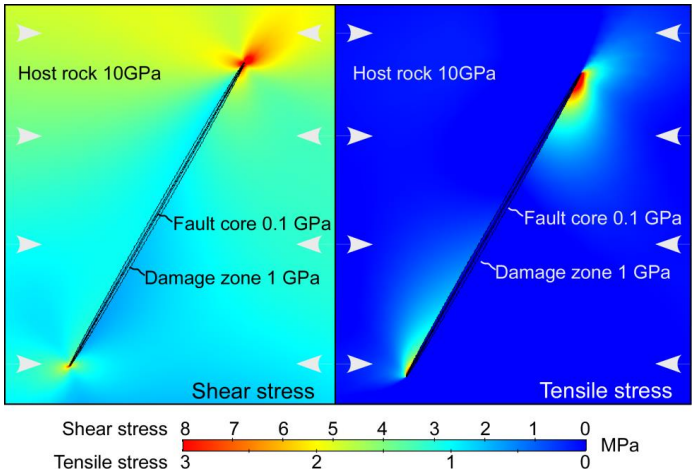

Figure 10. Stress results for the synthetic case of a fault zone with arbitrary dimensions in a homogeneous basin. The tensile and shear stress developed in a homogeneous basin with one fault subject to horizontal compressive stress of 5 MPa (indicated by horizontal arrows). The host rock has a Young's modulus value of 10 GPa, the damage zone is 1 GPa, and fault core 0.1 GPa.

As shown in Sections 3.3.1–3.3.3, magmatic sills will influence the diagenetic processes in their proximity (see Figures 5–7). In order to include this impact in the synthetic model, a second model featuring the same fault, but with one sill surrounded by a diagenetically altered area was added. The results (Figure 11) show that in addition to accumulating shear and tensile stresses at the fault tips, due to compression, stresses mainly build up in the sill and in the area modified by diagenesis surrounding the sill. This occurs as stresses tend to build up in layers/zones of stiffer rocks in contrast to softer rocks in heterogeneous basins (e.g., [111,118,119]). These shear stress accumulations are also present in the fault zone, particularly where the sill crosses the fault, and consequently, potential fault reactivation may start in this area. The accumulated shear stresses in the sill and diagenetically modified area may result in linking of present weaknesses and potentially initiate growth of new faults within this area, if the shear strength of the rock is exceeded [111]. Tensile stresses concentrating in the area modified by diagenesis along the fault zone and within the diagenetically altered damage zone may, if the tensile strength of the rock is exceeded, open fractures [111]. Similar results are obtained for the same model subject to extension, however, the resulting tensile stresses will be much larger compared to when subject to compression (not shown here) and accordingly the chance of opening fractures will increase.

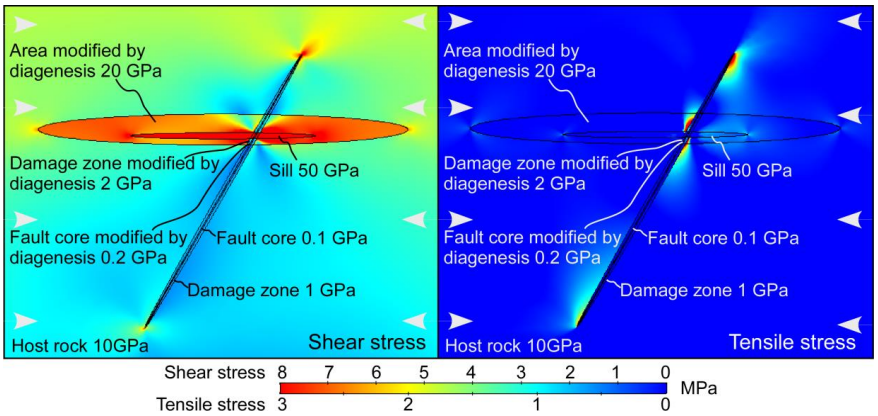

Figure 11. The resulting tensile and shear stresses of a fault with sill intruded through the fault zone with a surrounding area of diagenetic alteration when subject to horizontal compressive stress of 5 MPa (indicated by horizontal arrows). Dimensions are arbitrary in this synthetic model.

4.3. Example from the Vøring Area

For the transect VB-2-87-B in the Vøring Basin, the influence of sills and diagenetically altered area (as given in Sections 3.3.1–3.3.3) was included to investigate its effect on the stress accumulations. The mid-Norwegian margin is presently experiencing compression. However, this is not a specific study of the Vøring area, therefore, to study the response to compressive and tensile horizontal stresses the model was subjected to both. The area to the left (Figure 12a) with several faults and sills, is of particular interest as it displays the interaction between faults, sills, and areas modified by diagenesis. As the smectite to illite transition zones (Figure 7) show boundaries much like the one of opal A to opal CT (Figure 6) and quartz diagenesis (Figure 5), this transition was not included in the study, as the results are expected to be more or less the same as for the opal CT transition zone and quartz diagenesis.

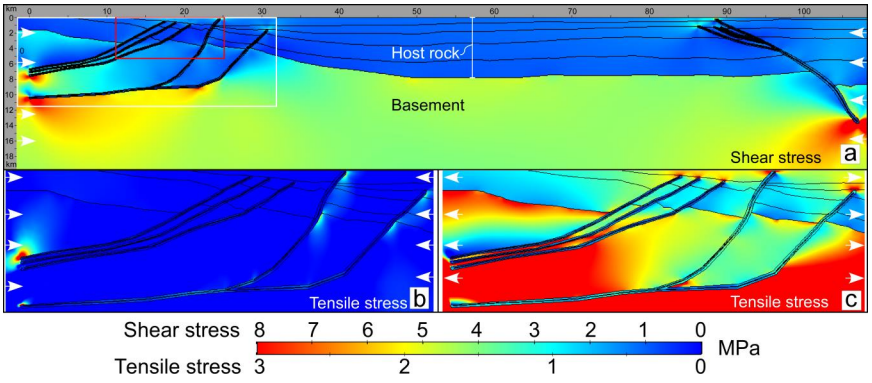

Figure 12. (**a**) Stress results for the Vøring profile when the sills are excluded, and diagenesis is disregarded. The results show the shear stresses due to 5 MPa compressive horizontal stress (indicated by horizontal arrows). The white box indicates the area enlarged in (**b**) and (**c**), the red box indicates the area enlarged in Figures 13 and 14. (b) The same scenario as in (a) but with the tensile stresses due to compression. (c) The same scenario as in (a) and (b), but with tensile stresses due to 5 MPa extension (indicated by horizontal arrows).

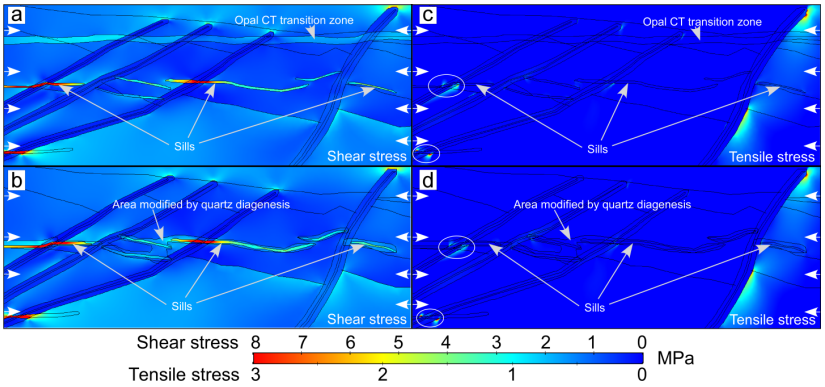

Figure 13. Stress results for the basin with 50 m thick sills subject to horizontal compressive stress of 5 MPa. The area and scale are shown by the red box in Figure 12. (**a**,**b**) The results for the basin when the sills and the transition zone of opal CT are accounted for. (**c**,**d**) The results when sills and quartz diagenesis are accounted for. White circles indicate areas where the sill does not penetrate the fault zone, however, parts of the fault zone have area altered by diagenesis.

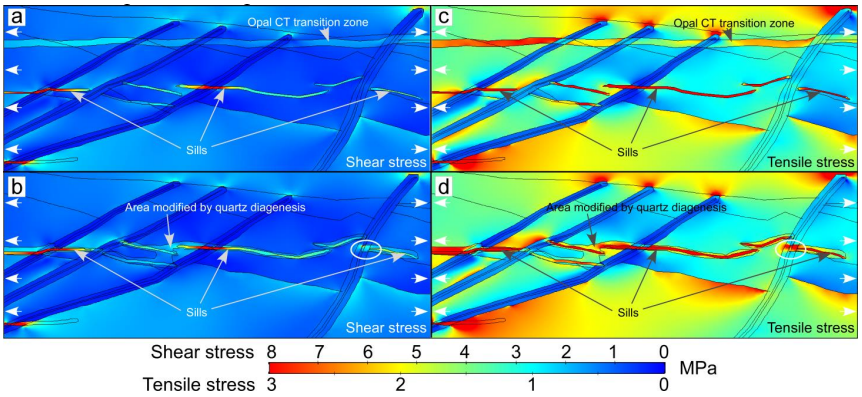

Figure 14. Stress results for the basin with 50 m thick sills subject to horizontal tensile stress of 5 MPa. The area and scale is shown by the red box in Figure 12. (**a**,**b**) Results for basin where sills and the transition zone of opal CT is accounted for. (**c**,**d**) Results for when sills and quartz diagenesis is accounted for. The white circle to the right indicates the area where the sill does not penetrate the fault zone, however, parts of the fault zone have area altered by diagenesis. This area concentrates stresses, and when high enough, may contribute to fault reactivation and fracture development. The sills are 50 m thick.

The transformation zone of opal A to opal CT starts when the porosity reduction is around 20% (cf. Figure 6; [23]) and is modeled to end around 200 m deeper (cf. [41]). Five different scenarios were tested and subject to horizontal compressive and tensile stresses of 5 MPa: (1) the basin with both sills and diagenesis disregarded (Figure 12), (2) the basin with sills but diagenesis disregarded, (3) the basin without sills but with opal A to opal CT transition zone included, (4) the basin with sills and opal A to opal CT transition zone included (Figures 13 and 14) and, (5) the basin with sills and quartz diagenesis (Figures 13 and 14).

Common results for all the models, whether subject to compressive or tensile stress, is that stresses build up at the fault tips (like the synthetic models), and in particular at the lower tips (Figure 12a–c). This is due to the larger contrast in rock stiffness between the fault zones and the basement compared

to the contrast between the fault zones and the host rock (cf. Table 3). Shear stresses are more or less the same with regard to location and strength of accumulations, whether they are subject to compression or extension. However, the tensile stresses are much lower for the models subject to compression (Figure 12b) than those subject to extension (Figure 12c).

When subject to both compression and extension, the synthetic models show that both shear and tensile stresses mainly concentrate in the sill and area modified by diagenesis, also where these features cross the fault zone (Figure 11). Figure 13 shows the results for the Vøring basin subject to compression and when sills and the opal CT transition zone are included (Figure 13a,c), as well as when sills and the quartz diagenetically modified area are accounted for (Figure 13b,d). For all cases, areas of increased tensile stresses are few and small, but potential fractures may open along the fault zone to the right and increase the permeability if the stresses become high enough (Figure 13c,d). In addition, areas indicated by white circles in Figure 13c,d, show elevated tensile stresses related to where the sill and diagenetically modified area cross the fault zone. Fractures may open or remain open if stress concentrations grow high enough, thereby contributing to increased permeability in these areas. The shear stresses tend to build up in the areas modified by diagenesis and in the sills. Where the sills cross the faults, stress concentrations are, without exceptions, particularly high (Figure 13a,b) and may reactivate the fault if they exceed the rock's shear strength of 1–12 MPa. Elevated shear stresses in the opal CT transition zone and area modified by quartz diagenesis, may potentially initiate growth of new faults if the stresses become high enough, and thereby contribute to increased permeability.

When the basin is subject to extension the shear stresses concentrate in the same location with the same strength (Figure 14a,b), as when subject to compression (Figure 13a,b), for all scenarios. If the shear stresses exceed the shear strength of the rocks, fault slip will be initiated in some areas (colored red and yellow). However, the tensile stresses are much larger for the basin subject to extension (Figure 14c,d) as opposed to compression (Figure 13c,d). The entire sills tend to concentrate tensile stresses, not just when crossing fault zones (Figure 14c,d). Additionally, the diagenetically altered area of both opal CT and quartz accumulate higher tensile stresses compared to their surroundings. The high concentrations of tensile stresses show that the basin is prone to open fractures and increase the permeability in several areas. Due to the particularly high stress concentrations in the sills and the areas that have undergone diagenetic transitions, fractures are expected to first open in these places.

5. Discussion

Magmatic intrusions may influence the location and amount of porosity loss due to diagenesis, given that the necessary physical, biogenic, and/or chemical conditions are present. Two specific topics are addressed in this study: (1) quantification of the effect of magmatic intrusions on several diagenetic processes (opal A to opal CT to quartz, smectite to illite, and quartz diagenesis) and (2) the effect of sills and diagenetically altered areas on the fracture and fault permeability in basins with emphasis on the effect of these factors on petroleum systems.

5.1. Effects of Diagenesis on Petroleum Systems

Diagenesis contributes to loss of porosity and permeability in petroleum reservoirs and thus essentially harm the reservoir quality [90]. However, the same processes may also enhance the porosity and permeability through development of secondary porosity by dissolution, grain coating, and fracturing of layers that have become brittle [90]. All diagenetic products can aid in calibrating the thermal history of basins, as the transformation of each diagenetic product commonly occurs over a specific temperature range. Thereby, they are markers for maximum temperatures and burial depths and may uncover areas exposed to unusual environments, i.e., uncommon heat flow or uplift and erosion, and they can be used together with for instance vitrinite reflectance and fluid inclusion data to calibrate thermal predictions.

The thermal conductivity of sediments could rise 4–5 times when opal CT transitions to quartz [120], as a result of the porosity loss. In the Bjørnøya Basin (Barents Sea) this difference in thermal conductivity

results in about 10 °C higher temperatures in the Paleocene/Eocene shales for opal CT rich shale compared to quartz rich shale [118]. This temperature difference is caused by the nature of clay minerals that have a flattened structure favoring horizontal over vertical heat transport [120]. This is an example of the importance of including diagenesis in basin modeling. Modeling of diagenesis will ensure good thermal models when assessing the petroleum potential of sedimentary basins [120].

When the effects of diagenetic processes on petroleum reservoirs are considered, it is important to realize that chemical compounds in subsurface fluids can be catalysts or quenchers for the processes. First of all, the transition of opal A to opal CT to quartz requires presence of amorphous silica in the sedimentary rocks. Kastner et al. [83] studied the chemical controls on the opal A to opal CT transition and found that the diagenetic process is increased in carbonate rocks and reduced in clay-rich rocks. The presence of magnesium and hydroxide ions was found to enhance the conversion of opal A to opal CT. Subsequent transformation of opal CT to quartz released magnesium and hydroxide ions [83] and fluids enriched in magnesium and hydroxide ions were expelled upwards along faults increasing the transformation of opal A to opal CT at shallower depths [121]. Conversion of smectite to illite requires the presence of clay minerals in the sedimentary rocks. Furthermore, the presence of potassium has proved to enhance this conversion process. The transformation rates of smectite to illite increases with high potassium concentrations and lower temperatures are needed to start the conversion [95]. The potassium is commonly sourced by k-feldspars, which requires such minerals to be present for diagenesis to occur [91]. On the other hand, laboratory studies indicate that the presence of magnesium ions retards the conversion process in the early phases of the smectite to illite conversion [94]. Therefore, although thermal requirements are met for diagenetic alterations to occur, it is ultimately the biogenic and/or chemical compounds in the rocks and pore fluids that determine the possible diagenetic processes.

5.2. Effect of Magmatic Sills on the Diagenetic Process in Reservoir Rocks

Earlier studies of magmatic intrusions and their effect on porosity evolution and diagenesis of reservoir rocks have come to contrasting conclusions (e.g., [14,15,122–124]). The diagenetic processes of sandstone reservoirs are likely to be controlled by the initial composition of the sand, original pore water composition, content of neighboring lithologies, burial and thermal history, and timing of cementation relative to accumulation of petroleum [17,47,82]. These criteria can largely explain the contrasting conclusions that are put forward in the referenced literature.

Haile et al. [14] conclude in their study at Edgeøya (Svalbard) that quartz cementation is unaffected by the short-lived heating of magmatic sills in reservoir rocks. They suggest that slow quartz cementation rates are in contrast to the relatively short-lived magmatic heating and will therefore not leave fingerprints on the diagenetic process. This conclusion contrasts from the results in our study which clearly show that magmatic sill intrusions affect the diagenesis in their proximity (Figures 5–7). Nejbert et al. [125] state that most sills in the Svalbard area are about 10–30 m thick. The sills are relatively thin and the distances between the sills are unknown in the study by Haile et al. [14], which could explain the contrasting conclusions of their study and ours. The magmatic sill thickness, distance from sills, and clusters of sills are pointed out in several studies to have significant importance on the thermal effect of magmatic intrusions (e.g., [3,5,6,9–11]). Our study shows that thermal effects will also affect diagenetic transformations (i.e., Figure 5). The location of sampling in the study by Haile et al. [14] might also be too far from sills to be thermally affected by them.

Another aspect is the temperature of the intruding magma. As the thermal effect of sills is a function of the temperature of the intruding magma, a lower magma temperature than 1000 °C (used in this study), would result in smaller thermal aureole surrounding the sills and consequently decrease the area affected by diagenesis. This could also to some degree explain the contrasting conclusions. The host rock pre-intrusion temperature is identified to be crucial for the thermal effect of magmatic intrusions (e.g., [5,8,11]), and ultimately the effect of magmatic intrusions on diagenetic processes. Factors such as fault displacement, time span of faulting and sediment deposition, fault angle, rock

thermal conductivity and specific heat capacity, basal heat flow, and restoration method used to simulate the fault movement through time, are all factors that influence the host rock pre-intrusion temperatures. For a specific, detailed area study, all these factors are crucial and require thorough assessment [11].

5.3. Silica Diagenesis

Silica diagenesis embraces two distinct types of chemical compaction processes, both of which are thermally dependent. The first studied here is quartz diagenesis and is related to pressure dissolution of quartz minerals, diffusion of dissolved silica and precipitation of quartz cement. Quartz cementation is the number one porosity reduction process in sandstones below 2000 m depth (e.g., [17,126,127]). Rapidly increasing porosity loss due to quartz cementation occurs when temperatures exceed 100–110 °C [75] and hydrocarbons do not seem to influence the porosity reduction process [91]. Grain coatings of clays have been found to inhibit quartz cementation and contribute to porosity preservation (e.g., [128–130]). Furthermore, at depths for peak mineral dissolution, such as quartz dissolution, the porosity is found to increase through secondary porosity production before it decreases again at deeper burial depth [130]. For basins without magmatic intrusions the porosity loss in petroleum reservoirs due to quartz diagenesis are expected to be found at depths corresponding to the mentioned temperature range (100–110 °C). As the results in this study show, magmatic intrusions in sedimentary basins contribute to abrupt changes in the diagenetic processes (Figure 5) and reservoirs with reduced porosity may thus be found at shallower depths than expected. Reservoirs located between sills in a cluster are particularly prone to porosity reduction due to quartz diagenesis.

The transition of siliceous sediments from opal A through opal CT to quartz, starts at lower temperatures than the silica transition discussed previously. Opal A dissolves and subsequently precipitates to opal CT at about 50–60 °C, and further transition into crystalline quartz starts around 80–90 °C [131]. These transformations are known to create hydrocarbon traps. In Onnagawa Formation, Yurihara oil and gas field (Japan) and Monterey Formation in California (USA), the opal CT/quartz boundary acts as a seal due to its low permeability, while the quartz rich layers underneath, with higher permeability, act as a reservoir [38,132]. For basins following the thermal development without particular interruptions, the transition zone of opal A to opal CT will normally be in the temperature range of 50–60 °C, and the opal CT to quartz transition at depths corresponding to 80–90 °C. Results from this study show that sills intruding at depths <1500 m moves the opal A/CT transition zone to significantly shallower depths. For basins with magmatic sill intrusions emplaced at shallow depths, such a hydrocarbon trap model would lie at shallower depths than basins without sills, and could possibly go undiscovered if sills are not included in the thermal and diagenetic calculations during basin modeling. The opal A/CT boundary has been mistaken for a flat spot as oil/water contact and drilled (e.g., [22]). When incorporating the diagenetic transition of opal A to opal CT in basin modeling, such errors may be avoided.

Opal CT Boundary in the Vøring Basin

The opal A to opal CT transition zone is found at surprisingly shallow depths in some areas of the Vøring Basin. Several reasons for this fossilized opal A/CT transition have been suggested. The transition zone is proposed to have developed during Miocene and died out in Early Pliocene (e.g., [44,49,133]). As the transition of amorphous silica to opal CT is a temperature dependent reaction (e.g., [22,24,73–75]) the fossilized transition is a record of peak paleo temperatures which may reflect max burial depth of the basin, uplift and erosion of the area, higher thermal gradient in the past, or another unknown thermal event [22,44,49,131]. The Eocene magmatic sills are, however, not the cause of the observed shallow opal A/CT zone because the extra heat provided by the intrusions did not affect the diagenesis as shallow as the Miocene/E Pliocene formations.

5.4. Smectite to Illite

The conversion of smectite to illite is one of many different clay diagenetic processes occurring in the subsurface. Illite has a fibrous texture and small amounts of this clay may dominate the pore space and largely reduce permeability [91]. The smectite to illite transition is of particular interest for the oil and gas industry as it may coincide with the onset of oil generation [90]. For the Vøring Basin, Peltonen et al. [24] found that major smectite to illite conversion occurred at depths corresponding to a temperature interval of 80–90 °C. For shales in the Gulf Coast (USA), the major rate of smectite to illite conversion was found at temperatures of 90–120 °C [134]. Other studies conclude that the illitization process starts at 50 °C and ceases around 100 °C [135]. These diverse temperature ranges for the smectite to illite conversion is also reflected in the modeling results in this study, when different published kinetic parameters are used (Figure 7). This emphasizes the complexity of the smectite to illite conversion, and possibly clay diagenesis in general. An area influenced by magmatic activity in western Pannonian Basin (Hungary), show a divergent effect of magmatic heating on clay minerals and the smectite to illite transformation [103]. Such results emphasize that, although thermal requirements are met for diagenetic processes to take place, other factors must also be fulfilled for chemical reactions to occur (cf., [136]). For the smectite to illite diagenetic functionality described here, caution must be exercised in the interpretation of the results. This means that the described method can be used to locate areas that fulfill the required kinetics for alterations to occur. This is a good first approximation in pin pointing areas prone to have undergone diagenetic changes in the basin. However, subsurface chemical knowledge is needed in order to examine if other necessary criteria are met for diagenetic alterations.

5.5. Influence of Sills and Diagenesis on Stress Accumulations

When sills have solidified and are subject to compressive and tensile stresses, this study shows that the sills and the diagenetically altered areas accumulate stress (Figures 10–14). When stresses exceed the shear and/or tensile strengths of the rock, the rocks will fail and fault movement will be initiated or fractures will develop, respectively. This occurs because stresses tend to build up in the stiffer layers as opposed to softer rocks (e.g., [111,116,117]), which will be decisive for where fractures develop and faults could be reactivated. From the models (Figures 10–14) it can be deduced that the higher the contrast in rock stiffness, the higher the stress concentration in the stiff layers. For diagenetically modified areas, with higher increase in rock stiffness than studied here (doubled the stiffness of the host rock), the potential stress accumulation in the area modified by diagenesis will be higher, and the likelihood of fault initiation and fracture opening is increased. On the other hand, in an opposite situation, the potential stress concentration will be lower and so will the likelihood of fault movement and fracture opening.

It has been proposed that diagenetic processes may affect the fluid flow properties in the subsurface (e.g., [14,47]), a statement which is confirmed by the results in this study. This is the case, not just due to how diagenesis modifies rocks porosity and permeability, but also to how these diagenetic alterations change the rock's physical properties. An active fault may increase the temporary permeability many times, and faults and fractures may dominate the fluid transport in the rock masses if they are interconnected [111]. The results in this study show that sills or diagenetically altered areas (Figures 11–14) could ultimately lead to opening of fractures or initiate fault movements if the tensile or shear stresses of the rocks are exceeded. For a petroleum system, such an outcome can be crucial, as opening of fractures and fault movement increase the permeability and supports fluid flow, possibly to new locations. Thus, we conclude that sills and their related diagenetically modified areas may influence the subsurface fluid migration pathways through time and space and increase the permeability, as opening of fractures and reactivation of faults may act as fluid conduits.

5.6. Limitations of the Calculations

All basins have their particular thermal and structural histories concerning e.g., sediment source, lithology, fluid circulation, pore fluid chemistry, and structural development. These variations all play a part in possible chemical alterations in the subsurface and lead to unique diagenetic development. Therefore, information regarding these elements must be included for more detailed local studies.

In numerical modeling there is a direct link between the quality of the input data and the quality of the output from the models. When studying a particular area, caution must be taken regarding various parameters. For instance, we only studied conductive heat transfer in the subsurface and heat convection by fluids is not accounted for. Convection by fluids could influence the resulting thermal and diagenetic calculations to various degrees (cf., [137–141]). The Vøring area shows proof of fluid convection (e.g., [142]), our results therefore show maximum porosity loss, at least for some areas. However, for basins that show little to no signs of convecting fluids, the presented estimations are adequate. We argue that the method presented here is a good approach to reveal areas needing further investigation of possible diagenetic alterations and thus possible alterations of reservoir properties.

6. Concluding Remarks

This study quantified the porosity loss due to the transition of opal A to opal CT to quartz, smectite to illite and quartz diagenesis and how magmatic intrusions may affect the diagenetic process. As the diagenetic alterations change the physical properties of the rock, it was shown how these alterations and the sills themselves influence location of stress accumulations in a basin and thus may contribute to changes in fracture and fault permeability. All these factors have implications for the petroleum system and the results are summarized as follows:

- Conductive thermal effects of sills significantly influence the diagenetic processes in sedimentary basins.
- The effect of magmatic intrusions on the diagenetic processes depends on the depth at which the magmatic sills intrude. Maximum diagenetic changes occur at different temperatures for the different processes. For sills to influence the transition of opal A to opal CT they must intrude at depths >1500 m.
- Sill thickness influences the size of the diagenetically altered area, particularly where clusters of sills are closely spaced.
- Sills and diagenetically modified areas influence location of stress accumulations and may contribute to initiation of fault movement and opening of fractures. As fractures and faults can act as conduits for fluid flow, sills and areas modified by diagenesis may therefore contribute to increased permeability.
- A thorough case study is required to determine the sill's specific effect on diagenetic processes and stress accumulations in the Vøring Basin and other volcanic basins. This is now made possible with the work done in this study.

Author Contributions: Conceptualization, M.S., W.F., I.G. and I.F.L.; methodology, M.S., W.F. and I.G.; software, M.S., W.F. and I.G.; formal analysis, M.S. and I.G.; investigation, M.S.; writing—original draft preparation, M.S.; writing—review and editing, W.F., I.G., I.F.L. and R.M.; visualization, M.S.; supervision, W.F. and R.M.; project administration, I.F.L.; funding acquisition, I.F.L.

Funding: This research was partly funded by The Research Council of Norway and Tectonor AS as a part of the PhD project 'Effects of magmatic intrusions on temperature history and diagenesis in sedimentary basins—and the impact on petroleum systems', RCN project number 257492.

Acknowledgments: We want to express gratitude for the support received. Inspiring conversations with Professors Olav Eldholm and Elen Roaldset, and valuable discussions with Professor Leiv K. Sydnes are highly appreciated. Two anonymous reviewers and Academic Editor are thanked for constructive and helpful comments that improved the contents and design of the paper.

Conflicts of Interest: The authors declare no conflict of interest.

References

1. Schutter, S.R. Hydrocarbon occurrence and exploration in and around igneous rocks. In *Hydrocarbons in Crystalline Rocks, Special Publications*; Petford, N., McCaffrey, K.J.W., Eds.; Geological Society: London, UK, 2003; Volume 214, pp. 7–33.
2. Svensen, H.; Planke, S.; Malthe-Sørenssen, A.; Jamtveit, B.; Myklebust, R.; Eidem, T.R.; Rey, S.S. Release of methane from a volcanic basin as a mechanism for initial Eocene global warming. *Nature* **2004**, *429*, 542–545. [CrossRef] [PubMed]
3. Fjeldskaar, W.; Helset, H.M.; Johansen, H.; Grunnaleite, I.; Horstad, I. Thermal modelling of magmatic intrusions in the Gjallar Ridge, Norwegian Sea: Implications for vitrinite reflectance and hydrocarbon maturation. *Basin Res.* **2008**, *20*, 143–159. [CrossRef]
4. Galushkin, Y.I. Thermal effects of igneous intrusions on maturity of organic matter: A possible mechanism of intrusion. *Org. Geochem.* **1997**, *26*, 645–658. [CrossRef]
5. Aarnes, I.; Svensen, H.; Connolly, J.A.D.; Podladchikov, Y.Y. How contact metamorphism can trigger global climate changes: Modeling gas generation around igneous sills in sedimentary basins. *Geochim. Cosmochim. Acta* **2010**, *74*, 7179–7195. [CrossRef]
6. Aarnes, I.; Svensen, H.; Polteau, S.; Planke, S. Contact metamorphic devolatilization of shales in the Karoo Basin, South Africa, and the effects of multiple sill intrusions. *Chem. Geol.* **2011**, *281*, 181–194. [CrossRef]
7. Peace, A.; McCaffrey, K.; Imber, J.; Hobbs, R.; van Hunen, J.; Gerdes, K. Quantifying the influence of sill intrusion on the thermal evolution of organic-rich sedimentary rocks in nonvolcanic passive margins: An example from ODP 210–1276, offshore Newfoundland, Canada. *Basin Res.* **2017**, *29*, 249–265. [CrossRef]
8. Spacapan, J.B.; Palma, J.O.; Galland, O.; Manceda, R.; Rocha, E.; D'Odorico, A.; Leanza, H.A. Thermal impact of igneous sill-complexes on organic-rich formations and implications for petroleum systems: A case study in the northern Neuquén Basin, Argentina. *Mar. Pet. Geol.* **2018**, *91*, 519–531. [CrossRef]
9. Spacapan, J.B.; D'Odorico, A.; Palma, O.; Galland, O.; Rojas Vera, E.; Leanza, H.A.; Medialdea, A.; Manceda, R. Igneous petroleum systems in the Malargüe fold and thrust belt, Río Grande Valley area, Neuquén Basin, Argentina. *Mar. Pet. Geol.* **2020**, *111*, 309–331. [CrossRef]
10. Sydnes, M.; Fjeldskaar, W.; Løtveit, I.F.; Grunnaleite, I.; Cardozo, N. The importance of sill thickness and timing of sill emplacement on hydrocarbon maturation. *Mar. Pet. Geol.* **2018**, *89*, 500–514. [CrossRef]
11. Sydnes, M.; Fjeldskaar, W.; Grunnaleite, I.; Løtveit, I.F.; Mjelde, R. Transient thermal effects in sedimentary basins with normal faults and magmatic sill intrusions—A sensitivity study. *Geosciences* **2019**, *9*, 160. [CrossRef]
12. Gudmundsson, A.; Løtveit, I.F. Sills as hydrocarbon reservoirs: Examples and models. *Geol. Soc. Lond. Spec. Publ.* **2012**, *374*, 251–271. [CrossRef]
13. Montanari, D.; Bonini, M.; Corti, G.; Agostini, A.; Del Ventisette, C. Forced folding above shallow magma intrusions: Insights on supercritical fluid flow from analogue modelling. *J. Volcanol. Geotherm. Res.* **2017**, *345*, 67–80. [CrossRef]
14. Haile, B.G.; Klausen, T.G.; Jahren, J.; Braathen, A.; Hellevang, H. Thermal history of a Triassic sedimentary sequence verified by a multi-method approach: Edgeøya, Svalbard, Norway. *Basin Res.* **2018**, *30*, 1075–1097. [CrossRef]
15. Haile, B.G.; Czarniecka, U.; Xi, K.; Smyrak-Sikora, A.; Jahren, J.; Braathen, A.; Hellevang, H. Hydrothermally induced diagenesis: Evidence from shallow marine-deltaic sediments, Wilhelmøya, Svalbard. *Geosci. Front.* **2019**, *10*, 629–649. [CrossRef]
16. Therkelsen, J. Diagenesis and reservoir properties of Middle Jurassic sandstones, Traill Ø, East Greenland: The influence of magmatism and faulting. *Mar. Pet. Geol.* **2016**, *78*, 196–221. [CrossRef]
17. Allen, P.A.; Allen, J.R. *Basin Analysis: Principles and Application to Petroleum Play Assessment*, 3rd ed.; Wiley-Blackwell: Chichester, UK, 2014.
18. Gluyas, J.; Swarbrick, R. *Petroleum Geosciences*; Blackwell Publishing: Oxford, UK, 2015.
19. Bjørlykke, K.; Ramm, M.; Saigal, G.C. Sandstone diagenesis and porosity modification during basin evolution. *Geol. Rundsch.* **1989**, *78*, 243–268. [CrossRef]
20. Bjørlykke, K. Relationships between depositional environments, burial history and rock properties. Some principal aspects of diagenetic process in sedimentary basins. *Sediment. Geol.* **2014**, *301*, 1–14. [CrossRef]

21. Nobes, D.C.; Murray, R.W.; Kuramoto, S.; Pisciotto, K.A.; Holler, P. Impact of silica diagenesis on physical property variations. In Proceedings of the Ocean Drilling Program, Scientific Results, College Station, TX, USA; 1992; Volume 127/128. [CrossRef]
22. Roaldset, E.; Wei, H. Silica-phase transformation of opal-A to opal_CT to quartz, Part I: An experimental diagenetic approach to natural observations. Prepared for submittal to AAPG. 1997.
23. Roaldset, E.; Wei, H. Silica-phase transformation of opal-A to opal-CT to quartz, Part II: Changes of physical properties. Prepared for submittal to AAPG. 1997.
24. Peltonen, C.; Marcussen, Ø.; Bjørlykke, K.; Jahren, J. Clay mineral diagenesis and quartz cementation in mudstones: The effects of smectite to illite reaction on rock properties. *Mar. Pet. Geol.* **2009**, *26*, 887–898. [CrossRef]
25. Neagu, R.C.; Cartwright, J.; Davies, R. Measurement of diagenetic compaction strain from quantitative analysis of fault plane. *J. Struct. Geol.* **2010**, *32*, 641–655. [CrossRef]
26. Elliot, W.C.; Aronson, J.L.; Matisoff, G.; Gautier, D.L. Kinetics of the smectite to illite transformation in the Denver Basin; clay mineral, K-Ar data, and mathematical model results. *AAPG Bull.* **1991**, *75*, 436–462.
27. Buryakovski, L.A.; Djevanshir, R.D.; Chilingar, G.V. Abnormally-high formation pressures in Azerbaijan and the South Caspian Basin (as related to smectite ↔ illite transformations during diagenesis and catagenesis). *J. Pet. Sci. Eng.* **1995**, *13*, 203–218. [CrossRef]
28. Worden, R.H.; Charpentier, D.; Fisher, Q.J.; Aplin, A.C. Fabric development and the smectite to illite transition in Upper Cretaceous mudstones from the North Sea: An image Analysis Approach. In *Understanding the Micro to Macro Behaviour of Rock-Fluid Systems*; Shaw, R.P., Ed.; Geological Society, Special Publications: London, UK, 2005; Volume 249, pp. 103–114.
29. Robin, V.; Hebert, B.; Beaufort, D.; Sardini, P.; Tertre, E.; Regnault, O.; Descostes, M. Occurrence of authigenic beidellite in the Eocene transitional sandy sediments of the Chu-Saryssu basin (South-Central Kazakhstan). *Sediment. Geol.* **2015**, *321*, 39–48. [CrossRef]
30. Dou, W.; Liu, L.; Wu, K.; Xu, Z.; Feng, X. Diagenesis of tight oil sand reservoirs: Upper Triassic tight sandstones of Yanchang Formation in Ordos Basin, China. *Geol. J.* **2018**, *53*, 707–724. [CrossRef]
31. Morley, C.K.; Maczak, A.; Rungprom, T.; Ghosh, J.; Cartwright, J.A.; Bertoni, C.; Panpichityota, N. New style of honeycomb structures revealed on 3D seismic data indicate widespread diagenesis offshore Great South Basin, New Zealand. *Mar. Pet. Geol.* **2017**, *86*, 140–154. [CrossRef]
32. Higgins, J.A.; Blättler, C.L.; Lundstrom, E.A.; Santiago-Ramos, D.P.; Akhtar, A.A.; Crüger Ahm, A.-S.; Bialik, O.; Holmden, C.; Bradbury, H.; Murray, S.T.; et al. Mineralogy, early marine diagensis, and the chemistry of shallow-water carbonate sediments. *Geochim. Cosmochim. Acta* **2018**, *220*, 512–534. [CrossRef]
33. Fawad, M.; Mondol, N.H.; Baig, I.; Jahren, J. Diagenetic related flat spots within the Paleogene Sotbakken Group in the vicinity of the Senja Ridge, Barents Sea. *Pet. Geosci.* **2019**, 122. [CrossRef]
34. He, J.; Wang, H.; Zhang, C.; Yang, X.; Shangguan, Y.; Zhao, R.; Gong, Y.; Wu, Z. A comprehensive analysis of the sedimentology, petrography, diagenesis and reservoir quality of sandstones from the Oligocene Xiaganchaigou (E_3) Formation in the Lengdong area, Qaidam Basin, China. *J. Pet. Explor. Prod. Technol.* **2019**, *9*, 953–969. [CrossRef]
35. Kruge, M.A. Biomarker geochemistry of the Miocene Monterey Formation, West San Joaquin Basin, California: Implications for petroleum generation. *Org. Geochem.* **1986**, *10*, 517–530. [CrossRef]
36. Behl, R.J. Chert spheroids of the Monterey Formation, California (USA): Early-diagenetic structures of bedded siliceous deposits. *Sedimentology* **2011**, *58*, 325–351. [CrossRef]
37. Weller, R.; Behl, R.J. Physical and Mechanical Characteristics of the Opal-A to Opal-CT Transition Zone: Enhanced Diatomite Permeabiltiy from Heterogeneous Diagenetic Embrittlement. *Search Discov. Artic.* **2015**, #51112, adapted from poster presentation given at Pacific section AAPG, SEG and SEPM Joint Technical Conference, Oxnard, California, USA, 3–5 May, 2015.
38. Dralus, D. Chemical Interactions between Silicates and Their Pore Fluids: How They Affect Rock Physics Properties from Atomic to Reservoir Scales. Ph.D. Thesis, Stanford University, Stanford, CA, USA, August 2013.
39. Dralus, D.; Lewan, M.D.; Peters, K. Kinetics of the Opal-A to Opal-CT Phase transition in Low- and High-TOC Siliceous Shale Source Rocks. *Search Discov. Artic.* **2015**, #41708, adapted form oral presentation given at AAPG Annual Convention & Exhibition, Denver, Colorado, USA, May 31–June 3, 2015.

40. Blystad, P.; Brekke, H.; Færseth, R.B.; Larsen, B.T.; Skogseid, J.; Tørudbakken, B. *Structural Elements of the Norwegian Continental Shelf, Part II: The Norwegian Sea Region*; Technical Report for Norwegian petroleum Directorate; Norwegian Petroleum Directorate: Stavanger, Norway, 1995; Volume 8, ISBN 82-7257-452-7.
41. Davies, R.J.; Cartwright, J.A. Kilometer-scale chemical reaction boundary patters and deformation in sedimentary rocks. *Earth Planet. Sci. Lett.* **2007**, *262*, 125–137. [CrossRef]
42. Peltonen, C.; Marcussen, Ø.; Bjørlykke, K.; Jahren, J. Mineralogical control on mudstone compaction: A study of Late Cretaceous to Early Tertiary mudstones of the Vøring and Møre basins, Norwegian Sea. *Pet. Geosci.* **2008**, *14*, 127–138. [CrossRef]
43. Davies, R.J.; Ireland, M.T.; Cartwright, J.A. Differential compaction due to the irregular topology of a diagenetic reaction boundary: A new mechanism for the formation of polygonal faults. *Basin Res.* **2009**, *21*, 354–359. [CrossRef]
44. Neagu, R.C.; Cartwright, J.; Davies, R.; Jensen, L. Fossilisation of a silica diagenesis reaction front on the mid-Norwegian margin. *Mar. Pet. Geol.* **2010**, *27*, 2141–2155. [CrossRef]
45. Davies, R.J.; Ireland, M.T. Initiation and propagation of polygonal fault arrays by thermally triggered volume reduction reactions in siliceous sediment. *Mar. Geol.* **2011**, *289*, 150–158. [CrossRef]
46. Ireland, M.T.; Davies, R.J.; Goulty, N.R.; Carruthers, D. Structure of a silica diagenetic transformation zone: The Gjallar Ridge, offshore Norway. *Sedimentology* **2011**, *58*, 424–441. [CrossRef]
47. Wrona, T.; Taylor, K.G.; Jackson, C.A.-L.; Huuse, M.; Najorka, J.; Pan, I. Impact of silica diagenesis on the porosity of fine-grained strata: An analysis of Cenozoic mudstones from the North Sea. *Geochem. Geophys. Geosyst.* **2017**, *18*, 1537–1549. [CrossRef]
48. Fjeldskaar, W.; Andersen, Å.; Johansen, H.; Lander, R.; Blomvik, V.; Skurve, O.; Michelsen, J.K.; Grunnaleite, I.; Mykkeltveit, J. Bridging the gap between basin modelling and structural geology. *Reg. Geol. Metallog.* **2017**, *72*, 65–77.
49. Brekke, H. The tectonic evolution of the Norwegian Sea Continental Margin with emphasis on the Vøring and Møre Basins. In *Dynamics of the Norwegian Margin*; Special Publications; Nøttvedt, A., Ed.; Geological Society: London, UK, 2000; Volume 167, pp. 327–378.
50. Bukovics, C.; Cartier, E.G.; Shaw, N.D.; Ziegler, P.A. Structure and development of the mid-Norway Continental Margin. In *Petroleum Geology of the North. European Margin*; Spencer, A.M., Ed.; Norwegian Petroleum Society: Stavanger, Norway; Graham and Trotman: Bristol, UK, 1984; pp. 407–423.
51. Gabrielsen, R.H.; Færseth, R.; Hamar, G.; Rønnevik, H. Nomenclature of the main structural features on the Norwegian Continental Shelf north of the 62nd parallel. In *Petroleum Geology of the North European Margin*; Spencer, A.M., Ed.; Norwegian Petroleum Society: Stavanger, Norway; Graham and Trotman: Bristol, UK, 1984; pp. 41–60.
52. Price, I.; Rattey, R.P. Cretaceous tectonics off mid-Norway: Implications for the Rockall and Faeroe-Shetland troughs. *J. Geol. Soc.* **1984**, *141*, 985–992. [CrossRef]
53. Surlyk, F.; Piasecki, S.; Rolle, F.; Stemmerik, L.; Thomsen, E.; Wrang, P. The Permian base of East Greenland. In *Petroleum Geology of the North European Margin*; Spencer, A.M., Ed.; Norwegian Petroleum Society: Stavanger, Norway; Graham and Trotman: Bristol, UK, 1984; pp. 303–315.
54. Brekke, H.; Riis, F. Tectonics and basin evolution of the Norwegian shelf between 62°N and 72°N. *Nor. Geol. Tidsskr.* **1987**, *67*, 295–322.
55. Doré, A.G.; Lundin, E.R. Cenozoic compressional structures on the NE Atlantic margin: Nature, origin and potential significance for hydrocarbon exploration. *Pet. Geosci.* **1996**, *2*, 299–311. [CrossRef]
56. Swiecicki, T.; Gibbs, P.B.; Farrow, G.E.; Coward, M.P. A tectonostratigraphic framework for the Mid-Norway region. *Mar. Pet. Geol.* **1998**, *15*, 245–276. [CrossRef]
57. Scheck-Wenderoth, M.; Raum, T.; Faleide, J.I.; Mjelde, R.; Horsfield, B. The transition from the continent to the ocean: A deeper view on the Norwegian margin. *J. Geol. Soc.* **2007**, *164*, 855–868. [CrossRef]
58. Mjelde, R.; Kodaira, S.; Shimamura, H.; Kanazawa, T.; Shiobara, H.; Berg, E.W.; Riise, O. Crustal structure of the central part of the Vøring Basin, mid- Norway margin, from ocean bottom seismographs. *Tectonophysics* **1997**, *277*, 235–257. [CrossRef]
59. Talwani, M.; Eldholm, O. Evolution of the Norwegian-Greenland Sea. *GSA Bull.* **1977**, *88*, 969–999. [CrossRef]
60. Eldholm, O.; Thiede, J.; Taylor, E. The Norwegian continental margin: Tectonic, volcanic, and paleoenvironmental framework. In Proceedings of the Ocean Drilling Program, Scientific Results, College Station, TX, USA; 1989; Volume 104. [CrossRef]

61. Stuevold, L.M.; Eldholm, O. Cenozoic uplift of Fennoscandia inferred from a study of the mid-Norwegian margin. *Glob. Planet. Chang.* **1996**, *12*, 359–386. [CrossRef]
62. Grunnaleite, I.; Fjeldskaar, W.; Wilson, J.; Faleide, J.I.; Zweigel, J. Effect of local variations of vertical and horizontal stresses on the Cenozoic structuring of the mid-Norwegian shelf. *Tectonophysics* **2009**, *470*, 267–283. [CrossRef]
63. Dalland, A.; Worsley, D.; Ofstad, K. *A Lithostrategraphic Scheme for the Mesozoic and Cenozoic Succession Offshore Mid- and Northern Norway*; Technical Report for Norwegian petroleum Directorate; Norwegian Petroleum Directorate: Stavanger, Norway, 1988; Volume 4, ISBN 82-7275-241-9.
64. Hjelstuen, B.O.; Eldholm, O.; Skogseid, J. Ceonzoic evolution of the northern Vøring margin. *GSA Bull.* **1999**, *111*, 1792–1807. [CrossRef]
65. Svensen, H.; Planke, S.; Corfu, F. Zircon dating ties NE Atlantic sill emplacement to initial Eocene global warming. *J. Geol. Soc.* **2010**, *167*, 433–436. [CrossRef]
66. Bungum, H.; Alsaker, A.; Kvamme, L.B.; Hansen, R.A. Seismicity and Seismotectonics of Norway and Nearby Continental Shelf Areas. *J. Geophys. Res.* **1991**, *96*, 2249–2265. [CrossRef]
67. Byrkjeland, U.; Bungum, H.; Eldholm, O. Seismotectonics of the Norwegian continental margin. *J. Geophys. Res.* **2000**, *105*, 6221–6236. [CrossRef]
68. Fjeldskaar, W.; Lindholm, C.; Dejls, J.F.; Fjeldskaar, I. Post-glacial uplift, neotectonics and seismicity in Fennoscandia. *Quat. Sci. Rev.* **2000**, *19*, 1413–1422. [CrossRef]
69. Hicks, E.C.; Bungum, H.; Lidholm, C.D. Stress inversion of earthquake focal mechanism solutions from onshore and offshore Norway. *Nor. Geol. Tidsskr.* **2000**, *80*, 235–250. [CrossRef]
70. Bungum, H.; Olesen, O.; Pascal, C.; Gibbons, S.; Lindholm, C.; Vestøl, O. To what extent is the present seismicity of Norway driven by post-glacial rebound? *J. Geol. Soc.* **2010**, *167*, 373–384. [CrossRef]
71. Lander, R.H.; Langfeldt, M.; Bonnell, L.; Fjeldskaar, W. *BMT User's Guide*; Tectonor AS Proprietary Publication: Stavanger, Norway, 1994.
72. Fjeldskaar, W. BMT^{TM}—Exploration tool combining tectonic and temperature modeling: Business Briefing: Exploration & Production. *Oil Gas Rev.* **2003**, 1–4.
73. Walderhaug, O.; Lander, R.H.; Bjørkum, P.A.; Oelkers, E.H.; Bjørlykke, K.; Nadeau, P.H. Modelling Quartz Cementation and Porosity in Reservoir Sandstones: Examples from the Norwegian Continental Shelf. In *Quartz Cementation in Sandstones, Special Publication*; Worden, R.H., Morad, S., Eds.; International Association of Sedimentologists: Algiers, Algeria, 2000; Volume 29, pp. 39–49.
74. Walderhaug, O. Precipitation rates for quartz cement in sandstones determined by fluid-inclusion microthermometry and temperature-history modeling. *J. Sediment. Res.* **1994**, *A64*, 324–333. [CrossRef]
75. Walderhaug, O. Kinetic Modeling of Quartz Cementation and Porosity Loss in Deeply Buried Sandstone Reservoirs. *AAPG Bull.* **1996**, *80*, 731–745.
76. Lander, R.H.; Walderhaug, O. Predicting Porosity through Simulating Sandstone Compaction and Quartz Cementation. *AAPG Bull.* **1999**, *83*, 433–449.
77. Angevine, C.L.; Turcotte, D.L. Porosity reduction by pressure solution: A theoretical model for quartz arenites. *Geol. Soc. Am. Bull.* **1983**, *94*, 1129–1134. [CrossRef]
78. Dewers, T.; Ortoleva, P. A coupled reaction/transport/mechanical model for intergranular pressure solution, stylolites, and differential compaction and cementation in clean sandstones. *Geochim. Cosmochim. Acta* **1990**, *54*, 1609–1625. [CrossRef]
79. Mullis, A.M. The Role of Silica Precipitation Kinetics in Determining the Rate of Quartz Pressure Solution. *J. Geophys. Res.* **1991**, *96*, 10007–10013. [CrossRef]
80. Ramm, M. Porosity-depth trends in reservoir sandstones: Theoretical models related to Jurassic sandstones offshore Norway. *Mar. Pet. Geol.* **1992**, *9*, 553–567. [CrossRef]
81. Stephenson, L.P.; Plumley, W.J.; Palciauskas, V.V. A model for sandstone compaction by grain interpenetration. *J. Sediment. Res.* **1992**, *62*, 11–22.
82. DeMaster, D.J. The supply and accumulation of silica in the marine environment. *Geochim. Cosmochim. Acta* **1981**, *45*, 1715–1732. [CrossRef]
83. Kastner, M.; Keene, J.B.; Gieskes, J.M. Diagenesis of siliceous oozes—I. chemical controls on the rate of opal-A to opal-CT transformation—An experimental study. *Geochim. Cosmochim. Acta* **1977**, *41*, 1041–1059. [CrossRef]

84. Grau, A.; Sterling, R.; Kidney, R. Success! Using Seismic Attributes and Horizontal Drilling to Delineate and Exploit a Diagenetic Trap, Monterey Shale, San Joaquin Valley, California. In Proceedings of the AAPG Annual Convention, Salt Lake City, Utah, USA, 11–14 May 2003.
85. Kidney, R.; Sterling, R.; Grau, A. Delineation of a diagenetic trap using P-wave and converted-wave seismic data in Miocene McLure Shale, San Joaquin Basin, CA. In *SEG Technical Program Expanded Abstracts 2005*; Society of Exploration Geophysicists: Tulsa, OK, USA, 2005; pp. 2329–2332.
86. Isaacs, C.M. Influence of rock composition on kinetics of silica phase changes in the Monterey Formation, Santa Barbara area, California. *Geology* **1982**, *10*, 304–308. [CrossRef]
87. Keller, M.A.; Isaacs, C.M. An Evaluation of Temperature Scales for Silica Diagenesis in Diatomaceous Sequences Including a New Approach Based on the Miocene Formation, California. *Geo-Mar. Lett.* **1985**, *5*, 31–35. [CrossRef]
88. Ernst, W.G.; Calvert, S.E. An Experimental Study of the Recrystallization of Porcelanite and its bearing on the Origin of some bedded Cherts. *Am. J. Sci.* **1969**, *267*, 114–133.
89. Castellan, G.W. *Physical Chemistry*, 3rd ed.; Addison-Wesley Publishing Company: Reading, MA, USA, 1969.
90. Jiang, S. Clay Minerals from the Perspective of Oil and Gas Exploration. In *Clay Minerals in Nature—Their Characterization, Modification and Application*; Valaškova, M., Martynkova, G.S., Eds.; IntechOpen: London, UK, 2012. [CrossRef]
91. Bjørkum, P.A.; Nadeau, P.H. Temperature Controlled Porosity/Permeability Reduction, Fluid Migration, and Petroleum Exploration in Sedimentary Basins. *APPEA J.* **1998**, *38*, 453–465. [CrossRef]
92. Pevear, D.R. Illite and hydrocarbon exploration. *Proc. Natl. Acad. Sci. USA* **1999**, *96*, 3440–3446. [CrossRef] [PubMed]
93. Boles, J.R.; Franks, S.G. Clay Diagenesis in Wilcox sandstones of southwest Texas: Implications of smectite diagenesis on sandstone cementation. *J. Sediment. Res.* **1979**, *49*, 55–70.
94. Huang., W.-L.; Longo, J.M.; Pevear, D.R. An experimentally derived kinetic model for smectite-to-illite conversion and its use as a geothermometer. *Clays Clay Miner.* **1993**, *41*, 162–177. [CrossRef]
95. Roaldset, E.; Wei, H.; Grimstad, S. Smectite to illite conversion by hydrous pyrolysis. *Clay Miner.* **1998**, *33*, 147–158. [CrossRef]
96. Nadeau, P.H.; Wilson, M.J.; McHardy, W.J.; Tait, J.M. Interstratified Clays as Fundamental Particles. *Science* **1984**, *225*, 923–925. [CrossRef]
97. Nadeau, P.H.; Wilson, M.J.; McHardy, W.J.; Tait, J.M. The conversion of smectite to illite during diagenesis: Evidence from some illitic clays from bentonites and sandstones. *Mineral. Mag.* **1985**, *49*, 393–400. [CrossRef]
98. Nadeau, P.H.; Bain, D.C. Composition of some smectites and diagenetic illitic clays and implications for their origin. *Clays Clay Miner.* **1986**, *34*, 455–464. [CrossRef]
99. Bjørlykke, K.; Aagaard, P.; Egeberg, P.K.; Simmons, S.P. Geochemical constraints from formation water analyses from the North Sea and the Gulf Coast Basins on quartz, feldspar and illilte precipitation in reservoir rocks. In *The Geochemistry of Reservoirs*; Special Publication; Cubitt, J.M., England, W.A., Eds.; Geological Society: London, UK, 1995; Volume 86, pp. 33–50.
100. Eberl, D.; Hower, J. Kinetics of illite formation. *Geol. Soc. Am. Bull.* **1976**, *87*, 1326–1330. [CrossRef]
101. Wei, H.; Roaldset, E.; Bjorøy, M. Parallel Reaction kinetics of smectite to illite conversion. *Clay Miner.* **1996**, *31*, 365–376. [CrossRef]
102. Hillier, S.; Matyas, J.; Matter, A.; Vasseur, G. Illite/Smectite diagenesis and its variable correlation with vitrinite reflectance in the Pannonian Basin. *Clays Clay Miner.* **1995**, *43*, 174–183. [CrossRef]
103. Sachsenhofer, R.F.; Rantitcsh, G.; Hasenhüttl, C.; Russegger, B.; Jelen, B. Smectite to illite diagenesis in early Miocene sediments from the hyperthermal western Pannonian Basin. *Clay Miner.* **1998**, *33*, 523–537.
104. Anell, I.; Thybo, H.; Artemieva, I.M. Cenozoic uplift and subsidence in the North Atlantic region: Geological evidence revisited. *Tectonophysics* **2009**, *474*, 78–105. [CrossRef]
105. Anell, I.; Thybo, H.; Stratford, W. Relating Cenozoic North Sea sediments to topography in southern Norway: The interplay between tectonics and climate. *Earth Planet. Sci. Lett.* **2010**, *300*, 19–32. [CrossRef]
106. Nielsen, S.B.; Gallagher, K.; Leighton, C.; Balling, N.; Svenningsen, L.; Jacobsen, B.H.; Thomsen, E.; Nielsen, O.B.; Heilmann-Clausen, C.; Egholm, D.L.; et al. The evolution of western Scandinavian topography: A review of Neogene uplift versus the ICE (isostasy–climate–erosion) hypothesis. *J. Geodyn.* **2009**, *47*, 72–95. [CrossRef]

107. Nielsen, S.B.; Clausen, O.R.; Jacobsen, B.H.; Thomsen, E.; Huuse, M.; Gallagher, K.; Balling, N.; Egholm, D. The ICE hypothesis stands: How the dogma of late Ceonozoic tectonic uplift can no longer be sustained in the light of data and physical laws. *J. Geodyn.* **2010**, *50*, 102–111. [CrossRef]
108. Sclater, J.G.; Christie, P.A.F. Continental stretching: An explanation of the post-mid-cretaceous subsidence of the central North Sea basin. *J. Geophys. Res.* **1980**, *85*, 3711–3739. [CrossRef]
109. Čermác, V.; Rybach, L. Thermal properties: Thermal conductivity and specific heat of minerals and rocks. In *Landolt-Börnstein Zahlenwerte und Functionen aus Naturwissenschaften und Technik, Neue Serie, Physikalische Eigenschaften der Gesteine*; Angeneister, G., Ed.; Springer: Berlin/Heidelberg, Germany; New York, NY, USA, 1982; pp. 305–343.
110. Pollastro, R.M. Considerations and Applications of the Illite/Smectite Geothermometer in Hydrocarbon-Bearing Rocks of Miocene to Mississippian Age. *Clays Clay Miner.* **1993**, *41*, 119–133. [CrossRef]
111. Gudmundsson, A. *Rock Fractures in Geological Processes*, 1st ed.; Cambridge University Press: Cambridge, UK, 2011.
112. Bell, F.G. *Engineering Properties of Soils and Rocks*, 4th ed.; Blackwell: Oxford, UK, 2000.
113. Farmer, I. *Engineering Behaviour of Rocks*, 2nd ed.; Chapman and Hall: London, UK, 1983.
114. Paterson, M.S.; Wong, T.F. *Experimental Rock Deformation: The Brittle Field*, 2nd ed.; Springer: Berlin, Germany, 2005.
115. Haimson, B.C.; Rummel, F. Hydrofracturing stress measurements in the Iceland research drilling project drill hole at Reydarfjördur, Iceland. *J. Geophys. Res.* **1982**, *87*, 6631–6649. [CrossRef]
116. Schultz, R.A. Limits on strength and deformation properties of jointed basaltic rock masses. *Rock Mech. Rock Eng.* **1995**, *28*, 1–15. [CrossRef]
117. Amadei, B.; Stephansson, O. *Rock Stress and Its Measurement*; Chapman and Hall: London, UK, 1997.
118. Gudmundsson, A.; Brenner, S.L. How hydrofractures become arrested. *Terra Nova* **2001**, *13*, 456–462. [CrossRef]
119. Gudmundsson, A.; Fjeldskaar, I.; Brenner, S.L. Propagation pathways and fluid transport of hydrofractures in jointed and layered rocks in geothermal fields. *J. Volcanol. Geotherm. Res.* **2002**, *116*, 257–278. [CrossRef]
120. Fjeldskaar, W.; Prestholm, E.; Guargena, C.; Stephenson, M. Mineralogical and diagenetic control on the thermal conductivity of the sedimentary sequences in the Bjørnøya Basin, Barents Sea. In *Basin Modelling: Advances and Applications, Special Publication*; Doré, A.G., Ed.; NPF: Stavanger, Norway, 1993; Volume 3, pp. 445–453.
121. Ireland, M.; Goulty, N.R.; Davies, R.J. Influence of pore water chemistry on silica diagenesis: Evidence from the interaction of diagenetic readtion zones with polygonal fault systems. *J. Geol. Soc.* **2010**, *167*, 273–279. [CrossRef]
122. McKinley, J.M.; Worden, R.H.; Ruffell, A.H. Contact Diagenesis: The effect of an intrusion on reservoir quality in the Triassic Sherwood Sandstone group, Northern Ireland. *J. Sediment. Res.* **2001**, *71*, 484–495. [CrossRef]
123. Bernet, M.; Gaupp, R. Diagenetic history of Triassic sandstone from the Beacon Supergroup in central Victoria Land, Antarctica. *N. Z. J. Geol. Geophys.* **2005**, *48*, 447–458. [CrossRef]
124. Grove, C. Direct and Indirect Effects of Flood Basalt Volcanism on Reservoir Quality Sandstone. Ph.D. Thesis, Durham University, Durham and Stockton-on-Tees, UK, 2014.
125. Nejbert, K.; Krajewski, K.P.; Dubinska, E.; Pécskay, Z. Dolerites of Svalbard, north-west Barents Sea Shelf: Age, tectonic setting and significance for geotectonic interpretation of the High-Arctic Large Igneous Province. *Polar Res.* **2011**, *30*, 7306. [CrossRef]
126. Ehrenberg, S.N. Relationship between Diagenesis and Reservoir Quality in Sandstones of the Garn Formation, Haltenbanken, Mid-Norwegian Continental Shelf. *AAPG Bull.* **1990**, *74*, 1538–1558. [CrossRef]
127. Bjørlykke, K.; Nedkvitne, T.; Ramm, M.; Saigal, G.C. Diagenetic processes in the Brent Group (Middle Jurassic) reservoirs of the North Sea: An overview. In *Geology of the Brent Group*; Special Publication; Morton, A.C., Haszeldine, R.S., Giles, M.R., Brown, S., Eds.; Geological Society: London, UK, 1992; Volume 61, pp. 263–287.
128. Ehrenberg, S.N. Preservation of Anomalously High Porosity in Deeply Buried Sandstones by Grain-Coating Chlorite: Examples from the Norwegian Continental Shelf. *AAPG Bull.* **1993**, *77*, 1260–1286.
129. Freiburg, J.T.; Ritzi, R.W.; Kehoe, K.S. Depositional and diagenetic controls on anomalously high porosity within a deeply buried CO_2 storage reservoir—The Cambrian Mt. Simon Sandstone, Illinois Basin, USA. *Int. J. Greenh. Gas Control* **2016**, *55*, 42–54. [CrossRef]

130. Lin, W.; Chen, L.; Lu, Y.; Hu, H.; Liu, L.; Liu, X.; Wei, W. Diagenesis and its impact on reservoir quality for the Chang 8 oil group tight sandstone of the Yanchang Formation (upper Triassic) in southwestern Ordos basin, China. *J. Pet. Explor. Prod. Technol.* **2017**, *7*, 947–959. [CrossRef]
131. PetroWiki.org. Available online: https://petrowiki.org/Diatomite (accessed on 27 September 2019).
132. Tsuji, T.; Masui, Y.; Yokoi, S. New hydrocarbon trap models for the diagenetic transformation of opal-CT to quartz in Neogene siliceaous rocks. *AAPG Bull.* **2011**, *95*, 449–477. [CrossRef]
133. Davies, R.J.; Cartwright, J. A fossilized Opal A to Opal C/T transformation on the northeast Atlantic margin: Support for a significantly elevated Palaeogeothermal gradient during the Neogene? *Basin Res.* **2002**, *14*, 467–486. [CrossRef]
134. Hall, P.L.; Astill, D.M.; McConnell, J.D.C. Thermodynamic and structural aspects of the dehydration of smectites in sedimentary rocks. *Clay Miner.* **1986**, *21*, 633–648. [CrossRef]
135. Singer, A.; Müller, G. Diagenesis in argillaceous sediments. In *Diagenesis in Sediments and Sedimentary Rocks*; Larsen, G., Chilingar, G.V., Eds.; Elsevier: Amsterdam, The Netherlands, 1983.
136. Essene, E.J.; Peacor, D.R. Clay mineral thermometry—A critical perspective. *Clays Clay Miner.* **1995**, *43*, 540–553. [CrossRef]
137. Podladchikov, Y.Y.; Wickham, S.M. Crystallization of Hydrous Magmas: Calculation of Associated Thermal Effects, Volatile Fluxes, and Isotopic Alteration. *J. Geol.* **1994**, *102*, 25–45. [CrossRef]
138. Iyer, K.; Rüpke, L.; Galerne, C.Y. Modeling fluid flow in sedimentary basins with sill intrusions: Implications for hydrothermal venting and climate change. *Geochem. Geophys. Geosyst.* **2013**, *14*, 5244–5262. [CrossRef]
139. Iyer, K.; Schmid, D.W.; Planke, S.; Millett, J. Modelling hydrothermal venting in volcanic sedimentary basins: Impact on hydrocarbon maturation and paleoclimate. *Earth Planet. Sci. Lett.* **2017**, *467*, 30–42. [CrossRef]
140. Wang, D.; Manga, M. Organic matter maturation in the contact aureole of an igneous sill as a tracer of hydrothermal convection. *J. Geophys. Res. Solid Earth* **2015**, *120*, 4102–4112. [CrossRef]
141. Annen, C. Factors affecting the thickness of thermal aureoles. *Front. Earth Sci.* **2017**, *5*, 1–13. [CrossRef]
142. Planke, S.; Rasmussen, T.; Rey, S.; Myklebust, R. Seismic characteristics and distribution of volcanic intrusions and hydrothermal vent complexes in the Vøring and Møre basins. In *Petroleum Geology: North-West Europe and Global Perspectives, Proceedings of the 6th Petroleum Geology Conference*; Dorè, A.G., Vining, B.A., Eds.; Geological Society: London, UK, 1 January 2005; pp. 833–844.

References

Aarnes, I. Svensen, H., Connolly, J.A.D., Podladchikov, Y.Y. (2010): How contact metamorphism can trigger global climate changes: Modeling gas generation around igneous sills in sedimentary basins. Geochimica et Cosmochimica Acta, 74, 7179-7195.

Aarnes, I., Svensen, H., Polteau, S., Planke, S. (2011): Contact metamorphic devolatilization of shales in the Karoo Basin, South Africa, and the effects of multiple sill intrusions. Chemical Geology, 281, 181-194.

Aarnes, I., Planke, S., Trulsvik, M., Svensen, H. (2015): Contact metamorphism and thermogenic gas generation in the Vøring and Møre basins, offshore Norway, during the Paleocene-Eocene thermal maximum. Journal of Geological Society, **172**, 588-598.

Allen, P.A., Allen, J.R. (2014): Basin Analysis: Principles and Application to Petroleum Play Assessment, 3rd ed.; Wiley-Blackwell: Chichester, West Sussex, UK.

Amadei, B., Stephansson, O. (1997): Rock stress and its Measurement. Chapman and Hall, London, UK.

Atkins, P., de Paula, J., Keller, J. (2017): Atkins Physical Chemistry; Oxford University Press, Oxford, UK.

Bell, F.G. (2000): Enigineering Properties of Soils and Rocks. Blackwell, Oxford.

Berndt, C., Skogly, O.P., Planke, S., Eldholm, O., Mjelde, R., (2000): High-velocity breakup-related sills in the Vøring basin, off Norway. Journal of Geophysical Research, 105, 28443-28454.

Bjørkum, P.A., Nadeau, P.H. (1998): Temperature Controlled Porosity/Permeability Reduction, Fluid Migration, and Petroleum Exploration in Sedimentary Basins. APPEA Journal, 38, 453–465.

Bostick, N.H., Pawlewicz, M.J. (1984): Paleotemperatures based on vitrinite reflectance of shales and limestones in igneous dike aureoles in the Upper Cretaceous Pierre Shale, Walsenburg, Colorado. In Hydrocarbon Source Rocks of the Greater Rocky Mountain Region; Woodward, J.G., Meissner, F.F., Clayton, C.J., Eds.; Rocky Mountain Association of Geologists Symposium: Denver, CO, USA, pp. 387–392.

Brady, B.H.G., Brown, E.T. (2005): Rock Mechanics for underground mining, 3rd edition; Springer Science, Business Medis, Inc., Dordrecht, Hollan

British Petroleum (BP) (2019): Energy Outlook. http://www.bp.com/content/dam/bp/business-sites/en/global/corporate/pdfs/energy-economics/energy-otlook/bp-energy-otlook-2019.pdf. Viewed 29.11.2019.

Chen, Y., Qin, Y., Ji, M., Duan, H., Wu, C., Shi, Q., Zhang; X., Wang, Z. (2020): Influence of lamprophyre sills on coal metamorphism, coalbed gas composition and coalbed gas occurrence in the Tongxin Minefield, Datong Coalfield, China. International Journal of Coal Geology, 217, 103286.

Coffin, M.F., Eldholm, O. (1994): Large Igneous Provinces: Crustal structure, dimensions, and external consequences. Reviews of Geophysics, 32, 1-36.

Dill, H.G. (2018): Gems and Placers – A Genetic Relationship Par Excellence. Minerals, 8, 470.

Dow, W.G. (1977): Kerogen studies and geological interpretations. Journal of Geochemical Exploration, *7*, 79–99.

Dralus, D. (2013): Chemical interactions between silicates and their pore fluids: How they affect rock physics properties from atomic to reservoir scales. PhD thesis, Stanford University, California, USA.

Eide, C.H., Schofield, N., Jerram, D.A., Howell, J.A., (2017a): Basin-scale architecture of deeply emplaced sill complexes: Jameson Land, East Greenland. Journal of the Geological Society, 174, 23-40.

Eide, C.H., Schofield, N., Lecomte, I., Buckley, S.J., Howell, J.A. (2017b): Seismic interpretation of sill complexes in sedimentary basins: implications for the sub-sill imaging problem. Journal of the Geological Society, 175, 193-209.

Eldursi, K., Branquet, Y., Guillou-Frottier, L., Martelet, G., Calcagno, P. (2018): Intrusion-Related Gold Deposits: New insights from gravity and hydrothermal integrated 3D modeling applied to the Tighza gold mineralization (Central Morocco). Journal of African Earth Sciences, 140, 199-211.

Essene, E.J., Peacor, D.R. (1995): Clay mineral thermometry – A critical perspective. Clays and Clay Minerals, 43, 540-553.

Farmer, I. (1983): Engineering Behaviour of Rocks, 2nd ed.; Chapman and Hall: London, England.

Fayol, N., Jébrak, M., Harris, L.B. (2016): The magnetic signature of Neoarchean alkaline intrusions and their realted gold deposits: Significance and exploration implications. Precambrian Research, 283, 13-23.

Fjeldskaar, W. (2003): BMT™ - Exploration Tool Combining Tectonic and Temperature Modelling: Business Briefing: Exploration & Production, The Oil and Gas Review, 1-4.

Fjeldskaar, W., Helset, H.M., Johansen, H., Grunnaleite, I., Horstad, I. (2008): Thermal modelling of magmatic intrusions in the Gjallar Ridge, Norwegian Sea: implications for vitrinite reflectance and hydrocarbon maturation. Basin Research, 20, 143-159.

Fjeldskaar, W.; Andersen, Å.; Johansen, H.; Lander, R.; Blomvik, V.; Skurve, O.; Michelsen, J.K.; Grunnaleite, I.; Mykkeltveit, J. (2017): Bridging the gap between basin modelling and structural geology. Regional Geology and Metallogeny, 72, 65–77.

Galushkin, Y.I. (1997). Thermal effects of igneous intrusions on maturity of organic matter: A possible mechanism of intrusion. Organic Geochemistry, 26, 645-658.

Gac, S., Hansford, P.A., Faleide, J.I. (2018): Basin modelling of the SW Barents Sea. Marine and Petroleum Geology, 95, 167-187.

Geoffroy, L. (2005): Volcanic passive margins. Comptes Rendus Geoscience, 337, 1395-1408.

Gluyas, J., Swarbrick, R. (2015): Petroleum Geoscience; Blackwell Publishing, Oxford, UK.

Grunnaleite, I., Mosbron, A. (2019): On the significance of salt modelling – Example from Modelling of Salt Tectonics, Tempeature and Maturity Around Salt Structures in Southern North Sea. Geosciences, 9, 363.

Gudmundsson, A. (1990): Emplacement of dikes, sills and crustal magma chambers at divergent plate boundaries. Tectonophysics, 176, 257-275.

Gudmundsson, A. (2001): Fluid overpressure and flow in fault zones: field measurements and models. Tectonophysics, 336, 183-197.

Gudmundsson, A., Brenner, S.L. (2001): How hydrofractures become arrested. Terra Nova, 13, 456-462.

Gudmundsson, A., Fjeldskaar, I., Brenner, S.L. (2002): Propagation pathways and fluid transport of hydrofractures in jointed and layered rocks in geothermal fields. Journal of Volcanology and Geothermal Research, 116, 257-278.

Gudmundsson, A. (2011a): Deflection of dykes into sills at discontinuities and magma-chamber formation. Tectonophysics, 500, 50-64.

Gudmundsson, A. (2011b): Rock Fractures in Geological Processes, 1st ed.; Cambridge University Press: Cambridge, UK.

Gudmundsson, A., Løtveit, I.F. (2012): Sills as hydrocarbon reservoirs: examples and models. Geological Society, London, Special Publications, 374, 251-271.

Guice, G.L., Törmänen, T., Karykowski, B.T., Johanson, B., Lahaye, Y. (2017): Precious metal mineralization in the Sotkavaara Intrusion, northern Finland: Peak Pt, Pd, Au, Cu, offsets in a small intrusion with poorly-developed magmatic layering. Ore Geology Reviews, 89, 701-718.

Haggerty, S.E. (1999): A Diamond Trilogy: Superplumes, Supercontinents, and Supernovae. Science, 285, 5429, 851-860.

Haile, B.G., Klausen, T.G., Jahren, J., Braathen A., Hellevang, H. (2018): Thermal history of a Triassic sedimentary sequence verified by a multi-method approach: Edgeøya, Svalbard, Norway. Basin Research, 30, 1075-1097.

Haile, B.G., Czarniecka, U., Xi, K., Smyrak-Sikora, A., Jahren, J., Braathen, A., Hellevang, H. (2019): Hydrothermally induced diagenesis: Evidence from shallow marine-deltaic sediments, Wilhelmøya, Svalbard. Geoscience Frontiers, 10, 629-649.

Haimson, B.C., Rummel, F. (1982): Hydrofracturing stress measurements in the Iceland research drilling project drill hole at Reydarfjördur, Iceland. Journal of Geophysical Research, 87, 6631-6649.

Hansen, D.M., Cartwright, J. (2006): The three-dimensional geometry and growth of forced folds above saucer-shaped igneous sills. Journal of structural Geology, 28, 1520-1535.

Hansen. J., Jerram, D.A., McCaffrey, K., Passey, S.R. (2011): Early Cenozoic saucer-shaped sills of the Faroe Islands: an example of intrusive styles in basaltic lava piles. Journal of the Geological Society, 168, 159-178.

Hart, B.S. (2000): 3-D Seismic Interpretation: A Primer for Geologists. Society for Sedimentary Geology Special Publication, Short Course, 48.

Hatch, J.R., Affolter, R.H. (2015): Resource Assessment of the Sprinfield, Herrin, Danville, and Baker Coals in the Illinois Basin. U.S. Geological Survey Professional Paper 1625-D.

Howell, S.M., Ito, G., Breivik, A.J., Rai, A., Mjelde, R., Hanan, B., Sayit, K., Vogt, P. (2014): The origin of the asymmetry in the Iceland hotspot along the Mid-Atlantic Ridge from continental breakup to present-day. Earth and Planetary Science Letters, 392, 143-153.

Huang., W.-L., Longo, J.M., Pevear, D.R. (1993): An experimentally derived kinetic model for smectite-to-illite conversion and its use as a geothermometer. Clays and Clay Minerals, 41, 162–177.

Ireland, M. T., Goulty, N.R., Davies, R.J. (2010): Influence of pore water chemistry on silica diagenesis: evidence from the interaction of diagenetic reaction zones with polygonal fault systems. Journal of Geological Society, 167, 273–279.

Iyer, K., Rüpke, L., Galerne, C.Y. (2013): Modeling fluid flow in sedimentary basins with sill intrusions: Implications for hydrothermal venting and climate change. Geochemistry, Geophysics, Geosystems, 14, 5244-5262.

Iyer, K., Schmid, D.W., Planke, S., Millett, J. (2017): Modelling hydrothermal venting in volcanic sedimentary basins: Impact on hydrocarbon maturation and paleoclimate. Earth and Planetary Science Letters, 467, 30-42.

Jackson, C.A.-L., Schofield, N., Golenkov, B. (2013): Geometry and controls on the development of igneous sill-related forced folds: A 2-D seismic reflection case study from offshore southern Australia. Geological Society of America Bulletin, 125, 1874-1890.

Jiang, J.-Y., Cheng, Y.-P., Wang, L., Li, W., Wang, L. (2011): Petrographic and geochemical effects of sill intrusions on coal and their implications for gas outbursts in the Wolonghu Mine, Huaibei Coalfield, China. International Journal of Coal Geology, 88, 55-66.

Kastner, M., Keene, J.B., Gieskes, J.M. (1977): Diagenesis of siliceous oozes—I. Chemical controls on the rate of opal-A to opal-CT transformation—an experimental study. Geochimica et Cosmochimica Acta, 41, 1041–1059.

Kjoberg, S., Schmiedel, T., Planke, S., Svensen, H.H., Millett, J.M., Jerram, D.A., Galland, O., Lecomte, I., Schofield, N., Haug, Ø.T. Helsem, A. (2017): 3D structure and formation of hydrothermal vent complexes at the Paleocene-Eocene transition, the Møre Basin, mid-Norwegian margin. Interpretation, 5, 65-81.

Lander, R.H., Langfeldt, M., Bonnell, L., Fjeldskaar, W. (1994): BMT user's guide. Tectonor AS proprietary publication.

Magee, C., Maharaj, S.M., Wrona, T., Jackson, C.A.-L. (2015): Controls on the expression of igneous intrusions in seismic reflection data. Geosphere, 11, 1024-1041.

Magee, C., Hoggett, M., Jackson, C.A.-L., Jones, S.M. (2019): Burial-Related Compaction modifies Intrusion-Induced Forced Folds: Implications for Reconciling Roof Uplift Mechanisms Using Seismic Reflection Data. Frontiers in Earth Science, 7, 37.

Maier, W.D., Hanski, E.J. (2017): Layered Mafic-Ultramaifc Intrusions of Fennoscandia: Europe's Treasure Chest of Magmatic Metal Deposits. Elements, 13, 415-420.

McKenzie, D. (1978): Some remarks on the development of sedimentary basins. Earth and Planetary Science Letters, 40, 25-32.

Michelsen, J.K. (2017): Personal communication.

Minakov, A., Mjelde, R., Faleide, J.I., Flueh, E.R., Dannowski, A., Keers, H. (2012): Mafic intrusions east of Svalbard imaged by active-source seismic tomography. Tectonophysics, 518-521, 106-118.

Mjelde, R., Kodaira, S., Digranes, P., Shimamura, H., Kanazawa, T., Shiobara, H., Berg, E.W., Riise, O. (1997a): Comparison between a Regional and Semi-regional Crustal OBS Model of the Vøring Basin, Mid-Norway Margin. Pure and applied Geophysics, 149, 641-665.

Mjelde, R., Kodaira, S., Shimamura, H., Kanazawa, T., Shiobara, H., Berg, E.W., Riise, O. (1997b): Crustal structure of the central part of the Vøring Basin, mid- Norway margin, from ocean bottom seismographs. Tectonophysics, 277, 235-257.

Mjelde, R., Breivik, A.J., Elstad, H., Ryseth, A.E., Skilbrei, J.R., Opsal, J.G., Shimamura, H., Murai, Y., Nishimura, Y. (2002): Geological development of the Sørvestsnaget Basin, SW Barents Sea, from ocean bottom seismic, surface seismic and potential field data. Norwegian Journal of Geology, 82, 183-202.

Mjelde, R., Kvarven, T., Faleide, J.I. Thybo, H. (2016): Lower crustal high-velocity bodies along North-Atlantic passive margins, and their link to Caledonian suture zone eclogites and Early Cenozoic magmatism. Tectonophysics, 670, 16-29.

Montanari, D., Bonini, M., Cori, G., Agostini, A., Ventisette, C.D. (2017): Forced folding above shallow magma intrusions: Insights on supercritical fluid flow from analogue modelling. Journal of Volcanology and Geothermal Research, 345, 67–80.

Moorcroft, D., Tonnelier, N. (2016): Contact Metamorphism of Black Shales in the Thermal Aureole of a Dolerite Sill Within the Karoo Basin. In *Origin and Evolution of the Cape Mountains and Karoo Basin, Regional Geology Reviews*; Linol, B., de Wit, M.J., Eds.; Springer International Publishing: Cham, Switzerland, 75–84.

Moorhouse, W.W. (1942): Gold mineralization in minor igneous intrusions. Economic Geology, 37, 318-329.

Neagu, R.C., Cartwright, J., Davies, R. (2010): Measurement of diagenetic compaction strain from quantitative analysis of fault plane. Journal of Structural Geology, 32, 641–655.

Nobes, D.C., Murray, R.W., Kuramoto, S., Pisciotto, K.A., Holler, P. (1992): Impact of silica diagenesis on physical property variations. In Proceedings of the Ocean Drilling Program, Scientific Results, Volume 127/128.

Nyblade, A.A., Pollack, H.N. (1993): A Global Analysis of Heat Flow From Precambrian Terrains: Implications for the Thermal Structure of Archean and Proterozoic Lithosphere. Journal of Geophysical Research, 98, 12207-12218.

Omosanya, K.O., Johansen, S.E., Eruteya, O.E., Waldmann, N. (2017): Forced folding and complex overburden deformation associated with magmatic intrusion in the Vøring Basin, offshore Norway. Tectonophysics, 706-707, 14-34.

Osagiede, E.E., Duffy, O.B., Jackson, C.A.-L., Wrona, T. (2014): Quantifying the growth history of seismically imaged normal faults. Journal of Structural Geology, 66, 382-399.

Parada, S.G., Stolyarov, V.V. (2012): Relation of Gold Mineralization on the Northern Flank of the Tyrnyauz Deposits to Intrusive Complexes, Kabardino-Balkar Republic. Doklady Earth Sciences, 445, 939-942.

Pascal, C., Balling, N., Barrère, C., Davidsen, B., Ebbing, J., Elvebakk, H., Mesli, M., Roberts, D., Slagstad, T., Willemoes-Wissing, B. (2010): HeatBar Final Report, Basement Heat Generation and Heat Flow in the western Barents Sea – Importance for hydrocarbon systems. NGU Report 2010.030.

Paterson, M.S., Wong, T. (2005): Experimental Rock Deformation – The Brittle Field, 2nd ed: Springer-Verlag, Berlin Heidelberg, Germany.

Peace, A., McCaffrey, K., Imber, J., Hobbs, R., van Hunen, J., Gerdes, K. (2017): Quantifying the influence of sill intrusion on the thermal evolution of organic-rich sedimentary rocks in nonvolcanic passive margins: an example from ODP 210-1276, offshore Newfoundland, Canada. Basin Research, 29, 249-265.

Peltonen, C., Marcussen, Ø., Bjørlykke, K., Jahren, J. (2009): Clay mineral diagenesis and quartz cementation in mudstones: The effects of smectite to illite reaction on rock properties. Marine and Petroleum Geology, 26, 887-898.

Phillips, T.B., Magee, C., Jackson, C.A.-L., Bell, R.E. (2018): Determining the three-dimensional geometry of a dike swarm and its impact on later rift geometry using seismic reflection data. Geology, 46, 119-122.

Planke, S., Rasmussen, T., Rey, S.S., Myklebust, R. (2005): Seismic characteristics and distribution of volcanic intrusions and hydrothermal vent complexes in the Vøring and Møre basins. In: A.G. Dorè, and B.A. Vining, eds., Petroleum Geology: North-West Europe and Global Perspectives – Proceedings of the 6th Petroleum Geology Conference, 833-844.

Planke, S., Millett, J.M., Maharjan, D., Jerram, D.A., Abdelmalak, M.M., Groth, A., Hoffmann, J., Berndt, C., Myklebust, R. (2017): Igneous seismic geomorphology of buried lava fields and coastal escarpments on the Vøring volcanic rifted margin. Interpretation, 5, 161-177.

Rahman, M.W., Rimmer, S.M., Rowe, H.D. (2018): The impact of rapid heating by intrusion on the geochemistry and petrography of coals and organic-rich shales in the Illinois Basin. International Journal of Coal Geology, 187, 45-53.

Raymond, A.C.; Murchison, D.G. (1988): Development of organic maturation in the thermal aureoles of sills and its relation to sediment compaction. FUEL, 67, 1599–1608.

Roaldset, E., Wei, H. (1997a): Silica-phase transformation of opal-A to opal-CT to quartz, Part I: Changes of physical properties. Unpublished results, prepared for submittal AAPG.

Roaldset, E., Wei, H. (1997b): Silica-phase transformation of opal-A to opal-CT to quartz, Part II: Changes of physical properties. Unpublished results, prepared for submittal AAPG.

Roaldset, E., Wei, H., Grimstad, S. (1998): Smectite to illite conversion by hydrous pyrolysis. Clay Minerals, 33, 147-158.

Robertson, E.C. (1988): Thermal properties of rocks. United States Department of the interior Geological Survey, Open-File Report 88-441.

Sachsenhofer, R.F., Rantitsch, G., Hasenhüttl, C., Russegger, B., Jelen, B. (1998): Smectite to illite diagenesis in early Miocene sediments from the hyperthermal western Pannonian Basin. Clay Minerals. 33, 523-537.

Schofield, N., Alsop, I., Warren, J., Underhill., J.R., Lehné, R., Beer, W., Lukas, V. (2014): Mobilizing salt: Magma-salt interactions. Geology, 42, 599-602.

Schultz, R.A. (1995): Limits on Strength and Deformation Properties of Jointed Basaltic Rock Masses. Rock Mechanics and Rock Engineering, 28, 1-15.

Schutter, S.R. (2003): Hydrocarbon occurrence and exploration in and around igneous rocks. In *Hydrocarbons in Crystalline Rocks*; Petford, N., McCaffrey, K.J.W., Eds.; Geological Society, Special Publications: London, UK, 214, 7–33.

Sclater, J.G., Christie, P.A.F. (1980): Continental stretching: an explanation of the post-mid-cretaceous subsidence of the central North Sea basin. Journal of Geophysical Research, 85, 3711-3739.

Scott, S., Driesner, T., Weis, P. (2015): Geologic controls on supercritical geothermal resources above magmatic intrusions. Nature Communications, 6:7837.

Scott, S., Driesner, T., Weis, P. (2018): A New Conceptual Framework for the Deep Roots og Magma-Driven Geothermal Systems. Proceedings, 43rd Workshop on Geothermal Reservoir Engineering, Stanford University, Stanford, California, February 12-14.

Senger, K., Millett, J., Planke, S., Ogata, K., Eide, C.H., Festøy, M., Galland, O., Jerram, D.A. (2017): Effects of igneous intrusions on the petroleum system: a review. First Break, 35, 47-56.

Sengör, A.M.C., Burke, K. (1978): Relative timing of rifting and volcanism on earth and its tectonic implications. Geophysical Research Letters, 5, 419-421.

Shi, Q., Qin, B., Bi, Q., Qu, B. (2018): An experimental study on the effect of igneous intrusions on chemical structure and combustion characteristics of coal in Daxing Mine, China. Fuel, 226, 307-315.

Sillitoe, R.H., Thompson, J.F.H. (1998): Intrusion-Related Vein Gold Deposits: Types, Tectono-Magmatic Settings and Difficulties of Distinction from Orogenic Gold Deposits. Resource geology, 48, 237-250.

Smallwood, J.R., Maresh, J. (2002): The properties, morphology and distribution of igneous sills: modelling, borehole data and 3D seismic from the Faroe-Shetland area. In: D.W. Jolley, and B.R. Bell, Eds., The North Atlantic Igneous Province: Stratigraphy, Tectonic, Volcanic and Magmatic processes: Geological Society, London, Special Publications, 197, 271-306.

Spacapan, J.B.; Palma, J.O.; Galland, O.; Manceda, R.; Rocha, E.; D'Odorico, A.; Leanza, H.A. (2018): Thermal impact of igneous sill-complexes on organic-rich formations and implications for petroleum systems: A case study in the northern Neuquén Basin, Argentina. Marine and Petroleum Geology, 91, 519–531.

Svensen, H., Planke, S., Jamtveit, B., Pedersen, T. (2003): Seep carbonate formation controlled by hydrothermal vent complexes: a case study from the Vøring Basin, the Norwegian Sea. Geo-Marine Letters, 23, 351-358.

Svensen, H., Planke, S., Malthe-Sørenssen, A., Jamtveit, B., Myklebust, R., Eidem, T.R., Rey, S.S. (2004): Release of methane from a volcanic basin as a mechanism for initial Eocene global warming. Nature, 429, 542-545.

Svensen, H., Planke, S., Corfu, F. (2010): Zircon dating ties NE Atlantic sill emplacement to initial Eocene global warming. Journal of the Geological Society, 167, 433-436.

Therkelsen, J. (2016): Diagenesis and reservoir properties of Middle Jurassic sandstones, Traill Ø, East Greenland: The influence of magmatism and faulting. Marine and Petroleum Geology, 78, 196-221.

Tsuji, T., Masui, Y., Yokoi, S. (2011): New hydrocarbon trap models for the diagenetic transformation of opal-CT to quartz in Neogene siliceous rocks. AAPG Bulletin 2011, 95, 449-477.

Tissot, B.P., Welte, D.H. (1984): Petroleum Formation and Occurrence, Second edition, Springer-Verlag.

Walderhaug, O. (1994): Precipitation rates for quartz cement in sandstones determined by fluid-inclusion microthermometry and temperature-history modeling. Journal of Sedimentary Research, A64, 324-333.

Walderhaug, O. (1996): Kinetic Modeling of Quartz Cementation and Porosity Loss in Deeply Buried Sandstone Reservoirs. AAPG Bulletin, 80, 731-745.

Wang, L., Cheng, L., Cheng, Y., Yin, G., Cai, C., Xu, C., Jin, K. (2014): Thermal effects of magmatic sills on coal seam metamorphism and gas occurrence. Bulletin of Volcanology , 76:803.

Xu, K., Yu, B., Gong, H., Ruan, Z., Pan, Y., Ren, Y. (2015): Carbonate reservoirs modified by magmatic intrusions in the Bachu area, Tarim Basin, NW China. Geoscience Frontiers, 6, 779-790.

Yao, Y., Liu, D., Huang, W. (2011): Influences of igneous intrusions on coal rank, coal quality and adsorption capacity in Hongyang, Handan and Huaibei coalfields, North China. International Journal of Coal Geology, 88, 135-146.

Yao, Y., Liu, D. (2012): Effects of igneous intrusions on coal petrology, pore-fracture and coalbed methane characteristics in Hongyang, Handan and Huaibei coalfields, North China. International Journal of Coal Geology, 96-97, 72-81.

Zou, C.; Zhang, G.; Zhu, R.; Yuan, X.; Zhao, X.; Hou, L.; Wen, B.; Wu, X. (2013): Volcanic Reservoirs in Petroleum Exploration: Petroleum Industry Press; Elsevier Inc.: Amsterdam, The Netherlands.

Grafisk design: Kommunikasjonsavdelingen, UiB / Trykk: Skipnes Kommunikasjon AS

uib.no

ISBN: 978-82-308-7081-5 (PRINT)
978-82-308-7170-6 (PDF)